DEVELOPMENT OF A BIPROPELLANT ROCKET ENGINE WITH A FOCUS ON THE INJECTOR

by

Enes Oğuz İskender

B.S., Mechanical Engineering, Boğaziçi University, 2019

Submitted to the Institute for Graduate Studies in
Science and Engineering in partial fulfillment of
the requirements for the degree of
Master of Science

Graduate Program in Mechanical Engineering

Boğaziçi University

2022

ACKNOWLEDGEMENTS

I would like to thank my advisor Prof. Murat ÇELİK for his guidance throughout this study. His support and enthusiasm has been a crucial source of motivation during this experimental research. His experience with experimenting paved the way for the development and realization of the daunting task of testing campaigns. I have learned a lot about research and experimenting from him during countless laboratory hours.

I would like to thank Prof. Şebnem ÖZÜPEK and Prof. Tufan Coşkun KARALAR for their time and contributions to my thesis.

I would like to thank İbrahim Safa UÇ for his invaluable friendship. We spent many hours of fruitful discussions in the laboratory together that contributed to this study. I would also like to thank Selcen YEDİYILDIZ for her support and friendship during many days of work throughout this study.

I would like to acknowledge the financial support of Scientific and Technological Research Council of Turkey (TÜBİTAK) under the scholarship program TÜBİTAK 2210 - A.

Last but not least, I would like to thank my dear family for their tremendous and endless support. I have been able to continue my studies with their continuous encouragement. I am always grateful to have them.

ABSTRACT

DEVELOPMENT OF A BIPROPELLANT ROCKET ENGINE WITH A FOCUS ON THE INJECTOR

Access to space relies on powerful propulsion systems to take a spacecraft out of the Earth's atmosphere. Currently, chemical propulsion systems are the only propulsion method that are able to provide the thrust levels required to carry out these missions. Among the chemical propulsion systems, bipropellant liquid rocket engines provide the highest specific impulse. In this study, a bipropellant liquid rocket engine, and specifically its injector, is designed, manufactured and tested. The used injector is a fixed area triple impinging injector. The tests include water tests, open injector cold flow tests, open injector hot flow tests and an engine hot fire test. BUSTLab (Boğaziçi University Space Technologies Laboratory) Liquid Rocket Engine is a pressure - fed liquid oxygen - ethanol (75% ethanol - 25% water) engine. The design point for the engine is $5.65kN$ thrust, $254s$ of specific impulse, 1.25 oxidizer to fuel ratio, total mass flow rate of $2.27kg/s$ at $30bar$ chamber pressure. The engine is hot fire tested at full thrust for 12 seconds. During this test, $0.83kg/s$ mass flow rate of oxidizer and $0.89kg/s$ mass flow rate of fuel are measured which gives $1.72kg/s$ total mass flow rate and 0.93 oxidizer to fuel ratio. Chamber pressure and thrust measurements during this test are inconclusive due to sealing and load cell issues. With the measured mass flow rates, the chamber pressure is calculated to be $21.2bar$ and the thrust is calculated as $3.62kN$.

ÖZET

SIVI YAKITLI ROKET MOTORUNUN ENJEKTÖR ODAKLI GELİŞTİRİLMESİ

Uzaya erişim, uzay araçlarını atmosferin dışına taşımak için güçlü itki sistemlerine dayalıdır. Günümüzde, kimyasal itki sistemler bu görevi gerçekleştirebilecek seviyelerde itki sağlayabilen tek itki sistemleridir. Sıvı yakıtlı roketlerden olan çift yakıtlı roketler, kimyasal itki sistemleri arasında en yüksek özgül itki değerine sahiptir. Bu çalışmada, çift yakıtlı bir sıvı yakıtlı roket motorunun, özellikle enjektörünün, tasarımı, üretimi ve testleri yapılmıştır. Kullanılan enjektör, sabit akış alanlı üçlü çarpışmalı bir enjektördür. Yapılan testler arasında su testleri, açık enjektör soğuk akış testleri, açık enjektör sıcak akış testleri ve motor sıcak ateşleme testi bulunmaktadır. BUSTLab (Boğaziçi Üniversitesi Uzay Teknolojileri Laboratuvarı) Sıvı Yakıtlı Roket Motoru basınç beslemeli, sıvı oksijen - etanol (75% etanol - 25% su) yakıtlı bir motordur. Motor tasarımı $5.65kN$ itki, $254s$ özgül itki, 1.25 oksitleyici kütlesel debisi / yakıt kütlesel debisi oranı, toplam $2.27kg/s$ kütlesel debi ve $30bar$ yanma odası basıncı değerleri elde edilecek şekilde yapılmıştır. Motor, 12 saniye boyunca tam itki değerinde test edilmiştir. Bu testte $0.83kg/s$ oksitleyici kütlesel debisi, $0.89kg/s$ yakıt kütlesel debisi ile toplam $1.72kg/s$ kütlesel debi ölçülmüştür. Yanma odası basıncı sızdırmazlık problemi nedeniyle ölçülememiştir. Yük hücresi arızası sebebiyle itki ölçümü yapılamamıştır. Yapılan kütlesel debi ölçümleri kullanılarak yanma odası basıncı $21.2bar$ ve üretilen itki $3.62kN$ olarak hesaplanmıştır.

TABLE OF CONTENTS

ACKNOWLEDGEMENTS . . . iii
ABSTRACT . . . iv
ÖZET . . . v
LIST OF FIGURES . . . viii
LIST OF TABLES . . . xiv
LIST OF SYMBOLS . . . xvi
LIST OF ACRONYMS/ABBREVIATIONS . . . xix
1. INTRODUCTION . . . 1
1.1. History of Rocketry . . . 2
1.2. Chemical Propulsion Systems . . . 3
1.2.1. Solid Propulsion . . . 7
1.2.2. Hybrid Propulsion . . . 9
1.2.3. Liquid Propulsion . . . 11
1.2.3.1. Monopropellant Propulsion . . . 12
1.2.3.2. Bipropellant Propulsion . . . 14
1.3. Electric Propulsion Systems . . . 15
1.3.1. Ion Engine . . . 15
1.3.2. Hall Effect Thruster . . . 17
1.3.3. Thermal / Resistojet Propulsion . . . 19
1.4. Scope of This Study . . . 19
2. BIPROPELLANT ROCKET ENGINE INJECTORS . . . 21
2.1. Showerhead Injectors . . . 22
2.2. Impinging Injectors . . . 23
2.3. Coaxial Injectors . . . 28
2.3.1. Swirl Injectors . . . 28
2.4. Pintle Injectors . . . 30
3. ENGINE DESIGN & MANUFACTURING . . . 34
3.1. Thrust Chamber . . . 40

3.2. Jacket 42
3.2.1. Saddle 42
3.3. Injector 43
3.3.1. Alternative Injector Design 1: A Coaxial Swirl Injector 52
3.3.2. Alternative Injector Design 2: A Pintle Injector 55
3.4. Dome 57
3.5. Thrust Stand 59
3.6. Feed System 60
3.6.1. Fuel Line 60
3.6.2. Oxidizer Line 61
3.6.3. Cooling Water Line 62
3.7. Igniter 63
4. INJECTOR TESTS 65
4.0.1. First Injector Water Tests 69
4.0.2. Second Injector Water Tests 70
4.1. Cold Flow Tests 71
4.2. Open Hot Flow Tests 76
5. HOT FIRE TEST 82
6. CONCLUSION 91
REFERENCES 94
APPENDIX A: NOZZLE THEORY 100

LIST OF FIGURES

Figure 1.1. Classification of rocket propulsion systems. 1

Figure 1.2. Hero of Alexandria's *aeolipile* [1]. 2

Figure 1.3. Isp and thrust values for various space propulsion systems [2]. . . 4

Figure 1.4. Flow separation during Space Shuttle Main Engine ignition [3]. . . 7

Figure 1.5. Grain configuration examples for initially high thrust followed by lower thrust combustion [4]. 8

Figure 1.6. General structure of a hybrid rocket engine [5]. 10

Figure 1.7. Green propellant reaction control system feeding schematic [6]. . . 13

Figure 1.8. Idealized selection process for propulsion systems [4]. 14

Figure 1.9. BURFIT - 80 RF ion thruster during operation inside BUSTLab vacuum chamber [7]. 16

Figure 1.10. Hall thruster operation schematic [8]. 17

Figure 1.11. HK40 Hall thruster during high power operation inside BUSTLab vacuum chamber. 18

Figure 1.12. General schematic of resistojet propulsion [9]. 19

Figure 2.1. Most common injector types. 21

Figure 2.2. Showerhead injector on the top (right) and swirl injectors on the sides (left) of V2 rocket [10]. 22

Figure 2.3. Typical showerhead injector geometry [11]. 23

Figure 2.4. Impinging injector types [11]. 24

Figure 2.5. PERSEUS project injector water test [12]. 26

Figure 2.6. A rendering of Sun Devil Rocketry injector's cross cut. Orange is used for fuel and blue is used for oxidizer [13]. 26

Figure 2.7. Impinging injector designed at University of Texas El Paso [14]. . 27

Figure 2.8. Schematic of a swirl injector [15]. 29

Figure 2.9. Cross - sectional view of the swirl injector 3D CAD model (left) [16] and the manufactured swirl injectors (right) [17]. 29

Figure 2.10. Pintle injector concept [18]. 30

Figure 2.11. Purdue liquid propellant sounding rocket pintle injector. Axial flow only (left), radial flow only (middle) and combined flow (right) [19]. 31

Figure 2.12. Flow fields of conventional (left) and pintle (right) engines [20]. . . 32

Figure 2.13. Pintle injector parts for a $5kN$ bipropellant injector [21]. 33

Figure 3.1. Summary of engine design process. 38

Figure 3.2. RS - 88 engine test [22]. 39

Figure 3.3. 3D model of the thrust chamber. 41

Figure 3.4. Manufacturing process of the thrust chamber. 41

Figure 3.5. Manufactured saddle. 42

Figure 3.6. 3D model of the first injector design. 43

Figure 3.7. Manufacturing process of the injector. 44

Figure 3.8. Technical drawing of the triplet used in the first version of BUST-Lab liquid rocket injector (units are in mm). 45

Figure 3.9. Discharge coefficients for various orifice geometries based on empirical data [4]. 46

Figure 3.10. Manufacturing misalignment in the first manufactured injector. . . 47

Figure 3.11. Technical drawing of the triplet used in the second version of BUST-Lab liquid rocket injector (units are in mm). 48

Figure 3.12. Front of the second injector design. 49

Figure 3.13. Back of the second injector design. 49

Figure 3.14. Cut view of the injector. Triple impingment of fuel and oxidizer orifices is visible. 50

Figure 3.15. Manufactured new injector. 50

Figure 3.16. Main geometry of the inner swirl flow [23]. 52

Figure 3.17. Schematic of the designed pintle injector [24]. 55

Figure 3.18. Pintle parameters [25]. 56

Figure 3.19. 3D model of the dome. 58

Figure 3.20. Manufactured dome. 58

Figure 3.21. Parts and assembly of the thruster. 59

Figure 3.22. Manufactured thrust stand. 60

Figure 3.23. LOX tank with cage - car before and after insulation. 62

Figure 3.24. The spark igniter in front of the injector before the open hot flow test. 64

Figure 4.1. Water test setup. 67

Figure 4.2. Triplet impingement of water at low pressure drop. 68

Figure 4.3. Cold flow test setup. 72

Figure 4.4. Cold flow test of the injector. 73

Figure 4.5. Pressure in the cold flow test with liquid nitrogen as the oxidizer. 73

Figure 4.6. Pressure in the cold flow test with water as the fuel. 74

Figure 4.7. Mass of the oxidizer tank in cold flow test with liquid nitrogen. . . 75

Figure 4.8. Mass of the fuel tank in cold flow test with water. 76

Figure 4.9. Open hot flow test setup. 77

Figure 4.10. Pressure measurements in open hot flow test for LOX. 78

Figure 4.11. Mass of the oxidizer tank - car in open hot flow test at 80 bar. . . 78

Figure 4.12. Pressure measurements in open hot flow test for fuel. 79

Figure 4.13. Mass of the fuel tank in open hot flow test at 80 bar. 80

Figure 4.14. Injector open hot flow test with liquid oxygen and ethanol - water mixture. 81

Figure 5.1. BUSTLab Liquid Rocket Engine hot fire thruster assembly on the thrust stand. 82

Figure 5.2. BUSTLab Liquid Rocket Engine hot fire test setup. 83

Figure 5.3. Pressure measurements on oxidizer side during hot fire test. 85

Figure 5.4. Oxidizer tank mass during hot fire test. 86

Figure 5.5. Pressure measurements on fuel side during hot fire test. 87

Figure 5.6. Fuel tank mass during hot fire test. 88

Figure 5.7. BUSTLab Liquid Rocket Engine hot firing. 90

Figure A.1. Area ratio (A/A_t), pressure ratio (P/P_0) and temperature ratio (T/T_0) along a converging - diverging nozzle as functions of Mach number (M) for $\gamma = 1.3$. 107

LIST OF TABLES

Table 1.1. Advantages and disadvantages of solid propulsion systems. 9

Table 1.2. Advantages and disadvantages of hybrid propulsion systems. 10

Table 1.3. Advantages and disadvantages of liquid propulsion systems. 12

Table 3.1. Effects of design choices on engine. 34

Table 3.2. Design results for the new configuration. 39

Table 3.3. Injector orifices of the two designs. 51

Table 3.4. Results of the fuel centered coaxial swirl injector design. 54

Table 3.5. Pintle design outline. 57

Table 3.6. Pintle design flow parameters & sizing. 57

Table 4.1. First injector water test results for the oxidizer orifices. 69

Table 4.2. First injector oxidizer flow with LOX. 69

Table 4.3. First injector water test results for fuel orifices. 70

Table 4.4. First injector fuel flow with ethanol - water mixture. 70

Table 4.5. Changes and expectations for the new injector oxidizer side. 71

Table 4.6. Changes and expectations for the new injector fuel side. 71

Table 5.1. Design and test result comparison of the BUSTLab Liquid Rocket Engine. 89

LIST OF SYMBOLS

A	Area
A_{ch}	Chamber area
A_e	Exit area
A_o	Orifice area
A_x	Area of section x
A^*	Throat area
C_d	Discharge coefficient
Cd_{an}	Annular region discharge coefficient
Cd_{in}	Inlet orifice discharge coefficient
Cd_{out}	Outlet orifice discharge coefficient
c	Local speed of sound
c_p	Specific heat at constant pressure
c_v	Specific heat at constant volume
Do	Exit diameter
Dp	Diameter of the inlet orifice
Ds	Swirl chamber internal diameter
Dso	Swirl chamber external diameter
D_e	Exit diameter
D_c	Chamber diameter
D_P	Pintle diameter
D_t	Throat diameter
g_0	Gravitational acceleration of Earth
h	Enthalpy
h_x	Enthalpy at section x
h_0	Stagnation enthalpy
Isp	Specific Impulse
Ls	Swirl chamber length
Lo	Exit lentgth

L_{ch}	Chamber length
L_{nozzle}	Nozzle length
L_s	Skip distance
L^*	Characteristic length
M	Mach number
M_e	Exit Mach number
M_x	Mach number at section x
M_f	Final mass
M_i	Initial Mass
$\dot{m}$	Mass flow rate
$\dot{m}_f$	Fuel mass flow rate
$\dot{m}_o$	Oxidizer mass flow rate
$\dot{m}_x$	Mass flow rate at section x
$\dot{m}_{orifice}$	Mass flow rate through orifice
$\dot{m}_{total}$	Total mass flow rate
$\mathbb{M}$	Molar mass
P_a	Ambient pressure
P_c	Chamber pressure
P_e	Exit pressure
ΔP	Pressure drop
p_0	Stagnation pressure
p_x	Pressure at section x
R	Specific gas constant
R_{univ}	Universal gas constant
T	Thrust
T_c	Combustion temperature
T_x	Temperature at section x
t	Annular region thickness
U	Injection velocity
u_e	Exit velocity
V	Velocity

V_{ch}	Chamber volume
V_e	Exhaust velocity
V_i	Initial velocity
V_f	Final velocity
ΔV	Change in velocity
v	Specific volume
v_x	Specific volume at section x
X	Open area ratio
$\#$	Number
γ	Specific heat ratio
θ	Half cone angle
ρ	Density
$\varnothing$	Diameter

LIST OF ACRONYMS/ABBREVIATIONS

BUSTLab	Bogazici University Space Technologies Laboratory
CAD	Computer aided design
CEA	Chemical equilibrium applications
CNC	Computerized numerical control
EDM	Electrical discharge machining
GOX	Gaseous Oxygen
JAXA	Japan Aerospace Exploration Agency
LOX	Liquid Oxygen
NASA	National Aeronautics and Space Administration
NI	National Instruments
NPT	National pipe thread
OF	Oxidizer to fuel
PERSEUS	Projet Étudiant de Recherche Spatiale Européen Universitaire et Scientifique
$RP-1$	Rocket propellant 1, Kerosene
TMR	Total momentum ratio
3D	Three dimensional

1. INTRODUCTION

Today, rockets are the only viable vehicles that can carry a payload to orbit or to another celestial body. Rockets use Newton's 3rd Law to move from point A to point B. However, this motion has different conditions depending on where it begins from. If a rocket is to begin its motion from the sea level on Earth, it is going to need very high thrusts exceeding the force exerted on it by the Earth's gravity, i.e., it's weight. On the other hand, an object at the Earth's orbit with the same mass as the rocket lifting off from the surface of the Earth can go to the farthest corner of our solar system with a thrust similar to the push of a gentle wind. For any of these motions, a spacecraft needs to be propelled. There are several methods used for propelling spacecraft in order to accelerate or maneuver them in desired directions or orientations. These methods can be seen in Figure 1.1.

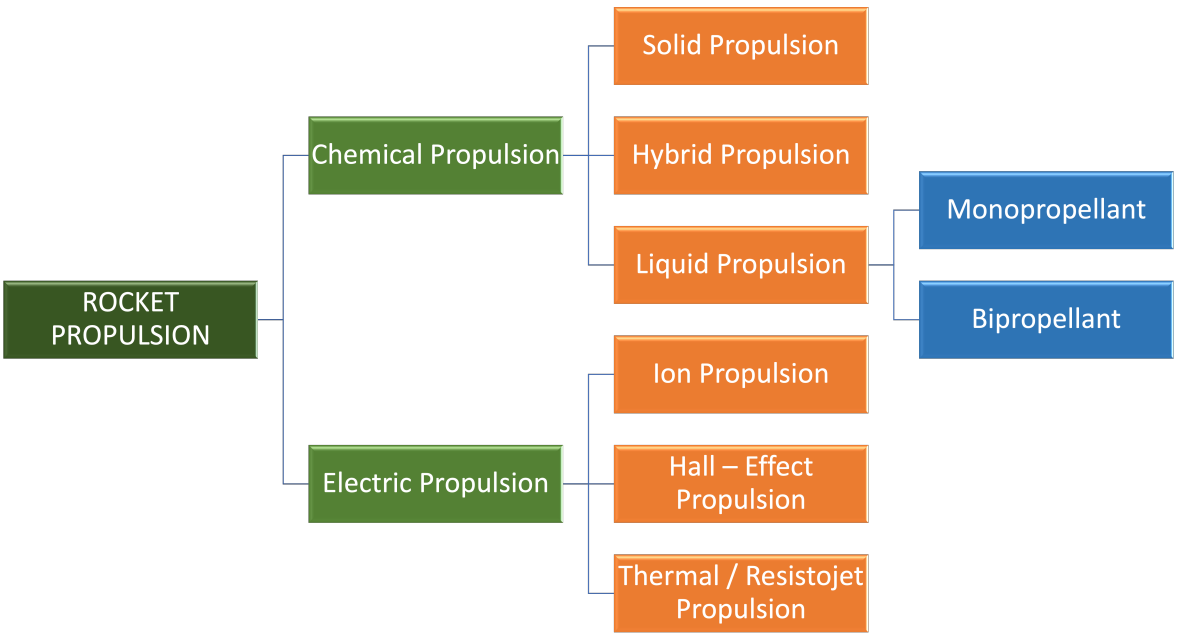

Figure 1.1. Classification of rocket propulsion systems.

1.1. History of Rocketry

The roots of today's advanced rockets go back many centuries in human history. The first known anecdote for the idea of a rocket is attributed to a Greek named Archytas in the year $360BC$. Using the action - reaction principle, that was not known to humanity as a law of motion by then, the flying pigeon of Arcyhtas suspended to a wire would be propelled with steam or compressed air to move along the wire [26].

Another story is attributed to a Greek named Hero of Alexandria in the 2nd century BC. Hero built a toy named *aeolipile*. A sphere with two L shaped orifices is placed on a boiler. As the boiler is heated with the fire underneath it, the generated steam passes through the sphere and exits through the orifices. With the action - reaction principle, the sphere is given a rotation around its axis. A schematic of this apparatus can be seen in Figure 1.2.

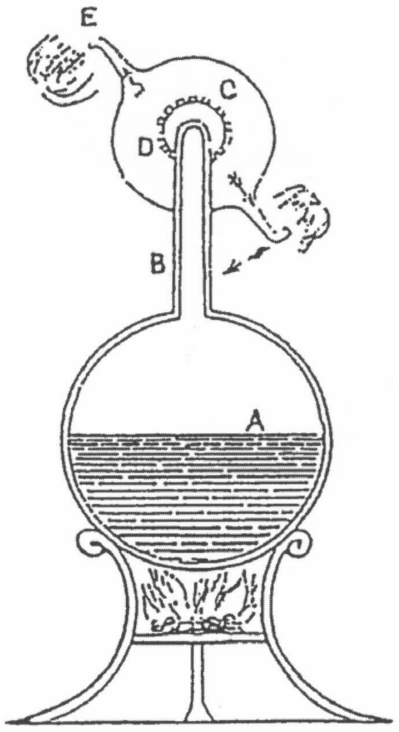

Figure 1.2. Hero of Alexandria's *aeolipile* [1].

Fast forwarding to the 20th century, Konstantin Tsiolkovsky derived the first formula for rocketry:

$$V_f = V_i + \Delta V = V_i + V_e \ln \frac{M_i}{M_f}. \tag{1.1}$$

In Equation 1.1, V_f is the final velocity, V_i is the initial velocity, ΔV is the change in velocity, V_e is the exhaust velocity of the propellant, M_i is the initial or wet mass and M_f is the final or dry mass of the rocket.

Rocket propulsion systems generate thrust by ejecting propellants in the opposite direction:

$$T = \dot{m} V_e. \tag{1.2}$$

In Equation 1.2, T is the thrust, $\dot{m}$ is the mass flow rate of the propellants and V_e is the exhaust velocity of the propellants. Specific impulse, Isp,

$$Isp = \frac{T}{\dot{m} g_0} = \frac{V_e}{g_0} \tag{1.3}$$

is a measure of how effectively a rocket uses its propellants. In Equation 1.3 g_0 is the gravitational pull of the Earth at sea - level. As it is seen in the third part of Equation 1.3, Isp can also be described as a measure of how fast a rocket exhausts the propellants. A rocket engine with higher Isp will produce more thrust than a rocket engine with lower Isp with the same amount of propellant flow rate. Among the propulsion systems listed in Figure 1.1, electric propulsion systems have the highest Isp. Figure 1.3 presents various propulsion systems' Isp and thrust values.

1.2. Chemical Propulsion Systems

The first part of any payload's journey to space is achieved by rocket engines that are categorized under chemical propulsion systems. These are systems that eject hot gases through a nozzle, and they are able to provide thrust in the order of hundreds of tons.

Unlike electric propulsion systems, chemical propulsion systems utilize the energy stored within the propellants to produce thrust. Comparison of Isp and thrust values of different propulsion systems can be seen in Figure 1.3.

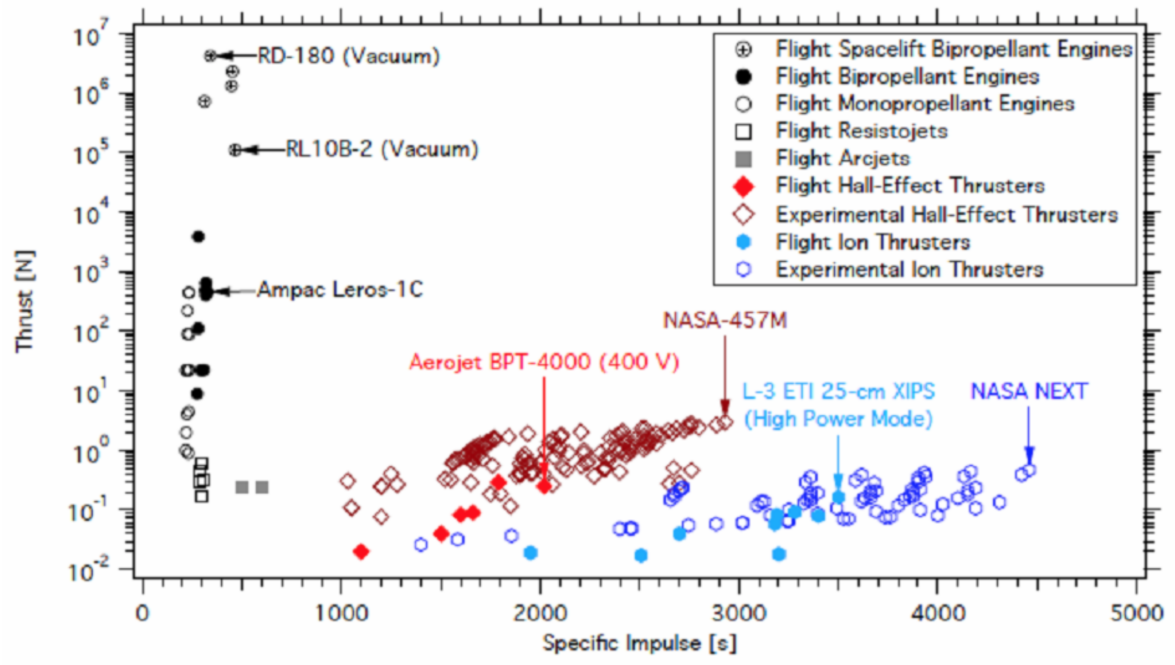

Figure 1.3. Isp and thrust values for various space propulsion systems [2].

Chemical propulsion systems rely on the chemical reactions, i.e., combustion or exothermic decomposition. The energy released by the chemical reactions creates a high temperature or enthalpy environment in the engine chamber. This thermal energy is the source of acceleration of the gases that are formed as the products of the chemical reaction.

Chemical propulsion systems have converging - diverging nozzles that are also known as de Laval nozzles. Invented by the Swedish engineer Gustaf de Laval, they were first used by Robert Goddard in a rocket engine. As the combustion products travel along the converging section of the nozzle, they reach to the part with the smallest cross - sectional area within the engine called the throat. Before reaching the throat, the combustion products flow at subsonic speeds. The converging part of the

nozzle accelerates the flow with venturi effect until it reaches the throat. At the throat, the flow is at local speed of sound, Mach 1, with choked conditions.

As the flow leaves the throat and starts expanding in the diverging section of the nozzle, it accelerates to supersonic speeds, cools down, and the pressure decreases. The diverging section of the nozzle determines the expansion ratio of the flow. The expansion ratio is defined as A_e/A_t, which is the area of the exit divided by the area of the throat. The expansion of the engine affects the exit pressure, P_e, of the flow, which affects the thrust provided by the engine. An engine with an exit pressure less than the ambient pressure is said to have an overexpanded nozzle. In an overexpanded nozzle, the flow of the combustion products expands to the ambient pressure before they leave the nozzle since the nozzle exit area is too large for an optimum expansion. An engine with an exit pressure higher than the ambient pressure is said to have an underexpanded nozzle. In an underexpanded nozzle, the flow completes its expansion after it leaves the nozzle because the nozzle exit area is smaller than that of an optimum rocket nozzle.

The space shuttle main engine (SSME) has an overexpanded nozzle. The SSME is an engine that is used both during the launch and after the solid rocket boosters are jettisoned. The ambient pressure, P_a, changes significantly during a launch as the space shuttle ascends to higher altitudes. SSMEs are designed so that during their burn time, they can give maximum power output in vacuum or space [27]. This is because the thrust provided by the engine is affected by both the exit pressure, P_e and ambient pressure, P_a, as it can be seen in the thrust equation:

$$T = \dot{m}u_e + A_e(P_e - P_a). \tag{1.4}$$

Also looking at the exit velocity equation,

$$u_e = \sqrt{\frac{2\gamma}{\gamma - 1} R_{univ} \left(\frac{T_c}{\mathbb{M}}\right) \left(1 - \left(\frac{P_e}{P_c}\right)^{\frac{\gamma-1}{\gamma}}\right)} \tag{1.5}$$

we can see that the exit velocity, u_e, increases as P_e decreases. In this equation, γ is the specific heat ratio of the combustion products, R_{univ} is the universal gas constant, T_c is the combustion temperature and $\mathbb{M}$ is the molecular weight of the combustion products. This means that having a greater expansion ratio will indeed increase u_e. However, this does not mean that it will increase the thrust indefinitely as it also affects the second term in Equation 1.4. One might think that we should have gigantic nozzles with huge expansion ratios for vacuum engines but it is also crucial to take into account the increase in the mass of an engine as its nozzle gets bigger. First stage rocket engines operate over a wide range of ambient pressures as they ascend from sea level to high altitudes. For this reason, they mostly operate in overexpanded or underexpanded conditions. Rocket engines are designed so that they give the maximum flight performance. Engine flight performance criteria can be total impulse, thrust or specific impulse depending on the mission. The expansion ratio for nozzle is designed as part of the mission requirements of the engine.

The other restriction to having a very large nozzle expansion, or opening ratio, is the flow separation. In one of the early studies on flow separation, Forster and Cowles found that when the flow is expanded to %40 of the ambient pressure, flow separation begins [28]. This is called Summerfield Criterion and it is now viewed as a conservative design criterion [29]. As discussed in the previous paragraph, rocket engines are designed for the maximum flight performance. However, safe operation of an engine is also as important as the flight performance.

The optimum expansion altitude, in other words optimum expansion ambient pressure, is chosen high enough to ensure that flow separation is avoided at sea level [30]. However, as the chamber pressure builds up during ignition, flow separation can occur in diverging nozzles. Flow separation in SSME during ignition, during chamber pressure build up, can be seen in Figure 1.4.



Figure 1.4. Flow separation during Space Shuttle Main Engine ignition [3].

Chemical propulsion systems can be classified under three main groups: solid, hybrid and liquid propulsion systems. The complexity of the design and manufacturing processes increases with the given order. These systems are further discussed in the following sections.

1.2.1. Solid Propulsion

A solid propellant rocket engine has both oxidizer and fuel stored in solid state. They are mixed and casted into a cylinder. A hole through the propellant is utilized as the combustion chamber. The combustion takes place on the flame front created with this hole through the fuel - oxidizer mixture propellant. The combustion takes place only on the surface of the fuel grain. The flame front and the area of combustion is

chosen depending on the designer's choice for the thrust curve. In Figure 1.5, several grain designs can be seen for passive control of thrust in solid rocket engines.

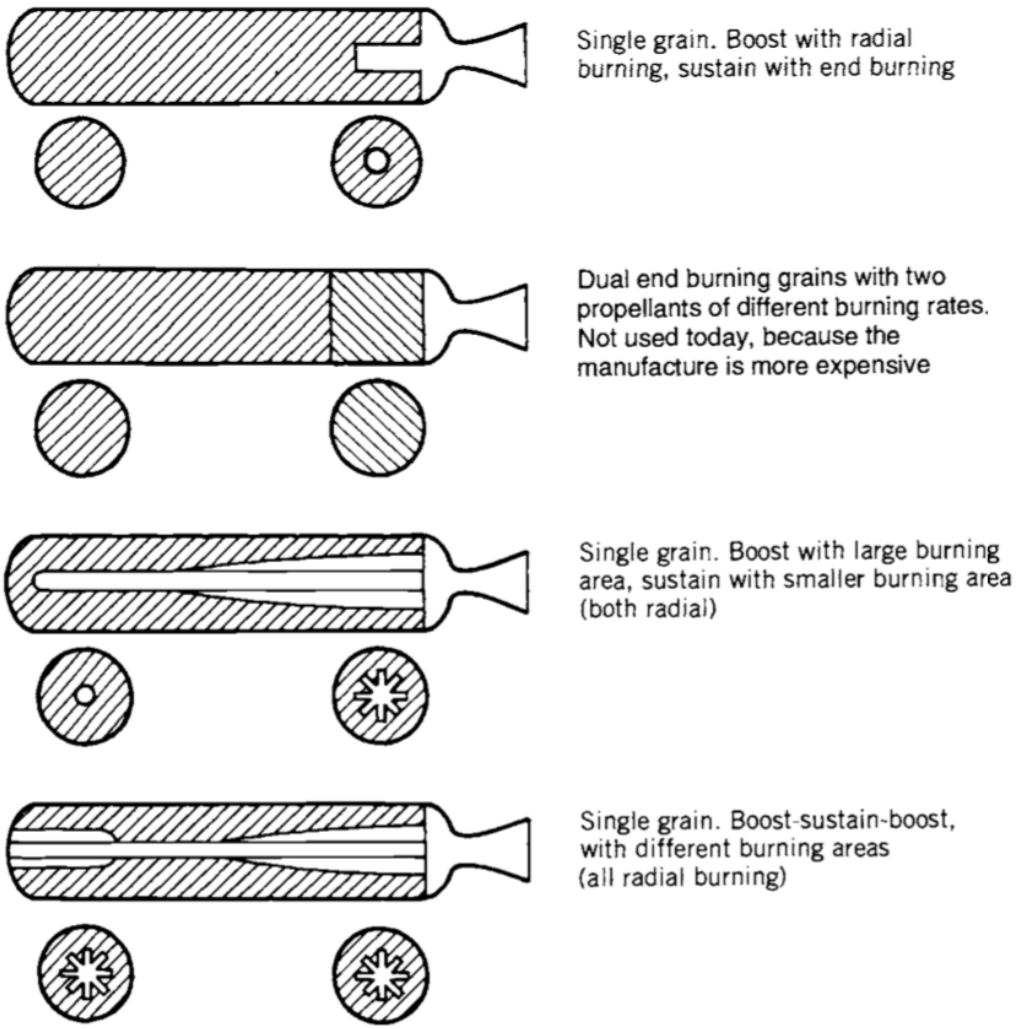

Figure 1.5. Grain configuration examples for initially high thrust followed by lower thrust combustion [4].

Combustion of the solid propellant results in a high enthalpy environment created by the hot product gases. Similar to other chemical propulsion systems, these hot gases are exhausted through a converging - diverging nozzle to produce thrust.

Solid propellant thrusters are reliable for long periods of storing. They are durable against propellant degradation and reliable to ignite. For these reasons, many military

systems are propelled with solid rocket thrusters. In the form of boosters, they are also used for launching payloads along with liquid propelled rockets. Smaller payloads can be launched to low Earth orbit with only solid rockets.

Solid rocket engines' thrust level cannot be actively controlled; in other words, they cannot be throttled or shut off easily. Once ignited, the combustion continues until the end. Some advantages and disadvantages of solid rocket engines are shown in Table 1.1.

Table 1.1. Advantages and disadvantages of solid propulsion systems.

Advantages	**Disadvantages**
• Simple design • Easy and quick operation readiness • Storable for long durations • Higher propellant density → small body → reduced mass & drag	• Explosion (detonation) risk • Exhaust gases can be toxic • Cannot be shut off easily • Active thrust control is not possible • Cannot be tested prior to ignition • Lower Isp than liquid and hybrid rockets

1.2.2. Hybrid Propulsion

Hybrid rockets generally use solid fuel and liquid oxidizer. If the configuration is reversed, i.e., liquid fuel and solid oxidizer, they are called reverse hybrids. Hybrid rocket fuel grains are made of polyethylene, paraffine, hydroxyl-terminated polybutadiene, etc. For oxidizer, hybrid rocket engines use liquid oxygen, hydrogen peroxide, nitrous oxide, dinitrogen tetroxide, etc.

General structure of a hybrid engine can be seen in Figure 1.6. The oxidizer is fed into a pre - combustion or vaporization chamber located before the solid fuel grain.

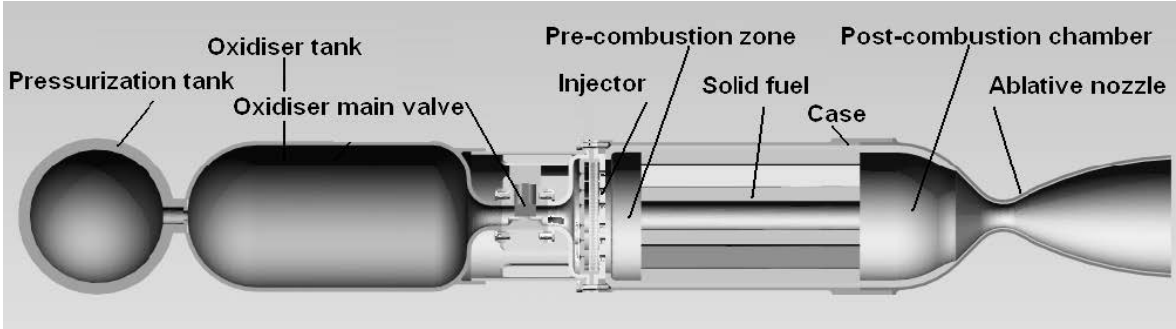

Figure 1.6. General structure of a hybrid rocket engine [5].

The solid fuel grain in hybrid thrusters have multiple axial channels through which the incomplete combustion products enter the fuel grain. These channels are called combustion ports. Combustion ports generate fuel vapor as a result of the heat transfer from the pre - combustion chamber. The number, shape and size of combustion ports depend on the designed surface area for the fuel. In order to ensure full combustion of the propellants, a post - combustion chamber is employed since the combustion is not completed in the pre - combustion chamber and combustion ports. [4]. After the post - combustion chamber, the hot product gases are exhausted through a converging - diverging nozzle and thrust is produced. Similar to liquid rocket engines, hybrid rocket engines can be throttled. Some advantages and disadvantages of hybrid rocket engines are presented in Table 1.2.

Table 1.2. Advantages and disadvantages of hybrid propulsion systems.

Advantages	**Disadvantages**
• Chemically simpler than solid rockets	• Cannot be tested prior to ignition
• Simple design compared to liquid rockets	• Mixture ratio variation during both
$\rightarrow$ low cost design and manufacturing	steady state operation and throttling
• Isp higher than solid rockets	• Isp lower than liquid rockets
• Safer to handle	• Unproven technology readiness
• Throttleable, restartable	

1.2.3. Liquid Propulsion

Liquid propellant rockets have the propellants stored in liquid form in one or more storage tanks. Liquid rockets may have multiple thrust chambers and therefore injectors.

In liquid rockets, the propellants are fed into the thrust chamber by a feeding mechanism. Forcing the propellants to the thrust chamber is done with gas driven turbo - pumps. These systems significantly increase the complexity of designing a rocket engine.

Forcing the propellants from the tanks to the thrust chamber can also be done with a pressure - fed system in which the propellant tanks are pressurized with a pressurant inert gas. Compared to turbo - pump - fed engines, pressure - fed engines have much simpler designs. However, they are inconvenient for high combustion chamber pressures. This is because the propellant tank mass increases significantly for storing the propellants at higher pressures.

Recently, with the advances in electric motor and battery technologies, studies on electric - pump - fed systems are being carried out as an alternative [31, 32]. Small launchers with electric - pump - fed engines are being developed for small satellite launches. The Electron Rocket, developed by Rocket Lab, uses pumps driven by electric motors energized by lithium polymer batteries to feed the LOX - $RP1$ Rutherford engines [33]. With a payload capacity of $300kg$, as of June 2021, they delivered 104 small satellites to Low - Earth - Orbit [34].

Liquid propulsion systems can be classified as monopropellant and bipropellant propulsion systems. Some of the advantages and disadvantages of liquid propulsion systems are presented in Table 1.3.

Table 1.3. Advantages and disadvantages of liquid propulsion systems.

Advantages	**Disadvantages**
• Highest Isp among chemical rockets • Storing is possible with storable propellants • Can be throttled, shut off, restarted and reused • Can be tested prior to operation • With pumps, feed system mass can be lowered	• Complex design - more components • Cannot be stored with cryogenic propellants • Combustion stability is more difficult to control • Sloshing in tanks may rise flight stability issues

1.2.3.1. Monopropellant Propulsion. Monopropellant propulsion systems use the energy released by the chemical reaction of only one substance. This chemical reaction is initiated by a catalyst which results in exothermic reactions. As a result of this exothermic reaction, hot gases are obtained in monopropellant propulsion systems.

Most common propellant used in these systems is hydrazine (N_2H_4). Hydrazine decomposes to hydrogen (H_2), nitrogen (N_2) and ammonia (NH_3) when it comes in contact with a catalyst. Iridium (Ir) supported alumina (Al_2O_3), also known as Shell 405, is a common material used as the catalyst for hydrazine systems [35].

Monopropellant thrusters are generally used for orbit maintenance and attitude control. These systems do not reach the Isp levels of bipropellant propulsion systems. Nonetheless, they are preferred in these applications due to their simple design and operation. Their simplicity also results in cheaper solutions for in - space missions. Many monopropellant thrusters use hydrazine as propellant. Hydrazine is a toxic substance to humans. In the past, hydrazine was considered to be a clean propellant by the space industry [36]. However, it has been listed as a substance of very high concern by the European Chemicals Agency in 2011 [37] which means hydrazine use in space industry might be banned in the future [38].

There have been numerous studies on alternative propellants to replace hydrazine with green propellants. These propellants can be described as environmentally friendly and non - toxic substances. They are safer and easier to handle which reduces the operational costs by eliminating the operational burdens created by the hazardous hydrazine. The Netherlands Organization for Applied Scientific Research (TNO) have been working on nitromethane (CH_3NO_2) as a green propellant alternative to hydrazine. They reported nitromethane as a promising green propellant for this purpose [39]. Researchers at Korea Advanced Institute of Science and Technology tested a $10N$ monopropellant thruster with hydrogen peroxide (H_2O_2) - ethanol (C_2H_5OH) mixture as the propellant and platinum with porous gamma - phase alumina support as the catalyst [40]. A hydroxylammonium nitrate ($H_4N_2O_4$), ammonium nitrate (NH_4NO_3), water (H_2O) and methanol (CH_3OH) mixture as the propellant has been used under the green propellant reaction control system project of JAXA by Uramachi, et al. [6]. A schematic of a monopropellant feeding system can be seen Figure 1.7.

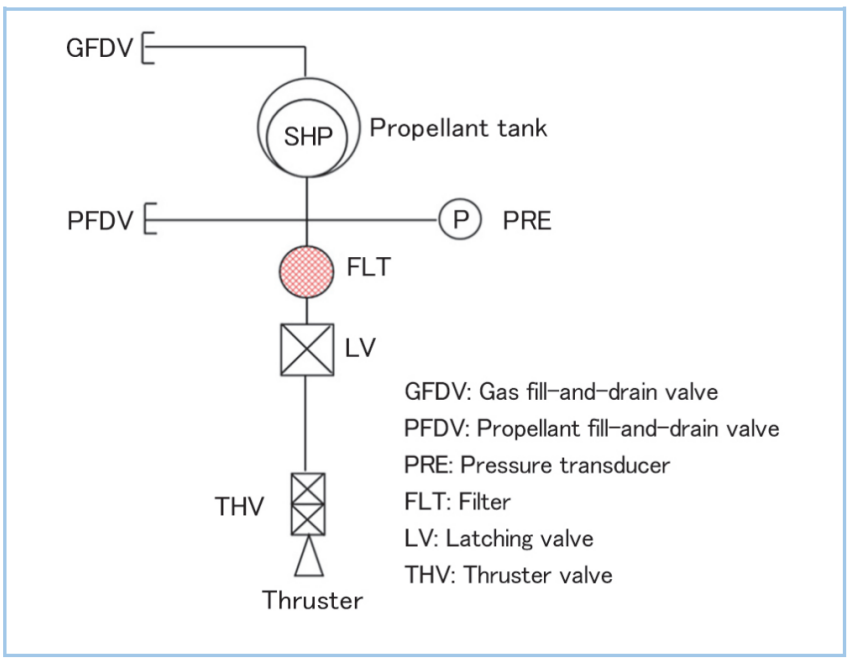

Figure 1.7. Green propellant reaction control system feeding schematic [6].

1.2.3.2. Bipropellant Propulsion. Bipropellant propulsion systems use two types of propellants: fuel and oxidizer. In these systems, both fuel and oxidizer are fed into a combustion chamber. Their mixture is then ignited in the combustion chamber to produce combustion products with high enthalpy. These gases are then accelerated in a converging - diverging nozzle and exhausted. The ideal nozzle assumptions and derivations are presented in APPENDIX A.

Bipropellant rocket engines have the highest performance among the chemical rocket engines, i.e., Isp. However, these systems require complicated design, manufacturing and control processes compared to other chemical propulsion systems. For these reasons, propulsion system selection is done based on not only the performance criteria but also based on the design, manufacturing and operational aspects. Idealized selection process for propulsion systems is presented in Figure 1.8.

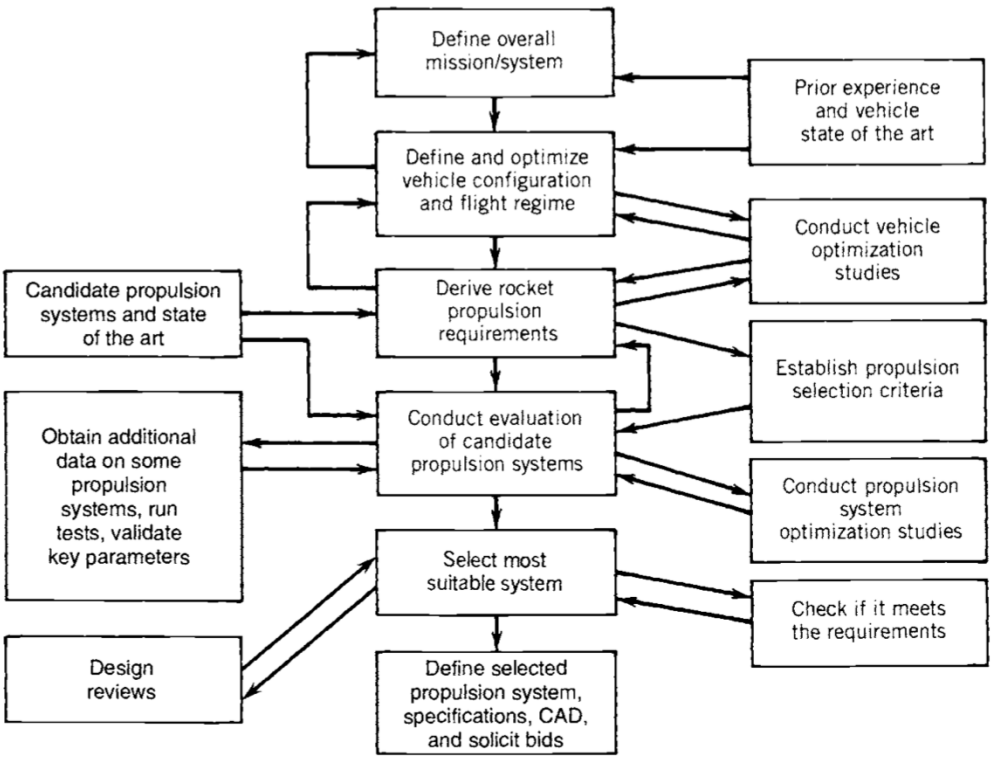

Figure 1.8. Idealized selection process for propulsion systems [4].

BUSTLab Liquid Rocket Engine is a bipropellant rocket engine. Our goal for the overall project is to gain knowledge and experience in this area in which we have no prior involvement or familiarity. Thus, the selection process given in Figure 1.8 is not of concern to us as we aim to lay our personal knowledge foundations in this area of engineering for educational and curiousity purposes. We began our project with the purpose of hot firing a liquid rocket engine only, without considering other chemical propulsion systems of any kind.

1.3. Electric Propulsion Systems

Electric propulsion systems generate thrust by using the energy acquired from the sun in the form of radiation or from a nuclear power source. These systems provide very low thrust with very high specific impulse levels compared to chemical propulsion systems. They are not suitable for launching an object from sea - level to space but they have great utility for in - space propulsion. Electric thrusters are used for various purposes including orbital station keeping, inter - orbital transfer and deep - space travel, etc. They are suitable for very long durations of operations. Electric propulsion systems can be classified as ion engines, Hall effect thrusters and thermal / resistojet thrusters.

1.3.1. Ion Engine

An ion thruster is a propulsion system that ionizes the propellant by electron bombardment. This electron bombardment is done with electrons emitted from a cathode placed inside the ionization chamber. This cathode, ionization cathode, is heated to elevated temperatures where a mechanism called thermionic emission releases electrons into the ionization chamber. These electrons are attracted to the chamber walls of the thruster. An ion thruster prevents these electrons from reaching the discharge chamber wall via the magnetic field created by the magnets around the ionization chamber. The neutral propellant is fed into the ionization chamber and ionized with the electron bombardment. The propellant now consists of neutral gas, positive ions and negative

electrons. The ions are now accelerated through perforated plates, grids, with a potential difference applied between them. This potential difference also prevents the electrons from leaving the discharge chamber. The electrons are collected by the anode of the ion engine. The ion engine, therefore the spacecraft, is prevented from negatively charging by releasing these electrons from an another cathode, neutralization cathode, located outside of the chamber. They are also released by the thermionic emission process and ejected into the ions leaving through the accelerator grid. The ions and the electrons now form a quasi - neutral plasma beam that produce thrust for the spacecraft. Another type of ionization method for ion thrusters is using radio - frequency (RF) waves. In this method, the propellant is ionized with the energy provided by the RF waves created by an RF antenna wrapped around the ionization chamber. An RF ion thruster developed and tested at BUSTLab can be seen in Figure 1.9.

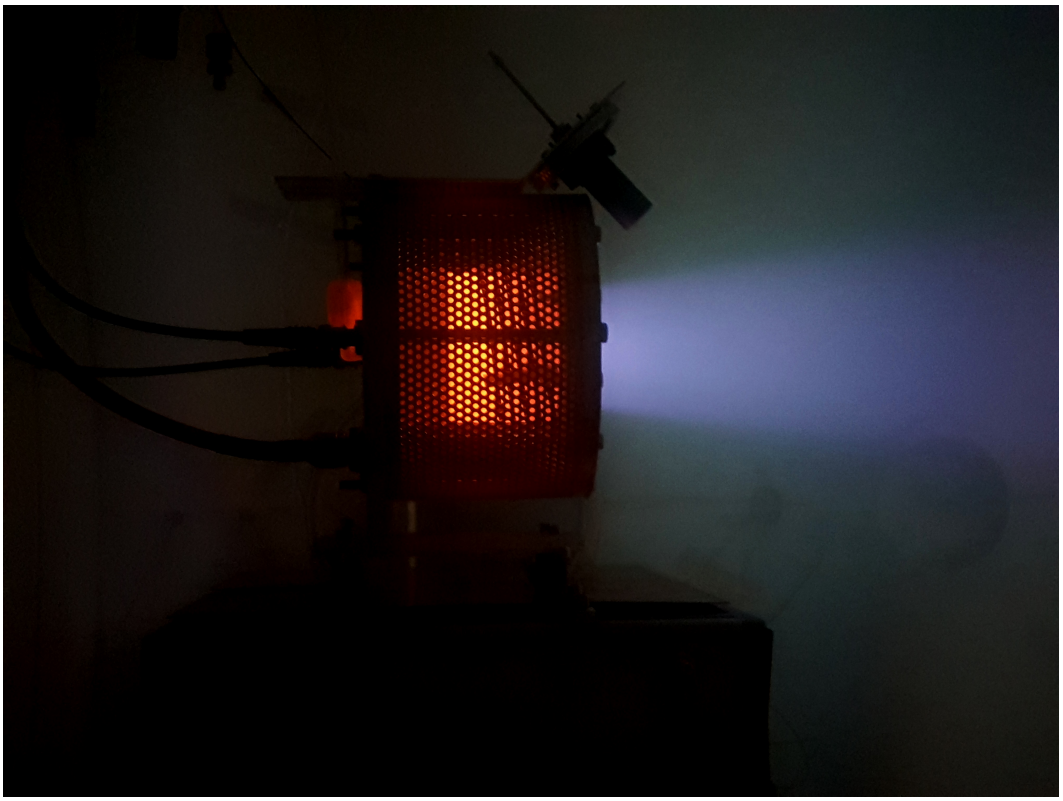

Figure 1.9. BURFIT - 80 RF ion thruster during operation inside BUSTLab vacuum chamber [7].

1.3.2. Hall Effect Thruster

Similar to ion engines, in Hall effect thrusters the neutral propellant is ionized with electron bombardment from a cathode. In Hall thrusters, the cathode is located externally. Unlike ion thrusters, Hall thrusters employ no perforated plates, i.e., grids.

A Hall thruster has a coaxial annular plasma cavity where the neutral propellant is ionized. The propellant is fed to this cavity through an annular anode. A schematic of a Hall thruster operation can be seen in Figure 1.10.

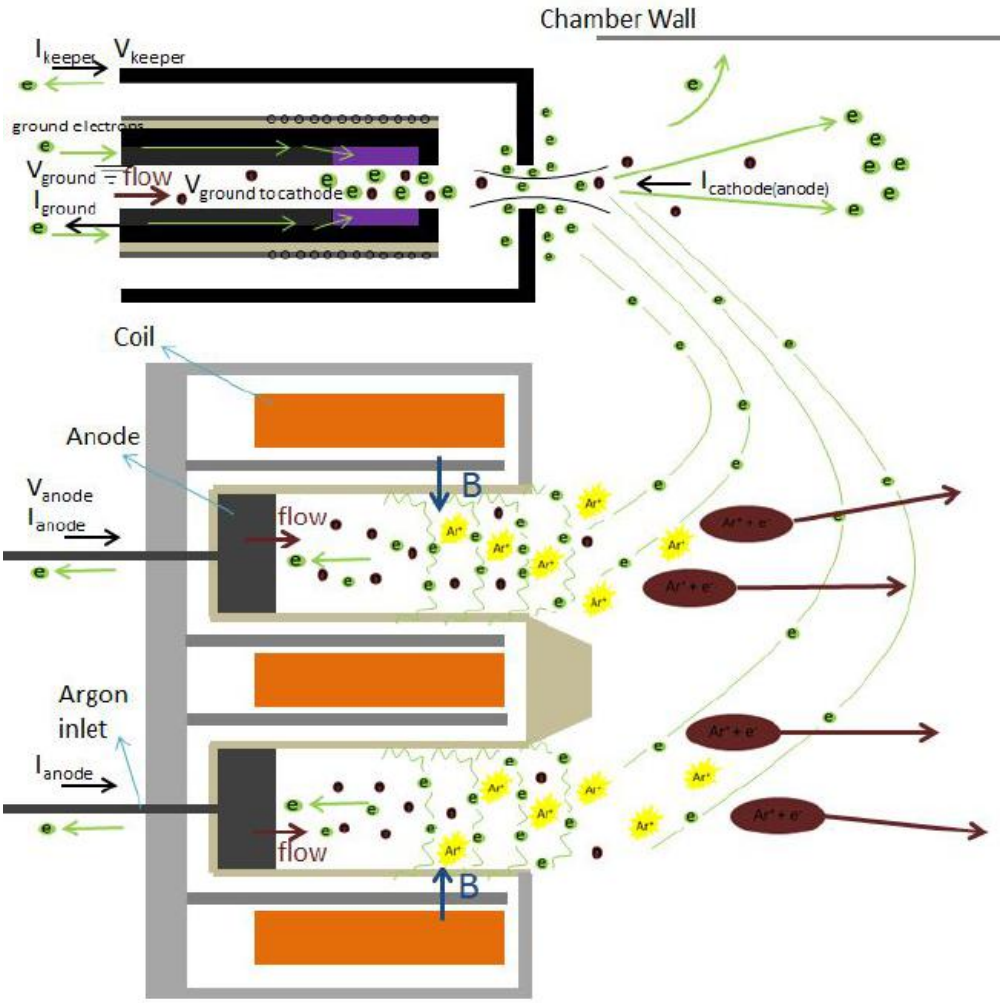

Figure 1.10. Hall thruster operation schematic [8].

Hall thrusters have radial magnetic fields created by permanent magnets or electromagnets. This magnetic field prevents the electrons from moving towards the annular anode. Instead, the electrons are confined in the plasma cavity with an azimuthal drift. On the other hand, the ions are only weakly affected by this magnetic field and have no azimuthal drift due to having a Larmor radius larger than the thruster's length.

Hall thrusters accelerate the positive ions with Lorentz force created by the axial electric field between the anode and the downstream potential. HK40 Hall thruster developed at BUSTLab during operation can be seen in Figure 1.11.

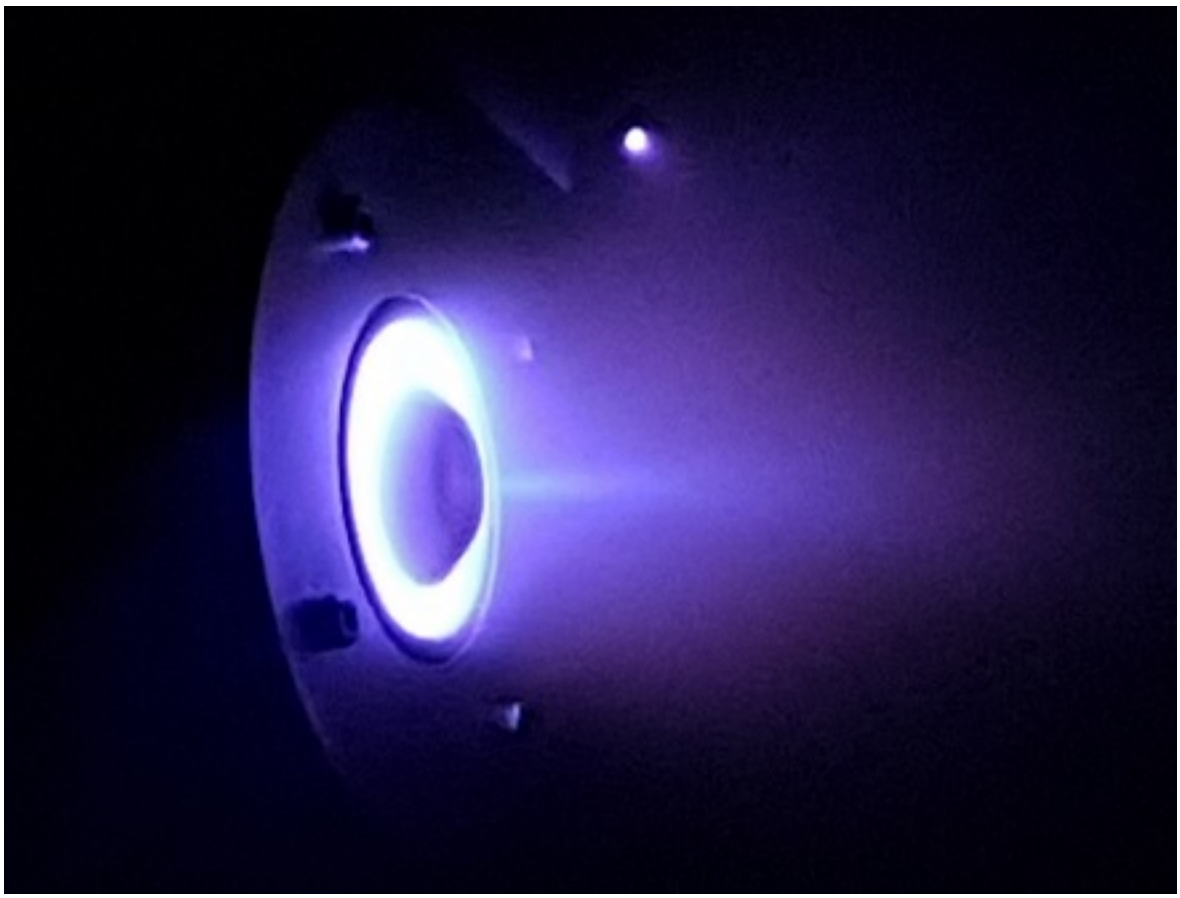

Figure 1.11. HK40 Hall thruster during high power operation inside BUSTLab vacuum chamber.

1.3.3. Thermal / Resistojet Propulsion

In a resistojet, the propellant is heated and exhausted through a converging - diverging nozzle. The heating of the propellant is done with a heat exchanger powered with electricity. Resistojets' performance is limited by the melting point of this heating element [9]. The main components of a resistojet propulsion system, i.e., propellant tank, heating element and nozzle, are shown in Figure 1.12.

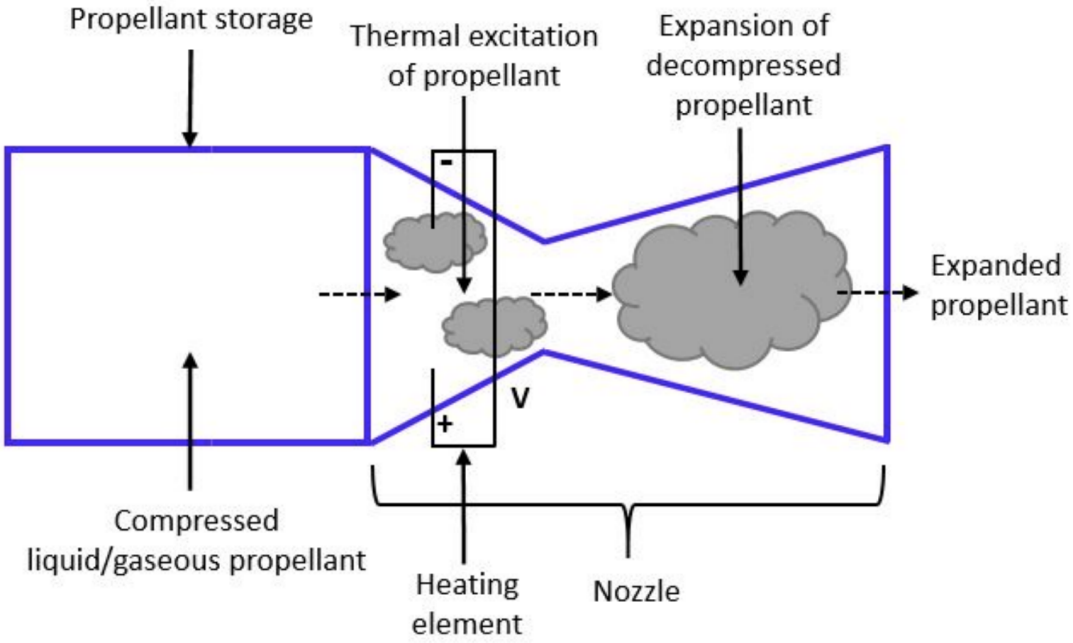

Figure 1.12. General schematic of resistojet propulsion [9].

1.4. Scope of This Study

In this study, the development of the BUSTLab Liquid Rocket Engine and specifically its injector is presented. BUSTLab Liquid Rocket Engine is a bipropellant engine. Common injector types used in bipropellant rocket engines, i.e., showerhead, impinging, coaxial, pintle, are presented in Chapter 2. An impinging injector is designed, manufactured and tested as part of this thesis. As an alternative, a pintle injector is designed and presented. As a second alternative a coaxial injector is also designed and presented.

The initial design of this engine was done for gaseous oxygen as oxidizer (GOX), kerosene ($RP-1$) as fuel, and oxidizer to fuel mass flow rate ratio (OF ratio) of 2.25, total mass flow rate of $3.45kg/s$, $50bar$ chamber pressure, $10kN$ thrust with $294s$ of Isp. The manufacturing of the engine parts were done in accordance with this design. Following the initial tests with the injector, there occurred a need to adjust the working configuration of the engine due to the issues rising from supplying the required mass flow rates of the oxidizer and acquiring the fuel. As a result, the engine and the injector is tested with liquid oxygen as the oxidizer and ethanol - water mixture as the fuel at $30bar$ chamber pressure. The design and manufacturing process details are given in Chapter 3.

In Chapter 4, water tests, cold flow tests and open hot flow tests with the injector are presented. Chapter 5 shows the results of the hot firing campaign with the BUST-Lab Liquid Rocket Engine. The results are presented and discussed with the obtained data and observed issues. Chapter 6 gives an overall summary of this thesis with the conclusions derived.

APPENDIX A gives the idealized calculations of nozzle flow characteristics using thermodynamic relations.

2. BIPROPELLANT ROCKET ENGINE INJECTORS

An injector is a device that delivers propellants into the thrust chamber in a rocket engine. While doing that, an injector breaks down the propellants into small droplets and ensures uniform and proper mixing of the fuel and the oxidizer. These are the two main goals of an injector. The first one is called atomization. By breaking down the propellants into small droplets, an injector increases the surface area to mass ratio of the propellants. Mixing of propellants is of utmost importance in rocket engines because it directly affects the combustion efficiency and stability. Poor mixing of propellants can be tolerated with a larger combustion chamber. However, this increases the mass of the engine. In order to achieve good atomization and mixing for stable and efficient combustion, injectors have passages on them to pass the flow into the combustion chamber in the form of jets or sheets. The most common injector types can be seen in Figure 2.1.

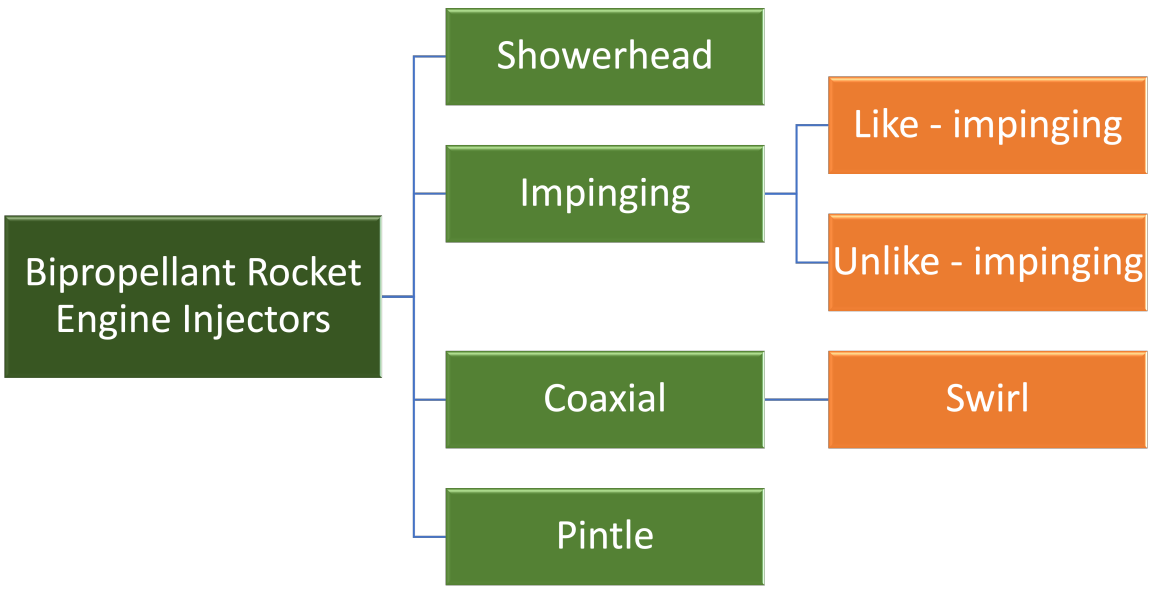

Figure 2.1. Most common injector types.

2.1. Showerhead Injectors

Showerhead injectors, also named as non - impinging, have the simplest geometry among the injector types. They deliver propellants into the combustion chamber in the form of axial jets only. Unlike other injector types, atomization and mixing of the propellants rely on turbulence and diffusion in the case of showerhead injectors. Although they have simple design, their low performance in atomization and mixing of the propellants puts them at great disadvantage compared to other injector types.

The famous German V-2 rocket used showerhead injectors at the top of their combustion chambers and swirl injectors on the sides [4]. A picture of V2 rocket engine injector can be seen in Figure 2.2.



Figure 2.2. Showerhead injector on the top (right) and swirl injectors on the sides (left) of V2 rocket [10].

Showerhead injectors are no longer used because they need large combustion chambers for good combustion of the propellants [4]. However, in some applications they are used for film cooling by near chamber wall placement and fuel injection only [41]. The schematic for the showerhead injector orifices can be seen in Figure 2.3.

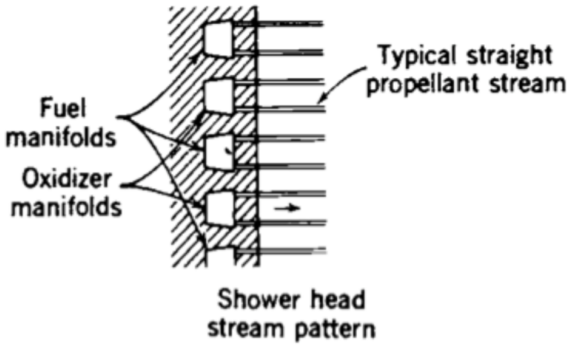

Figure 2.3. Typical showerhead injector geometry [11].

2.2. Impinging Injectors

Impinging injectors can be viewed as improved designs of showerhead injectors. Similar to showerhead injectors, impinging injectors have holes that deliver propellants into the combustion chamber in the form of jets. Unlike showerhead injectors, impinging injectors deliver the propellants into combustion chamber with an angle resulting in the collision of the propellant jets. As the jets of propellants collide in the combustion chamber, they scatter into a larger volume and break into smaller droplets. For this reason, impinging injectors have better atomization and mixing of the propellants. However, impinging injectors require higher accuracy in manufacturing. A failure in impingement of the jets would result in performance losses.

Doublet impinging injectors have one fuel and one oxidizer stream leaving the injector face with angles and impinging with each other. Doublet impinging injectors achieve atomization as the jets collide; however, the mixing occurs downstream of the impinging point.

The less complex doublet impinging type injector is the self - impinging injector which have 2 of either fuel or oxidizer jets at an angle to collide with each other. They are also named as like - impinging injectors. Propellant mixing in like - impinging elements rely on intermixing of neighbouring oxidizer and fuel fan sprays [41].

F-1, Atlas first stage booster and Titan-1 first stage are some of the famous rocket engines that used impinging jet injectors. These engines use self - impinging doublets arranged in such a way that they provide uniform mixing in the chamber core and a fuel rich combustion near the chamber walls. The fuel rich mixture near the walls is achieved by positioning the outer oxidizer doublets slightly closer to the center than the outer fuel doublets. This distribution of the doublet elements on the injector results in uniform and good mixing in the core and a transition zone, from oxidizer rich to fuel rich burn, near the walls. This configuration of the elements gives better results in terms of mixing losses compared to the film cooling introduced to the chamber with showerhead injectors near the chamber wall [41].

Triplet impinging injectors generally have a fuel jet perpendicular to the axis of combustion chamber and two jets of oxidizer at an angle. Doublet and triplet impinging injectors are also referred to as unlike - impinging injectors. The propellants are atomized an mixed with dissipative exchange of momentum near the point of impingement in unlike - impinging injectors. Therefore, the combustion begins near the impingement point resulting in high thermal loads on the injector face with unlike - impinging elements [41]. An image showing impinging injector types can be seen in Figure 2.4.

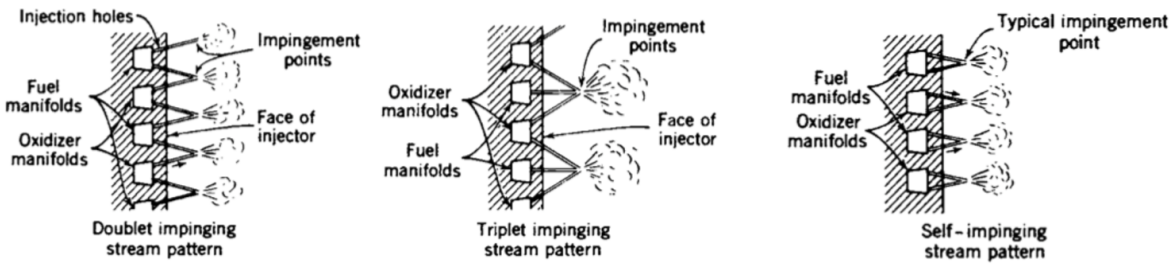

Figure 2.4. Impinging injector types [11].

Impinging injectors have fixed flow area. For this reason, throttling with impinging injectors is done through changing the upstream mass flow rate. In orifice flow, the pressure drop across the injector scales with the square of the mass flow rate. The mass

flow rate and pressure drop relation is calculated with Equation 3.14. The chamber pressure on the other hand scales linearly with the mass flow rate. This results in stiffness or hardness ratio, that is the ratio of pressure drop across the injector ΔP to the chamber pressure P_c, scaling linearly with the mass flow rate. Therefore, a 50% throttling of a fixed area injector would halve the hardness ratio. This may cause combustion stability issues due to the hardness ratio of the injector falling below 15%. Therefore, fixed area injectors require high pressure drops or hardness ratio at full thrust for safely throttling. Thus, it is possible to throttle impinging injectors but the high pressure drop at the full thrust level results in greater loads in the pressurization mechanism (propellant tanks for a pressure - fed engine or turbo - pumps). This results in increased mass for the feeding system. For this reason, rocket engines with fixed area injectors throttle down to a minimum of 35% of the rated thrust [18].

As part of French Space Agency's PERSEUS (Projet Étudiant de Recherche Spatiale Européen Universitaire et Scientifique) project, a $5kN$ ethanol - liquid oxygen engine was developed [12]. They have an impinging injector and an ablative combustion chamber for their thrust chamber. Their impinging injector has 7 triplet elements with oxidizer at the center of the triplet (F - O - F). During a 22 seconds long hot fire test, they measured $19bar$ chamber pressure, $2kg/s$ total mass flow rate, 1.5 OF ratio and $3.9kN$ thrust with 198s Isp. Figure 2.5 shows photographs from this injector's water tests in their MARTEL test bench.

A group of students in Sun Devil Rocketry group at Arizona State University designed a pressure - fed, regeneratively cooled liquid oxygen (LOX) - kerosene ($RP{-}1$) engine [13]. This design produces $405lbf$ ($1.8kN$) thrust at $250psig$ ($17bar$) chamber pressure. Their injector is a triplet impinging injector with 9 triplet elements. Relying on empirical results from the literature [4], they determined their discharge coefficients to be 0.70 for the fuel side and 0.75 for the oxidizer side. For an injector stiffness of 20%, they calculated the fuel orifice area to be $0.050in$ ($1.27mm$) and the oxidizer orifice area to be $0.058in$ ($1.47mm$). This results in a mass flow rate of $0.021slug/s$ ($0.31kg/s$) for RP - 1 and $0.033slug/s$ ($0.48kg/s$) for LOX. They also inject $RP-1$ into the



Figure 2.5. PERSEUS project injector water test [12].

combustion chamber near the chamber walls for film cooling in their design through 30 orifices with $0.033in$ ($0.84mm$) diameter that gives $0.019slug/s$ ($0.28kg/s$) mass flow rate. Their manufacturing and testing campaigns are yet to come. A rendering of their triplet impinging elements can be seen Figure 2.6.

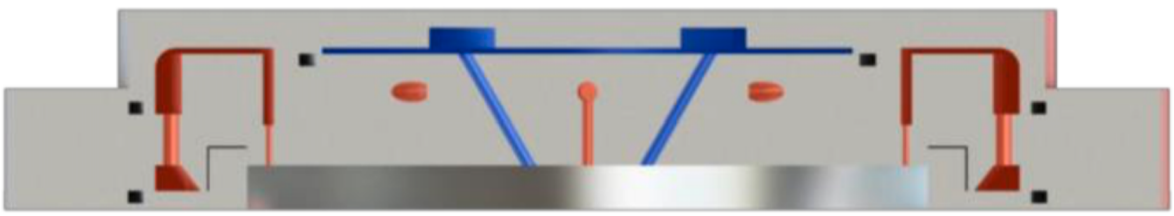

Figure 2.6. A rendering of Sun Devil Rocketry injector's cross cut. Orange is used for fuel and blue is used for oxidizer [13].

Another engine with an impinging injector is designed at the University of Texas El Paso [14]. They use liquid methane (LCH_4) as the fuel and LOX as the oxidizer for their design. Their injector has a $14psi$ ($0.96bar$) pressure drop, at low thrust configuration, that gives 20% stiffness ($70psi$ chamber pressure). Their total fuel injection

area is $0.018in^2$ $(11.6mm^2)$ and total oxidizer injection area is $0.030in^2$ $(19.4mm^2)$ giving $0.18lb/s$ $(0.08kg/s)$ and $0.48lb/s$ $(0.22kg/s)$ mass flow rates respectively. Their design also include film cooling orifices with fuel flowing through them. At $0.006in^2$ $(3.87mm^2)$ total flow area and $14psi$ pressure drop, $0.05lb/s$ $(0.023kg/s)$ fuel is injected for film cooling of the chamber walls. Figure 2.7 shows the impinging injector designed at the University of Texas El Paso.

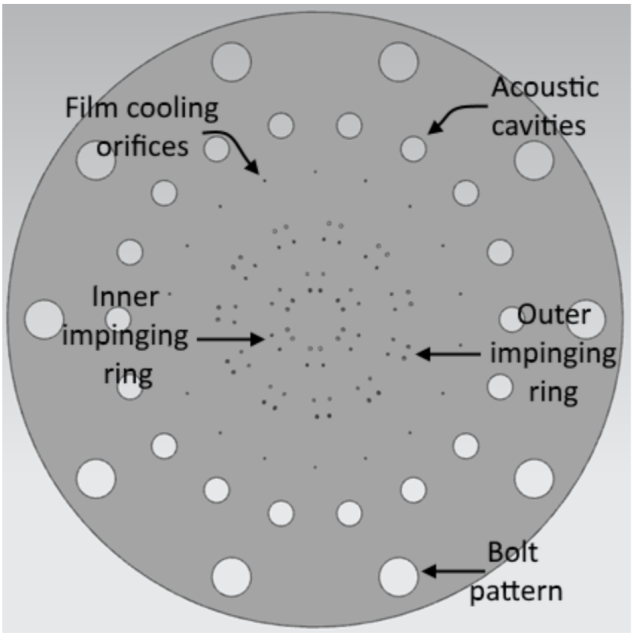

Figure 2.7. Impinging injector designed at University of Texas El Paso [14].

Impinging injectors provide a straightforward method for collision of the propellants for atomization and mixing. They are easier to manifold compared to coaxial and pintle injectors. It is seen in the literature that impinging injectors are preferred by beginner level designers because of these reasons. With a manufacturing process that can be carried out with computerized machining operations only, an impinging injector was our choice for designing a liquid rocket engine.

2.3. Coaxial Injectors

Coaxial or concentric tube injectors have one propellant flowing in a tube in the middle, and the other propellant flowing in a concentric pipe, between the pipe and the inner tube. If the propellant injection is done only in the axial direction, coaxial injectors do not provide great mixing. There is an exception to this for liquid hydrogen - liquid oxygen injectors. As the liquid hydrogen is heated from the cooling channels around the thrust chamber and gasified, it is injected into the chamber at very high velocity (typically $330 m/s$) whereas the liquid oxygen flows into the chamber at much lower velocity (typically $33 m/s$). This differential in velocities causes a shear action that breaks up the oxygen stream into small droplets [4].

Coaxial injectors usually require welding or brazing for sealing purposes. Since coaxial injectors have many elements, the welding part of the manufacturing process is of utmost significance. An improved version of the coaxial injectors is named as swirl injector.

2.3.1. Swirl Injectors

Swirl injectors have coaxial flow of propellants. The propellant flowing in the inner passage is introduced to this passage with angled holes on the wall. Thus, the propellant gains both angular and axial velocities. When leaving the passage, fluids form a conical sheet due to the centrifugal forces. The other propellant flows inside another annular passage coaxially and enter the combustion chamber axially. This flow forms a cylindrical sheet while entering the combustion chamber. A schematic of a swirl injector can be seen in Figure 2.8.

A swirl injector designed and built by Copenhagen Suborbitals [42], an amateur rocket group located in Denmark, can be seen in Figure 2.9.

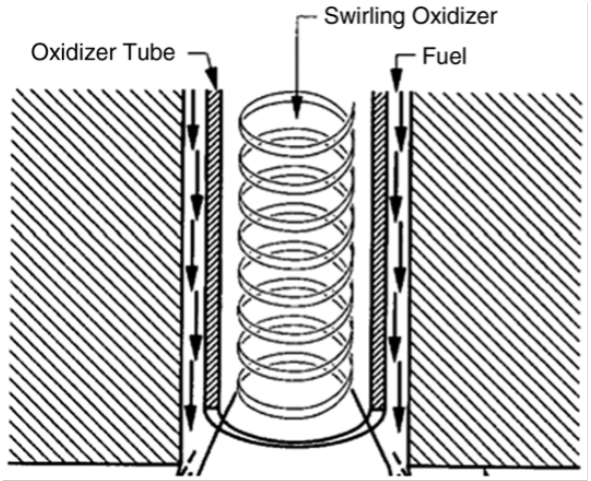

Figure 2.8. Schematic of a swirl injector [15].



Figure 2.9. Cross - sectional view of the swirl injector 3D CAD model (left) [16] and the manufactured swirl injectors (right) [17].

Compared to the jet injectors, swirl injectors' atomization characteristics are less sensitive to manufacturing flaws because they have much larger flow passages. Since the flow is conically injected into the combustion chamber, the sheet of the fluid becomes thinner as the flow further swirls and moves outwards. This results in droplet sizes up to 2.5 times smaller than that of jet injectors working under same conditions, i.e., mass flow rate and pressure drop [43]. The outward expansion of the flow also enables better

and more uniform mixing [44]. These advantages allow the use of smaller combustion chambers which results in reduced system mass [25].

Despite all of their advantages to the jet impinging injectors, we did not choose a coaxial injector for our engine because of all the welding and brazing of the parts. At our budget and level of experience in manufacturing, dealing with these details looked like something to avoid for us at the beginning of our design process.

2.4. Pintle Injectors

A pintle injector is a device that has a pintle or a rod at the center of a propellant passage. Depending on the design, a pintle injector can deliver both propellant flows into the combustion chamber in the form of jets or sheets. Pintle injectors generally do not force a swirl on either of the flows. A general conceptual drawing of a pintle injector is shown in Figure 2.10.

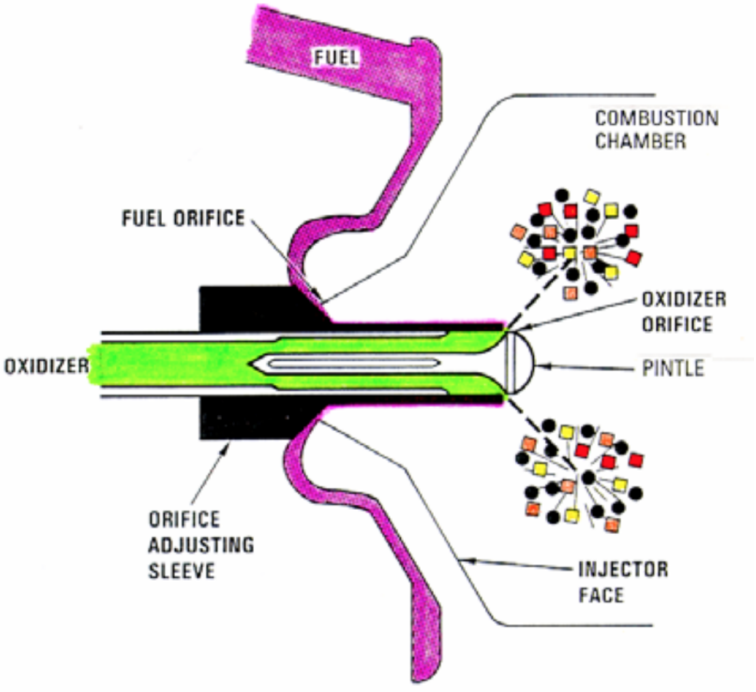

Figure 2.10. Pintle injector concept [18].

The pintle injector in Figure 2.10 has a movable sleeve that allows the change of flow area. In this conceptual drawing, the fuel is fed through the annular region in the form of sheet. The inner flowing oxidizer on the other hand can be injected radially in continuous (sheet) or discrete (jet) form depending on the design. The propellants impinge very close to the pintle head ensuring proper atomization and mixing.

A fixed flow area pintle injector can be seen in Figure 2.11. These images are from Purdue University's LOX and LCH_4 liquid propellant sounding rocket project [19]. The image on the left shows axial sheet flow only, the middle image shows radial jet flow only and the last image shows the combined flow of both propellants. These tests are carried out with water due to its abundance and safety compared to actual fuel and / or oxidizer.



Figure 2.11. Purdue liquid propellant sounding rocket pintle injector. Axial flow only (left), radial flow only (middle) and combined flow (right) [19].

Conventional rocket engine injectors generally have several orifices spread across the injector face. On the other hand, typical pintle injectors can deliver propellants from a single head located at the center of the injector face. Moreover, engines with typical injectors have flow fields directly leaving the combustion chamber axially, whereas pintle injectors create a flow field with 2 circulation zones. These flow fields can be seen in Figure 2.12.

The circulation zone on the left, or the upper toroidal zone, helps cooling the pintle head by the evaporation of the droplets within that zone while the circulation

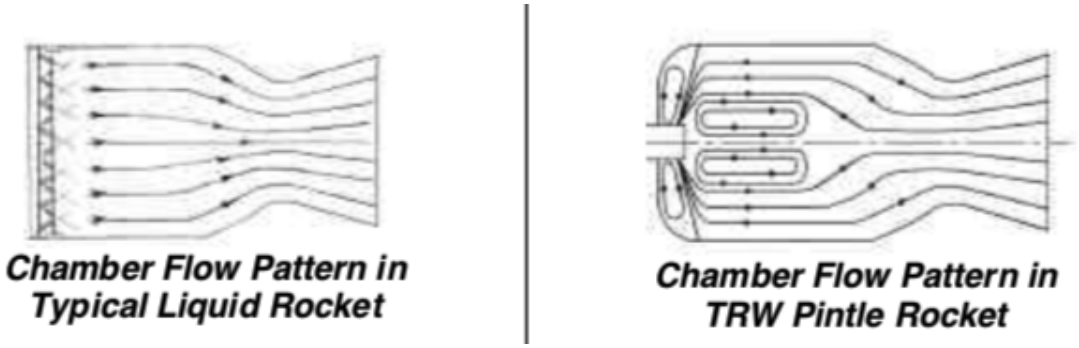

Figure 2.12. Flow fields of conventional (left) and pintle (right) engines [20].

zone at the middle, or the lower toroidal zone, regulates the combustion by circulating the unburned propellants that normally travel directly downstream in the conventional injector flow fields. This flow field created by the pintle injectors greatly improves the combustion stability even under modified operational conditions. This property of pintle injectors makes them easily scalable [20]. Hence, the pintle injectors are strong candidates for rocket engines with high throttleability because of their scalability.

In Figure 2.13, the simple structure and parts of a pintle injector, designed and built by researchers at Inotech [21], can be seen. Although these parts make a fixed area pintle injector when assembled, by simply changing the pintle tip or body, a whole new injector can be built. Moreover, a pintle injector can still provide stable combustion despite these changes.

Pintle injectors are preferable over other injector types since they create stable combustion. They are also superior in the ease of design for throttleability. The image in Figure 2.10 shows a movable sleeve. This sleeve can be adjusted during the firing of the engine to change the injector's flow area which is a known method of throttling.

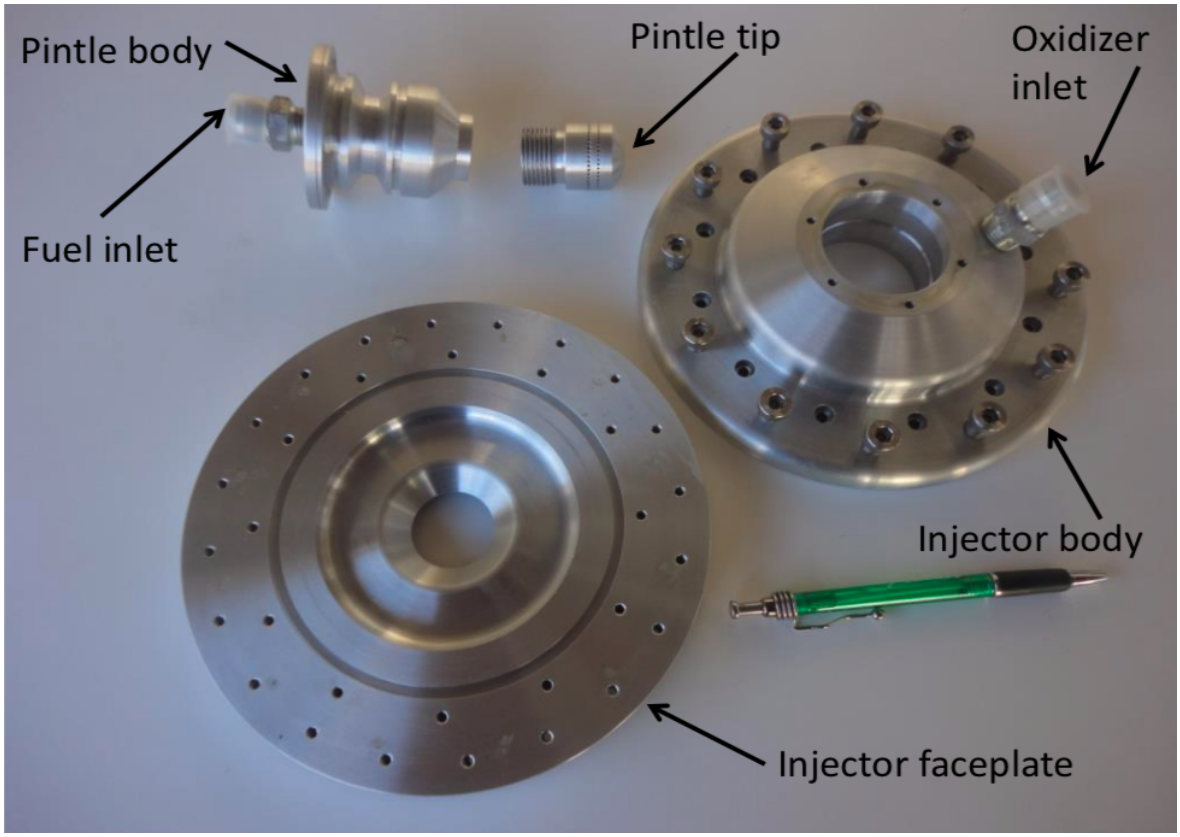

Figure 2.13. Pintle injector parts for a $5kN$ bipropellant injector [21].

3. ENGINE DESIGN & MANUFACTURING

The first design of BUSTLab liquid rocket engine was done for the following conditions: $10kN$ thrust, $50bar$ chamber pressure, kerosene as fuel and gaseous oxygen as oxidizer. We started our design with NASA's Chemical Equilibrim Applications (CEA) software. Propellant types, mixture ratio and chamber pressure were used as inputs for the CEA software. Using this software, we obtained molar mass ($\mathbb{M}$) of the combustion products, specific heat ratio (γ) of the combustion products and the stagnation temperature (T_c). Table 3.1 presents several parameters and their effects on the engine.

Table 3.1. Effects of design choices on engine.

Higher	$\Rightarrow$	Higher Isp		
Pressure	$\Rightarrow$	Increased hoop stress	$\rightarrow$	Engine mass increases
			$\rightarrow$	Feed system mass increases
	$\Rightarrow$	Increased T_c	$\rightarrow$	More cooling is needed
Fuel Rich	$\Rightarrow$	Lower $\mathbb{M}$	$\rightarrow$	Higher Isp
O/F Ratio	$\Rightarrow$	Lower T_c	$\rightarrow$	Lower Isp
Long/Narrow	$\Rightarrow$	Faster Flow	$\rightarrow$	Friction on flow increases
Chamber			$\rightarrow$	Heat transfer to walls increases
Short/Fat	$\Rightarrow$	Hoop stress increases	$\rightarrow$	Thicker walls
Chamber			$\rightarrow$	Engine mass increases

Once $\mathbb{M}$, γ and T_c were obtained, we calculated the dimensions for the targeted operation conditions. A MATLAB code was written. In the code, Equations 3.1, 3.2, 3.3, 3.4, 3.5, 3.6 and 3.7 are used to calculate the engine dimensions.

The following equation gives the throat area for the engine:

$$A^* = \frac{\dot{m}_{total}}{P_c}\sqrt{\frac{T_c R}{\gamma}}\left(1+\frac{\gamma-1}{2}\right)^{\frac{\gamma+1}{2(\gamma-1)}}, \tag{3.1}$$

where A^* is the throat area, $\dot{m}_{total}$ is the total mass flow rate, P_c is the chamber

pressure, T_c is the chamber temperature, R is the specific gas constant and γ is the ratio of specific heats.

The throat diameter, D_t, is calculated using:

$$D_t = \sqrt{\frac{4A^*}{\pi}}. \tag{3.2}$$

The following equation is used to calculate the chamber volume, V_{ch}:

$$V_{ch} = L^* A^* \tag{3.3}$$

where L^* is the characteristic length which is the length of the chamber if it was a straight tube, and it had no converging sections with the tube diameter equal to the throat diameter.

The cross sectional area of the combustion chamber, A_{ch}, is calculated using:

$$A_{ch} = A^*(8(D_t)^{-0.6} + 1.25). \tag{3.4}$$

The chamber length is represented by L_{ch} and it is calculated by using the formula:

$$L_{ch} = \frac{V_{ch}}{A_{ch}}. \tag{3.5}$$

The chamber diameter, D_c, is found using the equation:

$$D_c = \sqrt{\frac{4A_{ch}}{\pi}}. \tag{3.6}$$

The nozzle length, L_{nozzle} is calculated using the formula:

$$L_{nozzle} = 6.45D_t/2, \tag{3.7}$$

which is for the 80% bell contour nozzle.

The exit Mach number for the combustion products is found with the following

formula:

$$M_e = \sqrt{\frac{2\left(\left(\frac{P_e}{P_c}\right)^{-\frac{\gamma-1}{\gamma}} - 1\right)}{\gamma - 1}} \tag{3.8}$$

in which M_e is the exit Mach number and P_e is the exit pressure for the combustion products.

The exit area of the nozzle is calculated using Equation 3.8 in the following formula:

$$A_e = \frac{A^*}{M_e}\left[\frac{2}{\gamma+1}\left(1 + \frac{\gamma-1}{2}M_e^2\right)\right]^{\frac{\gamma+1}{2(\gamma-1)}}, \tag{3.9}$$

which is a version of Equation A.49 that is written for the throat and the exit of the nozzle.

After finding the exit area for the nozzle, the exit diameter, D_e is calculated using:

$$D_e = \sqrt{\frac{4A_e}{\pi}}. \tag{3.10}$$

Equation 1.5 is used to calculate the exit or exhaust velocity, u_e, of the combustion products. R_{univ} in this equation is the universal gas constant.

Using $\dot{m}$, u_e, A_e, P_e and P_a (ambient pressure) the thrust produced by the engine, T, is calculated using Equation 1.4. Finally, Equation 1.3 is used to find the Isp of the engine.

The MATLAB code is an iterative trial and error process for the total mass flow rate with the preset parameters until $10kN$ thrust is obtained. Once the code gives $10kN$ thrust, the iteration is stopped, and the total mass flow rate is obtained. Using

this, mass flow rates of the fuel and oxidizer are calculated using:

$$\dot{m}_f = \frac{\dot{m}_{total}}{1 + OFRatio} \tag{3.11}$$

and

$$\dot{m}_o = \dot{m}_{total} - \dot{m}_f \tag{3.12}$$

with the preset OF ratio given in:

$$OFRatio = \frac{\dot{m}_o}{\dot{m}_f}. \tag{3.13}$$

The code is written with the assumption of optimum expansion at sea level. Summary of the design process can be seen in Figure 3.1.

Using the results from the MATLAB code, the engine parts were manufactured. Material selection and manufacturing details of engine parts are presented in the following sections. The engine consists of several parts: combustion chamber, saddle, jacket, injector and dome. Overall, the system consists of engine, thrust stand and feed system. All of these parts are explained later in this chapter. The material selection for each part is done with several criteria: compatibility with the propellants and harsh chamber environment, machinability, cost and accessibility.

Our first design was done for a kerosene and gaseous oxygen engine. As we proceeded in our studies, we realized that kerosene was difficult to acquire. Consequently, we made the decision to change our fuel to ethanol - water mixture. In addition, after our tests with the injector, we also realized that providing the necessary oxidizer mass flow rate would require very high pressures in the oxidizer tank. Therefore, we changed our oxidizer to liquid oxygen which we first did not prefer because we did not want to deal with cryogenics. However, by the time we made these changes, the engine parts were already manufactured. We altered our MATLAB code and ran it with new numbers from CEA software for our new propellants for the manufactured engine. We also decided on a $30bar$ chamber pressure and $5kN$ thrust since the original

design creates several difficulties (budget, safety, etc.) for the rest of the system and the overall project. The results for %75 ethanol - %25 water and liquid oxygen are presented in Table 3.2.

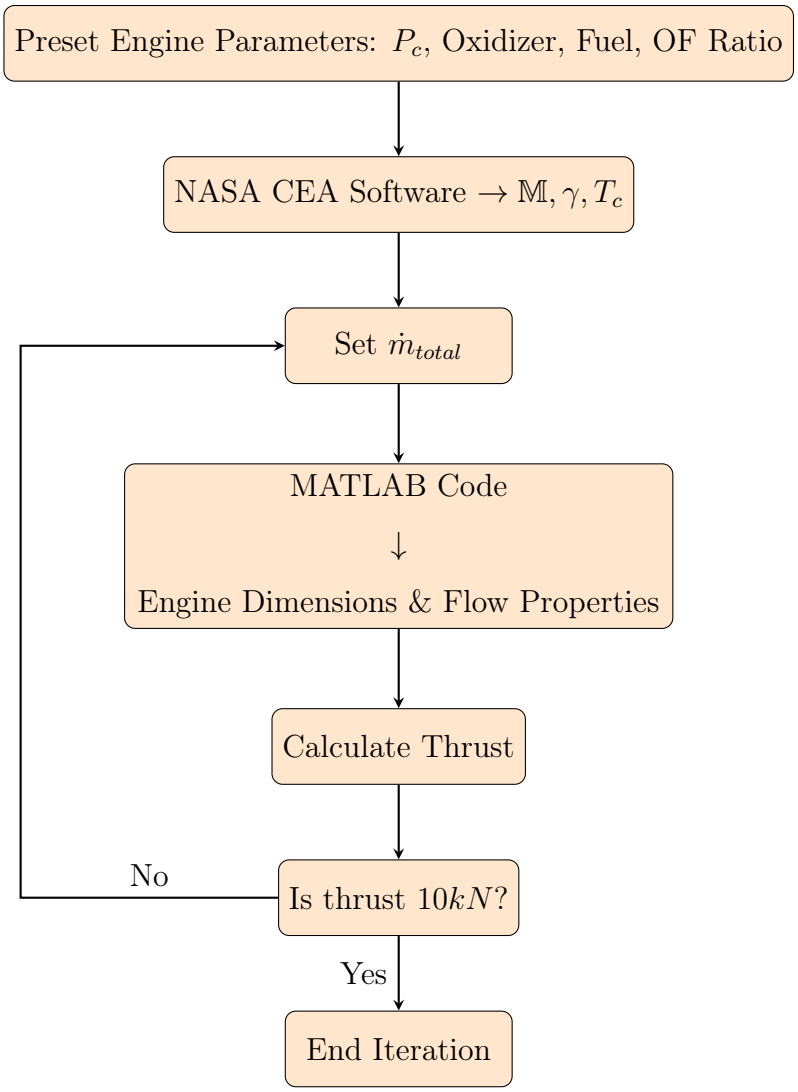

Figure 3.1. Summary of engine design process.

Ethanol is an environment friendly fuel. Its combustion products are only carbon dioxide and water. For this reason, ethanol is sometimes used as fuel for public transportation vehicles. Ethanol was used as rocket fuel in early stages of liquid fueled rockets. German V - 2 and American Redstone ballistic missiles are famous examples

Table 3.2. Design results for the new configuration.

Fuel mass flow rate, $\dot{m}_f$	$1.01kg/s$
Oxidizer mass flow rate, $\dot{m}_o$	$1.26kg/s$
Total mass flow rate, $\dot{m}_{total}$	$2.27kg/s$
OF Ratio	1.25
Chamber Pressure, P_c	$30bar$
Thrust, T	$5.65kN$
Specific impulse, Isp	$254s$

of ethanol fueled rockets. An ethanol fueled rocket engine RS-88 was designed and built by Rocketdyne for the NASA Bantam System Technology Program in 1997. In 2003, NASA tested the engine with 14 hot - fire tests totaling 55 seconds and measured the maximum thrust at sea level as $222kN$. The engine was employed by Boeing for the CST - 100 spacecraft as part of the launch abort - escape system [22]. RS - 88 engine during hot fire test can be seen in Figure 3.2.



Figure 3.2. RS - 88 engine test [22].

JAXA developed a 10 kN ethanol rocket engine with 280 Isp at sea level for a future reusable spaceplane project in 2009. The engine was designed to work at low combustion pressure for longer lifetime and it was tested at 10 bar in 2010 [45].

At New Mexico Institute of Mining and Technology, an ethanol - liquid nitrous oxide engine was developed. For an OF ratio of 4.71, at a chamber pressure of $63bar$ and total mass flow rate of $0.23kg/s$ they measured $592N$ thrust and $262s$ Isp [46].

As part of French Space Agency's PERSEUS (Projet Étudiant de Recherche Spatiale Européen Universitaire et Scientifique) project, a $5kN$ ethanol - LOX engine was developed. They had an impinging injector and an ablative combustion chamber. During a 22 seconds long hot fire test, they measured $19bar$ chamber pressure, $2kg/s$ total mass flow rate, 1.5 OF ratio and $3.9kN$ thrust with 198s Isp [12].

3.1. Thrust Chamber

BUSTLab bipropellant rocket engine thrust chamber was manufactured from a copper billet. Copper was the choice of material for our thrust chamber because it has high thermal conductivity (suitable for cooling purposes), high melting point and reasonable machinability. For these advantages, we decided to use copper for our thrust chamber despite it being a relatively expensive metal.

The copper billet was lathed to combustion chamber's and nozzle's geometry with a CNC (computer numerical control) lathe. After the turning process was completed, the workpiece was mounted on an indexing head (division head) inside a CNC milling machine and the cooling channels were machined. The combustion chamber geometry was created using the dimensions obtained from the MATLAB code. The nozzle geometry was created with %80 *Bell Contour* properties. Thrust chamber 3D model can be seen in Figure 3.3. Manufacturing steps and manufactured thrust chamber can be seen in Figure 3.4.

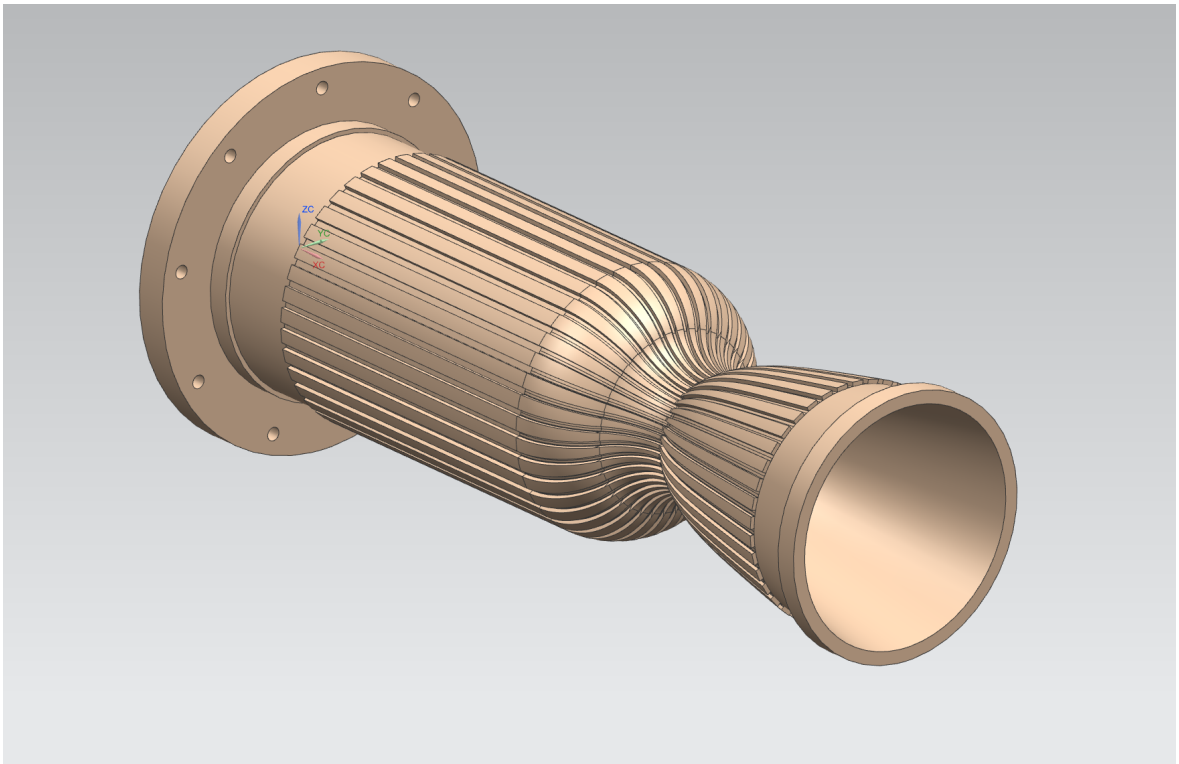

Figure 3.3. 3D model of the thrust chamber.

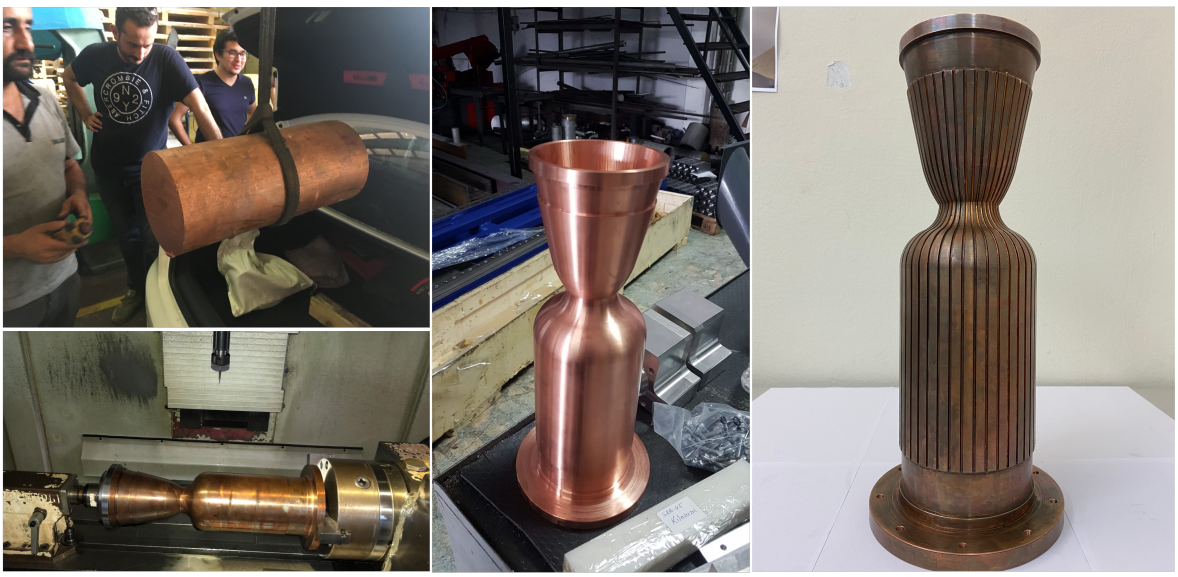

Figure 3.4. Manufacturing process of the thrust chamber.

3.2. Jacket

A jacket is manufactured from aluminium. The jacket surrounds the thrust chamber and encloses the water cooling channels. Jacket design had two 1/2" NPT (national pipe thread) water inlets near the thrust chamber exit and two 1/2" NPT water outlets near the combustion chamber uppermost side. The combustion chamber is first assembled with the saddle and then inserted into the jacket. An aluminium flange is screwed to the jacket prior to the combustion chamber. The combustion chamber is assembled with the jacket by screwing it to this flange with cap screws. Finally, the thrust chamber assembly is completed with a stainless steel cover at the chamber exit. This cover ensures cooling water is leak - proof and the chamber is fixed.

3.2.1. Saddle

In order to create proper flow passages for the cooling channels around the thrust chamber, a saddle was manufactured. Saddle hugs the thrust chamber around the throat and prevents a water manifold around it. Saddle was manufactured out of an aluminium billet.



Figure 3.5. Manufactured saddle.

First, it was shaped in a CNC lathe to the design geometry and then it was cut in half with wire EDM (electrical discharge machining). Aluminium was selected as material here because it is cheaper and lighter than stainless steel. Manufactured saddle can be seen in Figure 3.2.1.

3.3. Injector

BUSTLab liquid rocket engine has an impinging injector. The injector is a triple impinging type with one fuel jet in the axial direction and two oxidizer jet at an angle with this axis. All of our injectors were manufactured out of brass billets. Brass was selected for injector material because it has high melting point and good machinability. Stainless steel was not used for injector manufacturing because we had tiny and angled orifices in our design and drilling those holes would be challenging.

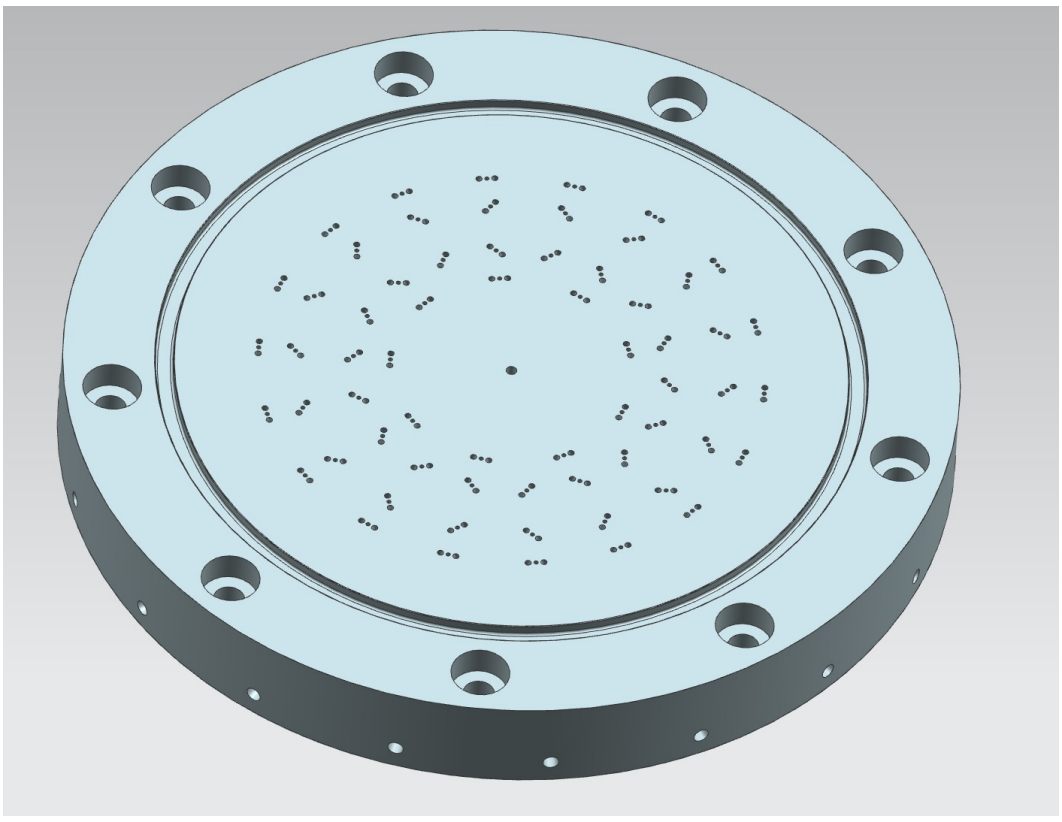

Figure 3.6. 3D model of the first injector design.

Aluminium was not chosen because it has much lower melting point compared to other materials mentioned. Manufacturing started with turning of brass billet into the injector diameter and thickness. Injector holes were drilled with a 5 - axis CNC mill. 3D model of the first design is presented in Figure 3.6. Manufacturing process of the injector can be seen in Figure 3.7.

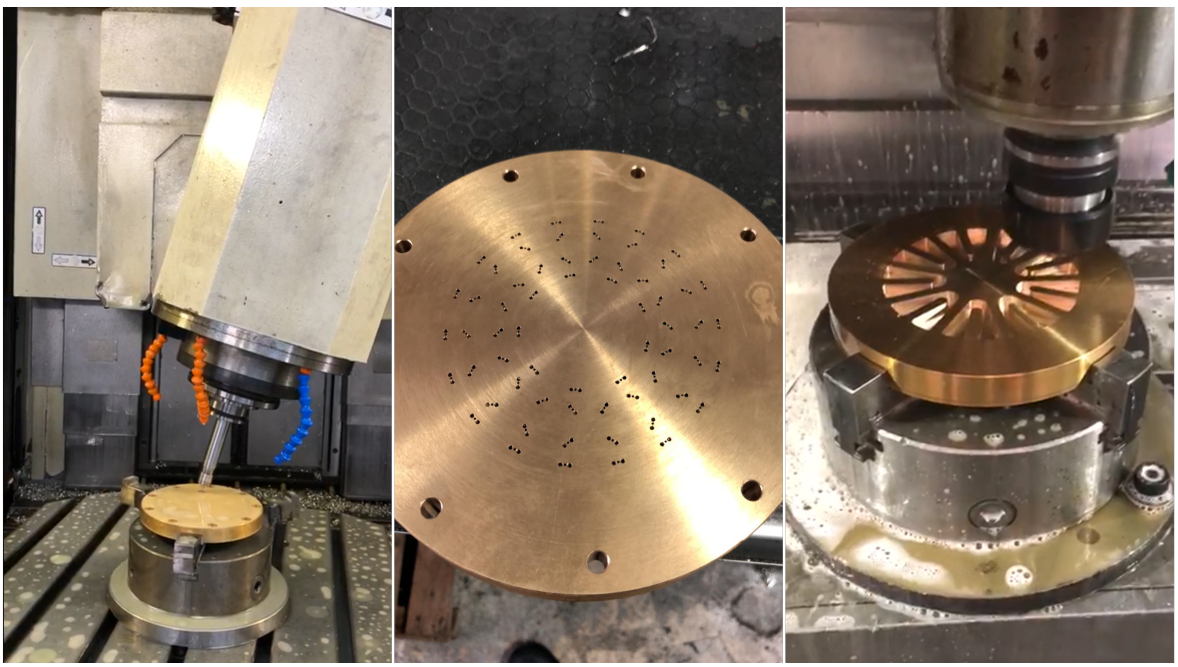

Figure 3.7. Manufacturing process of the injector.

The first design of the injector was done for a kerosene ($RP-1$) - gaseous oxygen engine (GOX). This injector has 126 oxidizer orifices and 63 fuel orifices. Oxidizer orifices are angled at 15 degrees, and they are $1.2mm$ in diameter. Fuel orifices are perpendicular the injector face, and they are $0.8mm$ in diameter. The technical drawing for each triplet in our first design can be seen in Figure 3.8.

The mass flow rate for jet injector orifices for liquid propellants is calculated with the following equation:

$$\dot{m}_{orifice} = C_d A_o \sqrt{2\rho\Delta P}. \tag{3.14}$$

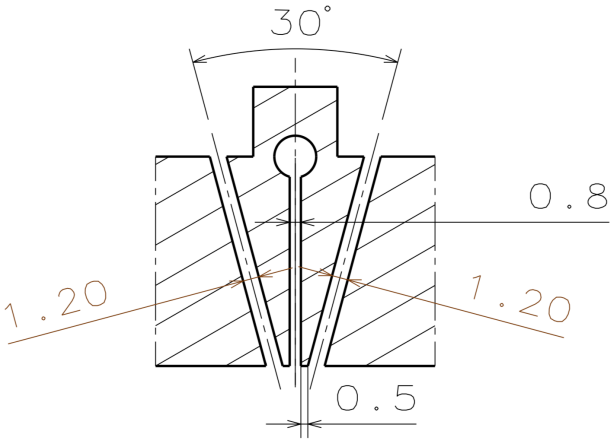

Figure 3.8. Technical drawing of the triplet used in the first version of BUSTLab liquid rocket injector (units are in mm).

The injection velocity of the propellant jets, U, is calculated using:

$$U = C_d\sqrt{\frac{2}{\rho}\Delta P}. \tag{3.15}$$

In Equation 3.14, $\dot{m}_{orifice}$ is the mass flow rate, A_o is the flow cross - sectional area of the orifice, ρ is the density of the fluid and ΔP is the pressure difference between the upstream and downstream of the orifice. According to the experimental and theoretical studies, the ratio of pressure drop, ΔP, to the combustion chamber pressure, P_c, sometimes referred to as stiffness or hardness ratio, should be around 15 - 20% to ensure combustion stability [18, 41, 47]. This limitation is one of the most difficult conditions when throttling a rocket engine. Thus, impinging injectors are not favorable for throttleable rocket engines because of their fixed flow area. The final term in this equation, that is C_d, is a dimensionless coefficient called the discharge coefficient. C_d mainly depends on the orifice geometry and is calculated empirically [48]. In Figure 3.9, types and values for the discharge coefficients of orifices calculated based on experiments can be seen.

Orifice Type	Diagram	Diameter (mm)	Discharge Coefficient
Sharp-edged orifice	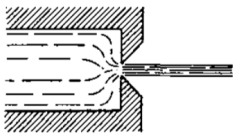	Above 2.5 Below 2.5	0.61 0.65 approx.
Short-tube with rounded entrance $L/D > 3.0$	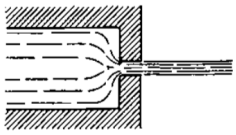	1.00 1.57 1.00 (with $L/D \sim 1.0$)	0.88 0.90 0.70
Short tube with conical entrance	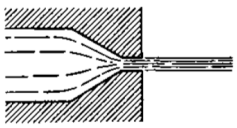	0.50 1.00 1.57 2.54 3.18	0.7 0.82 0.76 0.84–0.80 0.84–0.78
Short tube with spiral effect	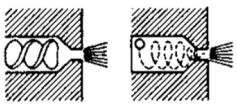	1.0–6.4	0.2–0.55
Sharp-edged cone	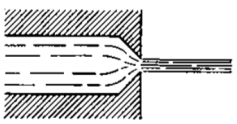	1.00 1.57	0.70–0.69 0.72

Figure 3.9. Discharge coefficients for various orifice geometries based on empirical data [4].

We were not able to use the first manufactured part of this version because of a referencing error. Injector holes were not aligned with the fuel feed lines; thus, this one was never used. Therefore, the first design was manufactured once again and this one is used in the tests. The misalingment can be seen in Figure 3.10.

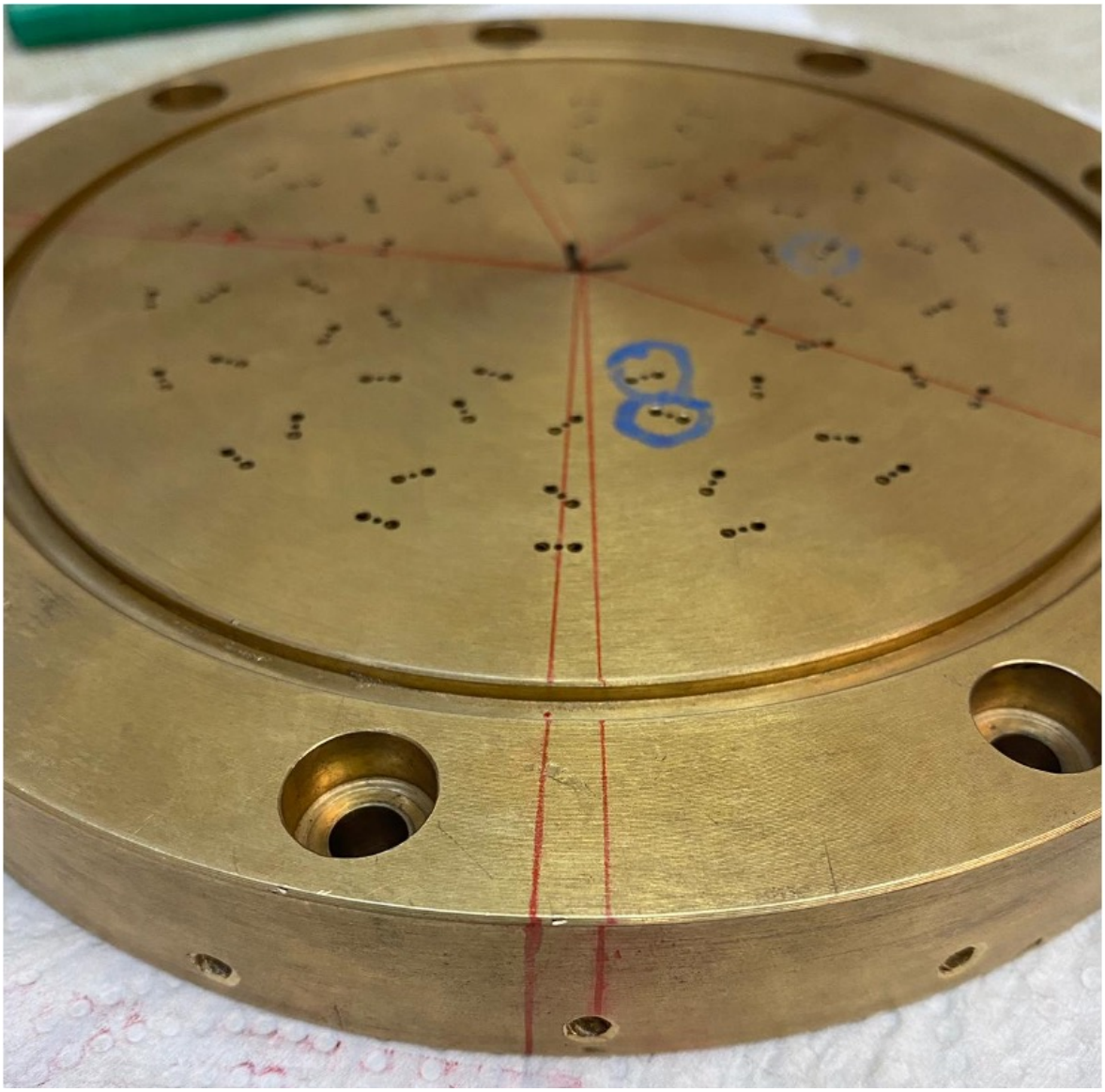

Figure 3.10. Manufacturing misalignment in the first manufactured injector.

First version of the injector was tested with water and compressed air. We had not been able to get the required mass flow rates for oxidizer with this injector and propellant selection. The injector would actually be able provide those mass flow rates for gaseous oxygen; however, it would put immense pressure loads on the oxidizer tank, i.e., the tank would not hold. Therefore, we made the choice to change our oxidizer to liquid oxygen. Tests with the first injector are presented in Chapter 4.

After changing the propellants, the injector was tested again with water in both fuel and oxidizer lines. Changing the oxidizer to a liquid resulted in inadequate pressure drop across the oxidizer orifices. This is because the oxidizer orifices were originally sized for a gaseous propellant. They were able to provide the required mass flow rate with liquid oxygen but the pressure drop was too small for a safe operation of the combustion chamber due to rising combustion instability issues.

In order to solve this problem, we made changes in our injector design. In the second version of the injector, 72 oxidizer orifices with $1mm$ diameter and 36 fuel orifices with $1.3mm$ diameter were used. The technical drawing for each impinging triplet can be seen in Figure 3.11. 3D model for the second version of the injector can be seen in Figure 3.12 and 3.13. A cut view of this injector can be seen in Figure 3.14. Manufactured new injector can be seen in Figure 3.15.

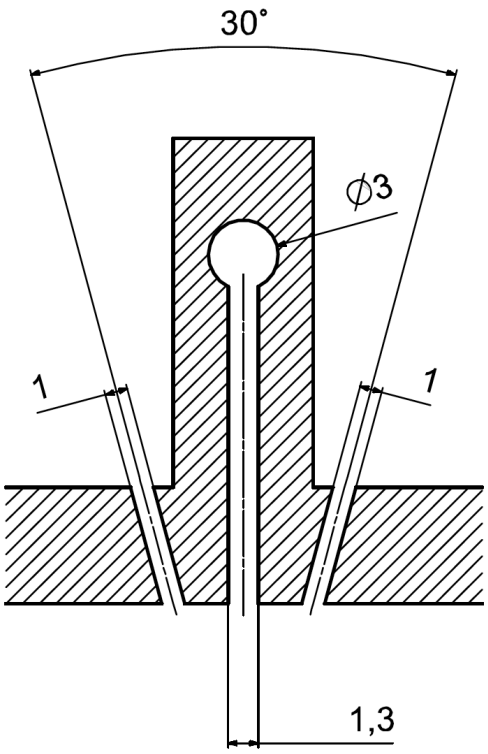

Figure 3.11. Technical drawing of the triplet used in the second version of BUSTLab liquid rocket injector (units are in mm).

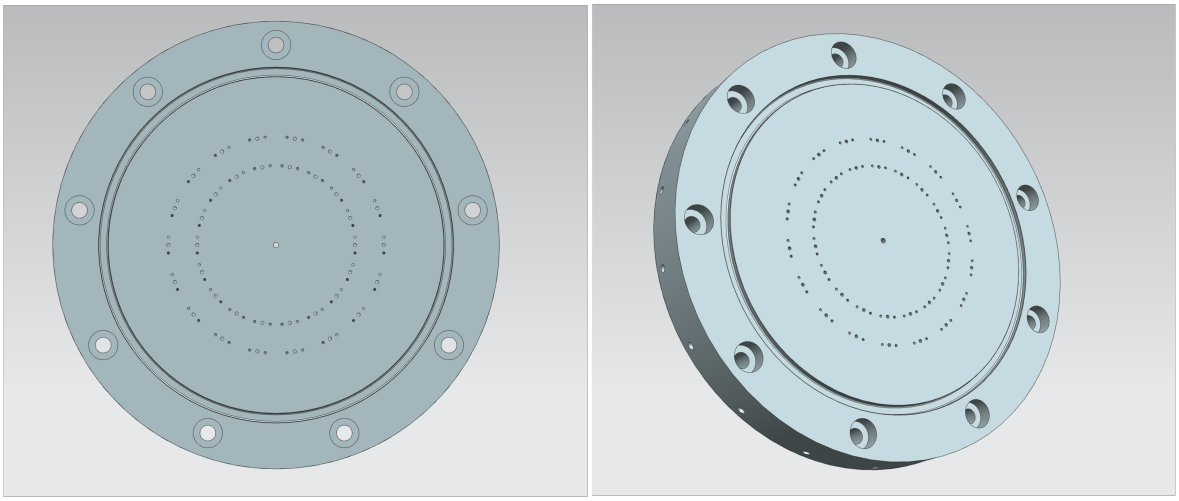

Figure 3.12. Front of the second injector design.

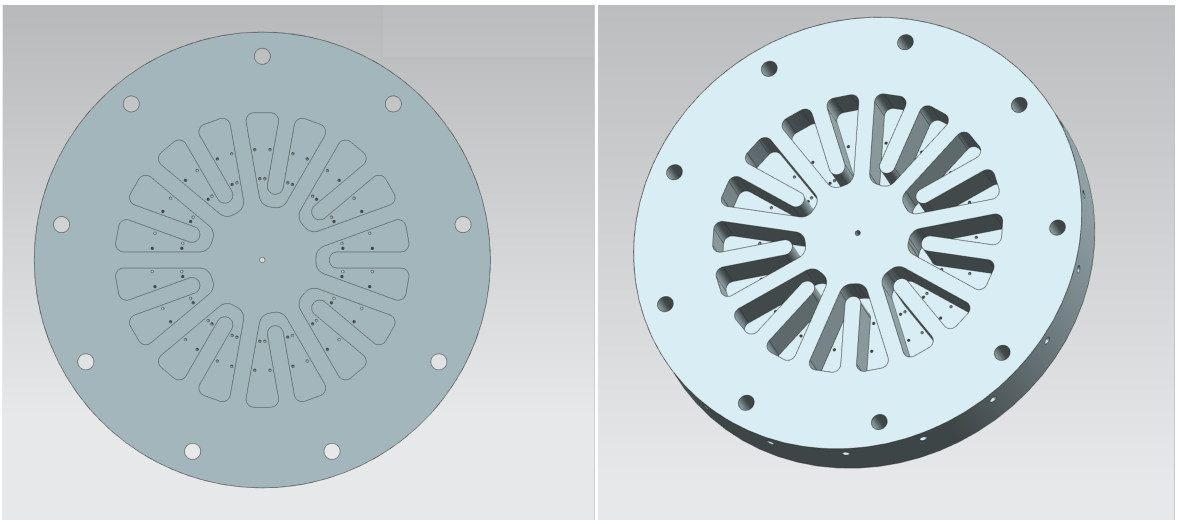

Figure 3.13. Back of the second injector design.

In order to have a stable combustion, we needed to reduce the oxidizer flow area for the purpose of increasing the pressure difference across injector. We first reduced the oxidizer orifice diameter. However, they needed to be very small to meet the pressure drop requirement. At this point, reducing the diameter alone was not a feasible option because drilling the holes would be very challenging and the overall manufacturing would be costly.

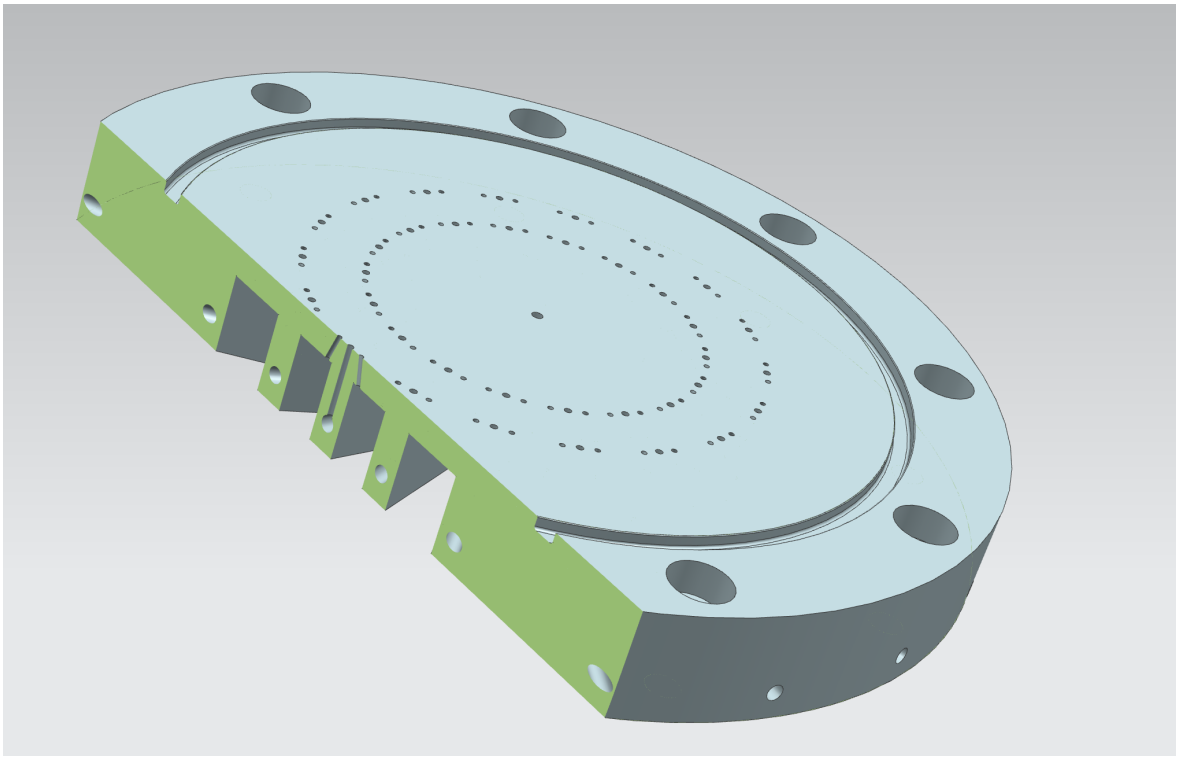

Figure 3.14. Cut view of the injector. Triple impingment of fuel and oxidizer orifices is visible.



Figure 3.15. Manufactured new injector.

As an alternative, we reduced both the number and the diameter of the oxidizer orifices. Another problem with this injector was that the total fuel flow area was too

small for our operation. The injector could supply the required mass flow rate with ethanol - water mixture; however, this would result in high pressure drop across the injector. Adding the combustion pressure to the pressure drop, this gives a rather high pressure in the fuel dome. We wanted to have lower pressure in the dome and therefore we also needed to increase the fuel injection area for the purpose of reducing the pressure drop across the injector. This way, the upstream pressure in the dome would also be lowered. This pressure drop reduction is done keeping the injector hardness ratio in mind. As the number of oxidizer orifices was decreased, many fuel orifices were left alone, without an impingement. For the purpose of having a decent mixing and atomization of the propellants, the decision was made to also decrease the number of fuel orifices. This way, all of the injection into the combustion chamber is done through triple impingement of propellants. We then increased the fuel orifice diameter to once again have enough mass flow rate and to reduce the pressure drop to a feasible level. The distribution and alignment of the triple impingement groups were simplified in this version. This was done to reduce manufacturing difficulty and cost of the injector. In this version, oxidizer holes were drilled in a 3 - axis CNC mill with the help of a division head. The number and diameter of injector orifices for both of the designs are presented in Table 3.3.

Table 3.3. Injector orifices of the two designs.

	# of Oxidizer Orifices	**Oxidizer Orifice ∅ (mm)**	**# of Fuel Orifices**	**Fuel Orifice ∅ (mm)**
First Design	126	1.2	63	0.8
Second Design	72	1	36	1.3

3.3.1. Alternative Injector Design 1: A Coaxial Swirl Injector

The following calculations are done based on the design process given in reference [23] for the swirling inner flow. The discharge coefficient for the annular flow, Cd_{an}, is chosen approximately using reference [21] . Annular flow enters the combustion in the form of a cylindrical sheet whereas inner flow enters the chamber in the from of a conical sheet. Figure 2.8 shows the general schematic of an oxidizer centered swirling coaxial injector. The designed coaxial swirl injector is the fuel centered version of this schematic. This design is done for 5 coaxial elements with 2 tangential inlets on the injector face.

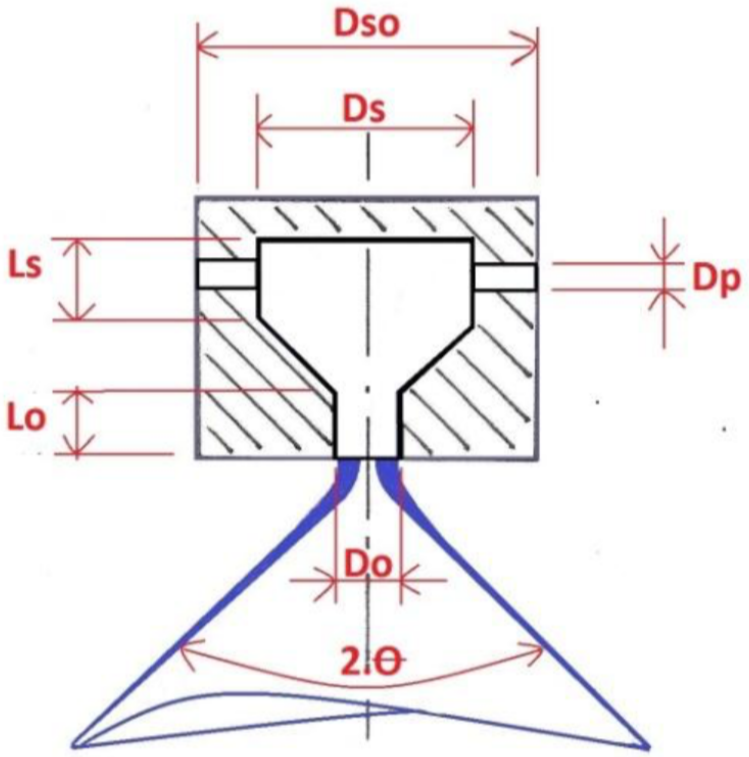

Figure 3.16. Main geometry of the inner swirl flow [23].

Figure 3.16 shows the cross cut of the fuel swirling injector. In this figure, Dso is the swirl chamber external diameter, Ds is the internal diameter, Ls is the length of the swirl chamber, Dp is the diameter of the inlet orifice, Lo is the length of the exit,

Do is the diameter of the exit and 2θ is the spray cone angle whereas θ is the half cone angle.

The design procedure begins by setting the spray cone angle for the swirler. Reference [49] suggests a cone angle of 90° for minimizing the combustion chamber length. The cone angle is selected as 90°. The cone angle is related to the open area ratio, X, as given in Equation 3.16:

$$\sin\theta = \frac{X\sqrt{8}}{(1+\sqrt{X})\sqrt{(1+X)}}. \tag{3.16}$$

The open area ratio defines the relation between the flow area and the air core are in the swirl. Open area ratio can take values from 0 to 1. Open area ratio is zero when the air core area is zero (no air core) and one when the flow area is zero (no liquid flow).

Solving Equation 3.16 for X gives:

$$X = 0.0042\theta^{1.2714}. \tag{3.17}$$

Solving Equation 3.17 with $\theta = 45$ gives $X = 0.53$. Equation 3.18 gives the formula for the discharge coefficient of the outlet orifice, Cd_{out}:

$$Cd_{out} = \sqrt{\frac{(1-X)^3}{1+X}}. \tag{3.18}$$

With the obtained value for X, Cd_{out} is calculated as 0.74. Using Equation 3.14 with $6bar\ \Delta P$ assumption and $1.01kg/s$ mass flow rate of fuel, the total fuel injection area is calculated as $42.7mm^2$. For 5 coaxial elements, this gives an area per element of $8.53mm^2$ and the exit orifice diameter, Do, is calculated as $3.30mm$.

Reference [23] gives the following relations:

$$Ds = 3.3Do = 9.90mm, \tag{3.19}$$

$$Ls = 3.3Do = 9.90mm \tag{3.20}$$

$$Lo = 0.5Do = 1.65mm \tag{3.21}$$

for the swirler injector.

With $Ds = 9.90mm$, the swirl chamber external diameter, Dso, is set to be $14mm$ by intuition. The calculations for the swirl chamber geometry except the inlet orifices and exit orifice are now complete. The inlet discharge coefficient, Cd_{in}, is calculated with the formula given in Equation 3.22:

$$Cd_{in} = \sqrt{\frac{(X)^3}{2 - X}}. \tag{3.22}$$

With the known X value of 0.53, Cd_{in} is calculated as 0.32. For 5 coaxial elements with 2 tangential inlets for each of them, the inlet orifice area is calculated as $9.96mm^2$ from Equation 3.14. This gives an inlet diameter of $3.56mm$ for each 10 elements.

Table 3.4. Results of the fuel centered coaxial swirl injector design.

# of elements	5
# of tangential inlets for each element	2
Swirl chamber external diameter, Dso (mm)	14
Swirl chamber internal diameter,, Ds (mm)	9.90
Swirl chamber length, Ls (mm)	9.90
Inlet diameter, Dp (mm)	3.56
Length of the exit, Lo (mm)	1.65
Diameter of the outlet, Do (mm)	3.30
Cone angle, 2` (degrees)	90
Open area ratio, X	0.53
Swirl inlet discharge coefficient, Cd_{in}	0.32
Swirl outlet discharge coefficient, Cd_{out}	0.74
Annular discharge coefficient, Cd_{an}	0.8
Annular region thickness, t (mm)	0.19

Similar to Subsection 3.3.2, the discharge coefficient for the annular oxidizer passage is taken approximately to be 0.80 from reference [21]. For 5 coaxial injector elements, Equation 3.14 gives a flow area of $8.51mm^2$. With the $14mm$ swirl chamber external diameter, this gives an annular region thickness, t, of $0.19mm$ for each element. The design results for the coaxial swirl injector are presented in Table 3.4.

3.3.2. Alternative Injector Design 2: A Pintle Injector

In this section, an alternative pintle injector design for the BUSTLab Liquid Rocket is presented. The rest of the thrust chamber is taken to be the same as the manufactured design. The designed pintle injector has radial discrete flow of fuel through the inner tube and axial sheet flow of oxidizer through the annular region. This configuration, fuel centered, can be seen in Figure 3.17.

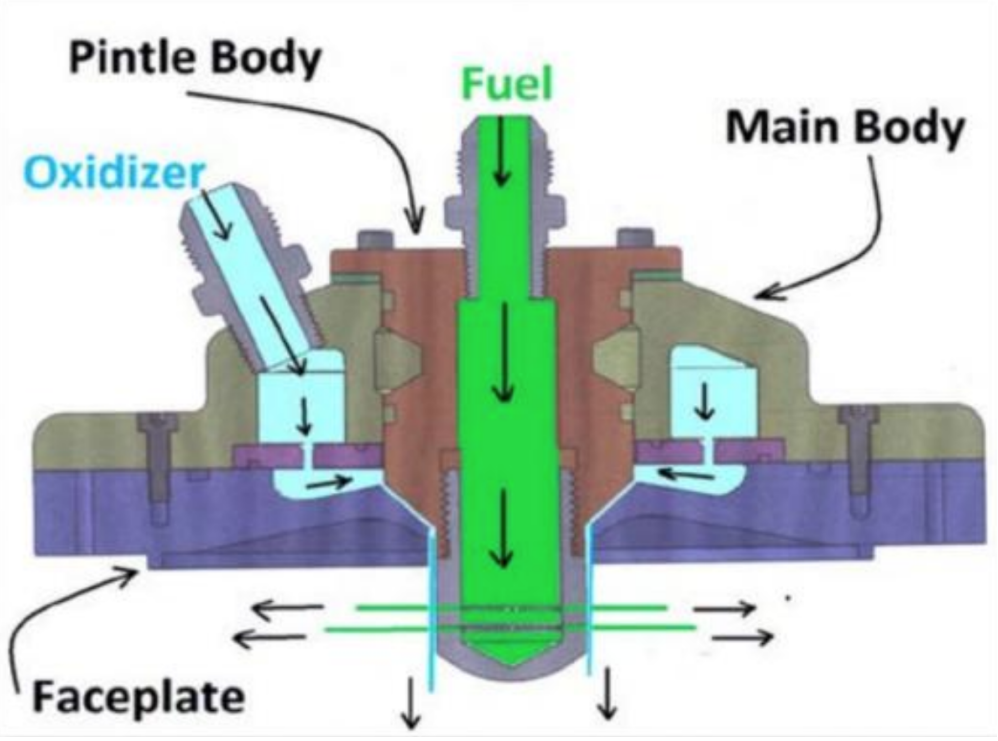

Figure 3.17. Schematic of the designed pintle injector [24].

Sizing of the pintle injector begins with the pintle diameter. Pintle diameter, D_p, is related to the chamber diameter, D_c, with the relation $1/3D_c > D_p > 1/5D_c$ [21,50]. Figure 3.18 shows the geometric parameters of a pintle element. Skip distance, L_s, is the distance at which annular axial flow collides with the radial discrete flow. The ratio of skip distance to pintle diameter is named as the skip ratio, L_s/D_p, and it is typically equal to 1 [51], giving $L_s = D_p$. Larger skip ratios result in the deceleration of the flow due to the friction against the pintle post and smaller skip ratios may cause spray impingement on the head end of the combustion chamber [25].

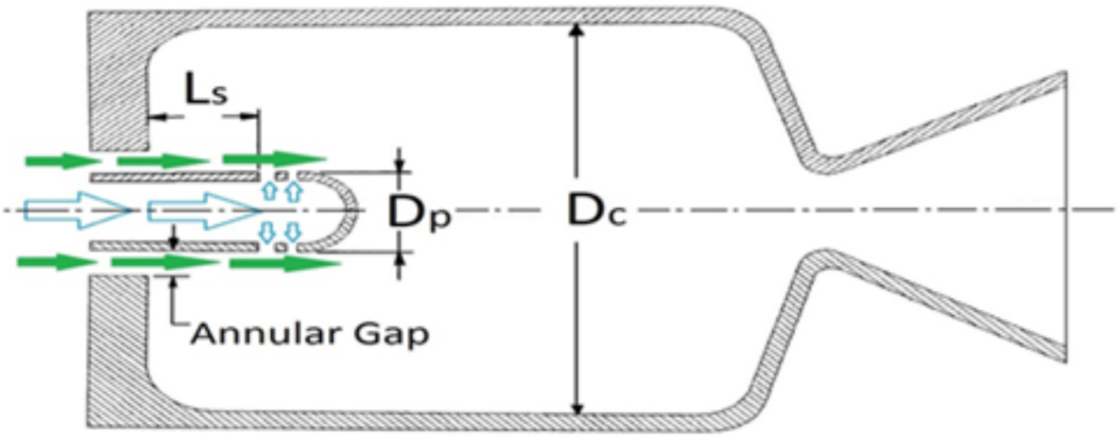

Figure 3.18. Pintle parameters [25].

Another design parameter named the total momentum ratio, TMR, is the ratio of central flow total momentum to outer flow total momentum. TMR is calculated as:

$$TMR = \frac{(\dot{m}U)_{radial}}{(\dot{m}U)_{axial}}, \tag{3.23}$$

which provides optimum performance for values near 1 [25]. The mass flow rates in this equation are preset parameters for our purposes. The injection velocities, U, are calculated from Equation 3.15. When using a fuel centered design, TMR can be set to be $TMR > 1$ so that the fuel jets penetrate the oxidizer sheet and reach the chamber walls to enable film cooling [25].

Our design has an oxidizer mass flow rate of $1.26kg/s$ and a fuel mass flow rate of $1.01kg/s$. Using Equation 3.14, the total flow areas for the oxidizer and the fuel side are calculated. From Figure 3.9 and reference [48], the C_d value for the radial flow is chosen approximately. From reference [21], the discharge coefficient for the annular flow, Cd_{an}, is chosen approximately. Pintle injector design results are presented in Table 3.5 and Table 3.6.

Table 3.5. Pintle design outline.

Pintle diameter, D_p (mm)	26.75
Skip distance, L_s (mm)	26.75
Skip ratio	1
Annular region outer diameter, (mm)	27.75
Total momentum ratio, TMR	1.01

Table 3.6. Pintle design flow parameters & sizing.

	FUEL	**OXIDIZER**
Mass flow rate, $\dot{m}$ (kg/s)	1.01	1.26
Discharge coefficient, C_d	0.75	0.80
Pressure Drop, ΔP (bar)	7	6
Total Area (mm^2)	39.46	42.56
# of orifices	24	1
Orifice ∅(mm)	1.45	-
Annular region thickness (mm)	-	0.50

3.4. Dome

The dome was manufactured out of stainless steel. Oxidizer is fed to the dome axially from the 3/4" NPT inlet at the back. A 1/4" NPT hole in the center was drilled for chamber pressure measurements and the other 1/4" NPT hole was used for pressure measurement in the oxidizer dome. Fuel is fed to the dome through 4

circumferential 1/2" NPT holes. 3D CAD model of the dome can be seen in Figure 3.19. Manufactured dome can be seen in Figure 3.20. In this figure, the manifold at the center is the oxidizer dome and the annular manifold is the fuel dome. All parts of the thrust chamber and its assembly can be seen in Figure 3.21.

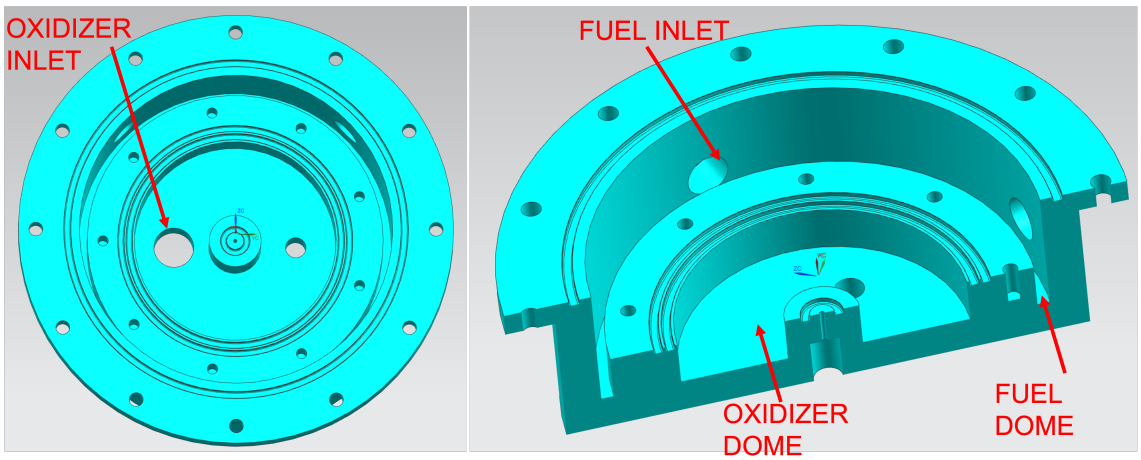

Figure 3.19. 3D model of the dome.

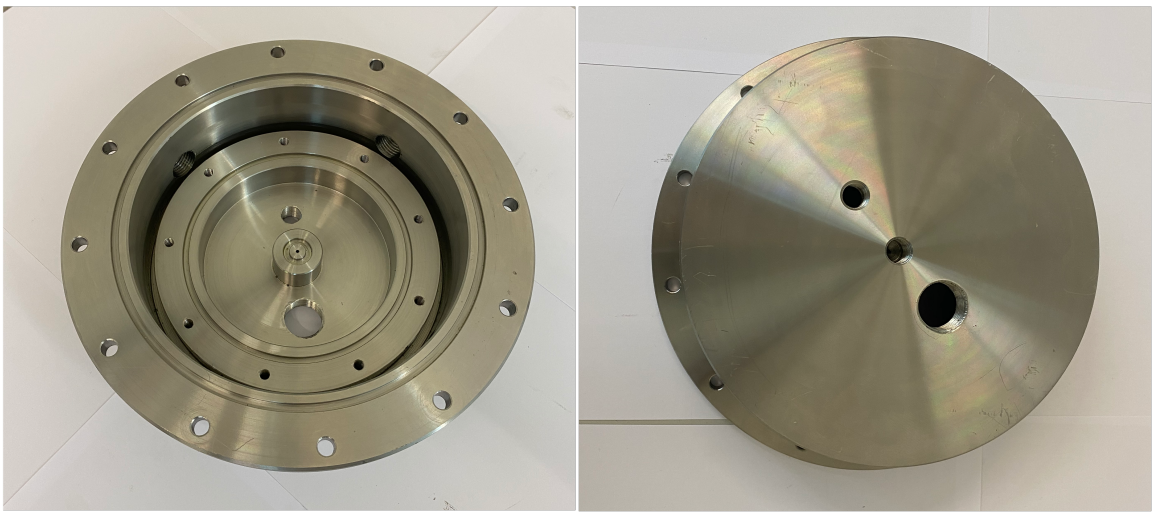

Figure 3.20. Manufactured dome.



Figure 3.21. Parts and assembly of the thruster.

3.5. Thrust Stand

A thrust stand was manufactured for the hot fire thrust measurements of the engine. The main frame of the thrust stand was constructed by welding steel square pipes. The thrust stand has a rail - car platform on which the engine is mounted. Aluminium clamps, cut from a thick plate with a waterjet cutting machine, are used to position and lock the engine on the thrust stand. Rail car has a smooth movement in the thrust axis thanks to the good alignment and leveling of the two rails. 4 round columns made out of steel are used to connect the engine and the thrust plate. The columns are screwed to the engine from the extra threads on the bolts that are used to

assemble the dome and the thrust chamber. The thrust force produced by the engine is transferred to the thrust plate through these 4 columns. The thrust plate is a $10mm$ thick steel plate and it is connected to the load cell at the center with a threaded steel bar. The load cell is connected to the stand with another threaded bar. Manufactured thrust stand can be seen in Figure 3.22.

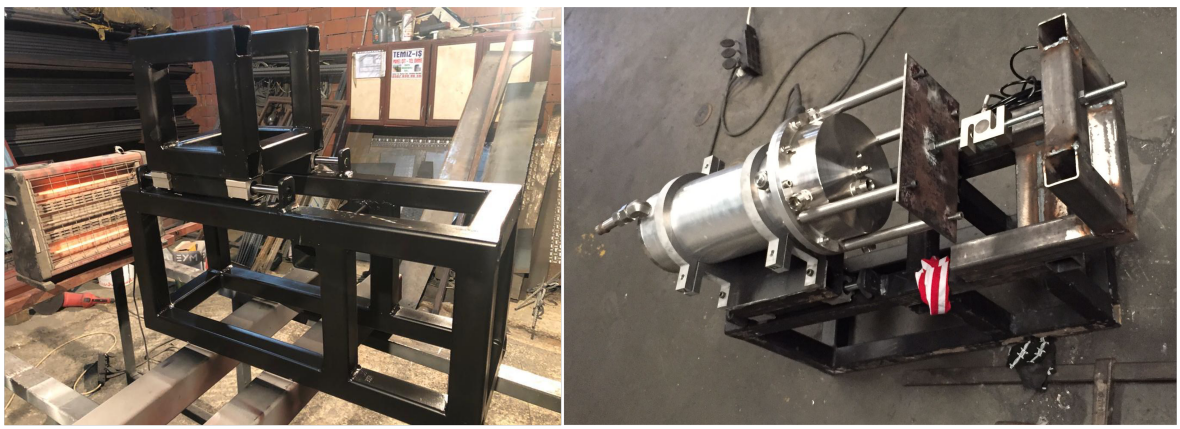

Figure 3.22. Manufactured thrust stand.

3.6. Feed System

The feed system pressurizes the propellants and feeds them into the combustion chamber through the injector. BUSTLab liquid rocket engine is a pressure - fed engine. Pressurization is done with gaseous nitrogen (N_2). Pressurizer gases are stored in standard industrial pre - filled nitrogen bottles. For each line, a group of 15 $50l$ nitrogen bottles at $235bar$ pressure are used.

3.6.1. Fuel Line

A $100l$ steel vessel was manufactured for the fuel tank. This tank has a 3/4" outlet at the bottom. At the top, the fuel tank has two 3/4", one 1/2" and two 1/4" ports. These ports are used for filling and pressurizing the tank, sensor connections and attaching a pressure relief valve. All of the threads are NPT.

After the fuel tank, the fuel feed line consists of check valves, ball valves with pneumatic actuators, pressure sensors, temperature sensors, a cavitating venturi for passive flow control and a flow - meter. Pneumatic actuators are actuated with solenoid actuators.

Piping from the fuel tank to the engine is done with 3/4" seamless stainless steel pipes. The fuel tank is placed on a scale to measure its mass for both filling and calculating the mass flow during operation. The fuel tank is pressurized to 80bar during the hot firing of the engine.

3.6.2. Oxidizer Line

A 100l stainless steel vessel was manufactured for the oxidizer tank. Similar to the fuel tank, the oxidizer tank has a 3/4" outlet at the bottom. At the top, two 3/4", one 1/2" and two 1/4" holes are present. These ports are used for filling and pressurizing the tank, sensor connections and attaching a pressure relief valve just like the fuel tank. All of the threads are NPT. The oxidizer tank is covered with an insulation for storing the liquid oxygen. Without the insulation it is not possible to store liquid oxygen in the tank as it has only one wall. It would be possible to store the liquid oxygen in a pressure vessel with two walls with vacuum in the middle but this would be beyond our budget.

Prior to the insulation, a cage - like car was built and the tank is mounted to it. The car was built for easily moving the tank after the insulation. The oxidizer tank can be seen before and after the insulation in Figure 3.23.

After the oxidizer tank, the oxidizer feed line consists of check valves, cryogenic ball valves with pneumatic actuators, pressure sensors, temperature sensors and a cavitating venturi for passive flow control. Pneumatic actuators are actuated with solenoid actuators. Piping from the fuel tank to the engine is done with 3/4" seamless stainless steel pipes. The LOX tank car is placed on a scale to measure its mass for

both loading and calculating the mass flow during operation. The oxidizer tank is pressurized to 80*bar* during the hot firing of the engine.



Figure 3.23. *LOX* tank with cage - car before and after insulation.

3.6.3. Cooling Water Line

The cooling water is only used for the hot fire test. A commercial 16*bar*-80*l* air tank is employed for storing the cooling water. A TESCOM ER - 5000 regulator is used to pressure the tank to 15*bar* during the hot fire test. The tank has a 16*bar* relief valve on one of the ports at the top. Gaseous nitrogen supplied from an industrial 50*l* - 235*bar* bottle is used for pressurizing the cooling water tank. The cooling water is directly fed into the cooling channels of the chamber from the inlets on the jacket near the nozzle.

3.7. Igniter

Torch igniters are used in many applications in the literature [14, 52–54]. However, they require additional feed lines and flow control mechanisms which increases the complexity of the system and overall workload. For these reasons, torch igniters are not considered for the ignition system in this study. On the other hand, pyro igniters provide a rather simple way to ignite a rocket engine. They are also used by rocket engine developers for ignition [13]. We actually considered a pyro igniter and experimented with commercially available amateur solid rocket grains. The ones we experimented with did not have successful burns and a good portion of them exploded themselves during their burn time so they were deemed unreliable. Purchasing and acquiring better quality grains from more established firms would take time so we eliminated this method as well.

For the ignition of the engine, a simple electric spark device was built. The ignition system consisted of 2 electrodes, a transformer and a 1 - axis translation pneumatic piston. The electric spark is created between the sharpened tips of the electrodes with $+14kV$ and -$14kV$ potential. All of these components are standard industrial products. These components are used in standard industrial gas burner igniters.

The igniter was located at the center of the nozzle exit. With a pneumatic cylinder, it was lowered and taken out of the exhaust plume. The electrodes have ceramic insulation around them. They are mounted on the piston tip with a simple steel clamp. This igniter was used in 3 open hot flow injector tests and 1 full system hot fire test. In all of the 4 tests, the ignition occurred instantly. A photo of the igniter can be seen Figure 3.24.

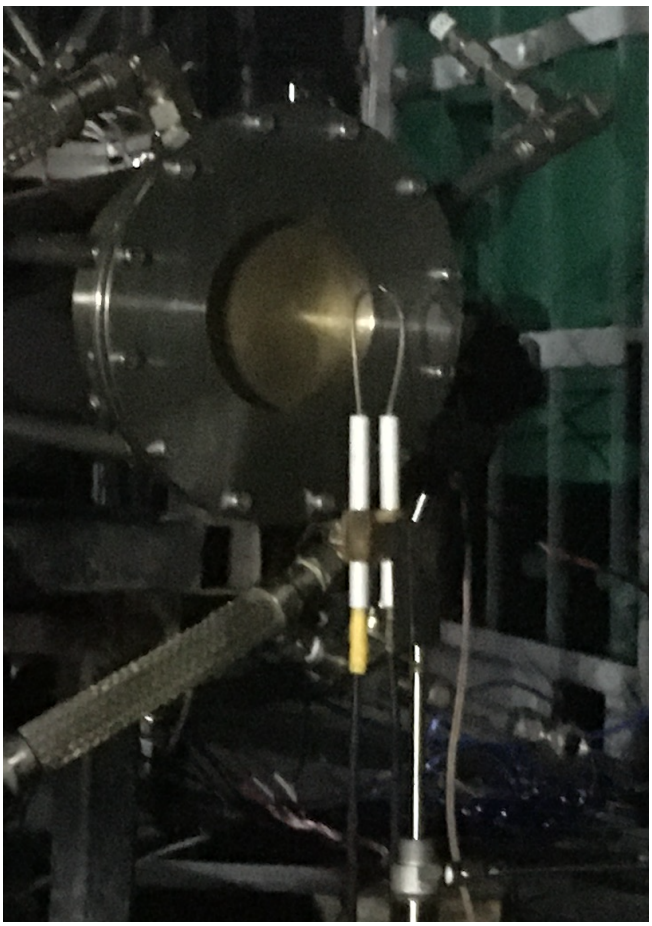

Figure 3.24. The spark igniter in front of the injector before the open hot flow test.

4. INJECTOR TESTS

The first version of the injector was tested many times with water and compressed air. Initial tests were done with an air compressor to pressurize the fuel tank. Initial oxidizer tests were done with this compressor too. Both tanks were filled with water and pressurized with a $50l$ - $8bar$ compressor. This compressor does not have enough capacity for pressurizing the tanks during the tests. We later swapped this compressor with $50l$ - $235bar$ industrial pre - filled nitrogen bottles for the water tests. The compressor was still used in the tests for supplying the pneumatic actuator valves through the solenoid valves.

The fuel and oxidizer tanks are placed on separate scales for measuring their masses. They are both loaded and pressurized through inlets on top of each of them. Both tanks have a single outlet at the bottom. Manual ball valves are used at the inlet of each tank's propellant loading port. A manual ball valve for the fuel tank and a manual cryogenic ball valve for the oxidizer tank are used as primary outlet valves. These valves are followed by pneumatic valves in each line. The propellants are fed to the lines once these valves are opened.

Water test setup consists of two feed lines to the injector, one for the fuel and one for the oxidizer. The pipes for both of the lines are mounted on a table with wheels. This table is built with aluminium sigma profiles. Two plywood plates are mounted on this table for the early tests with water. Later, these are changed with steel sheets to strengthen the connections. The first one is placed on top of the table. Pneumatic valves are mounted on this plate. These valves connect the pressurizer nitrogen bottles to the propellant tanks. Each of the pressurization lines on the table has an extra outlet to open air devoted to depressurizing the tanks in case of an over - pressurization and relief valve failure. These outlets are also used for controlling the propellant tanks' pressure and keeping them at the desired level.

Another plywood plate is mounted to the side of the desk. After exiting the tanks, the propellants are fed into the pipes mounted and fixed on this plate. Two check valves, a cavitating venturi, a temperature sensor, a pressure sensor before the venturi and a pressure sensor after the venturi are used in both lines. The oxidizer line is covered with sponge insulation for the tests with cryogenics.

For the water tests, an injector flange was manufactured. In thruster assembly, the oxidizer sealing for the injector is done with an o - ring placed between the injector and the dome. This o - ring's groove is located on the dome side. The fuel is sealed into the dome with an o - ring placed in the groove on injector's front face. This o - ring is compressed between the combustion chamber and the injector in the full thruster assembly. In the water tests, this o - ring is compressed between the injector's front face and the aforementioned flange.

The injector water test assembly is placed on another desk built from aluminium sigma profiles. A large bucket is employed for collecting the water after it exits the injector. Mass flow rate measurements are done with this large bucket placed on a scale. The weight of the bucket is measured before and after the test and mass flow rate is calculated. Setup for water tests can be seen in Figure 4.1. This setup is also used for the second injector water tests.

The pressurization of the tanks is done with a bang - bang controller. Including this, the test setups, i.e., water tests, cold flow tests, open hot fire tests and hot fire test, are all controlled with two NI (National Instruments) USB - 6008 and an NI USB - 6009 data acquisition systems.

Most of the pneumatic valves in the test setups are in normally - closed configuration. Only the emergency depressurization valves on the feed lines are in normally - open configuration. These are the extra outlets on the desk that are mentioned before. These outlets are also used to regulate the tanks' pressure if it exceeds the targeted value during bang - bang controlled pressurization. The pneumatic valves and the rest

of the test setup are designed for safely shutting the system and depressurizing the lines in case of a power loss or any other issues.

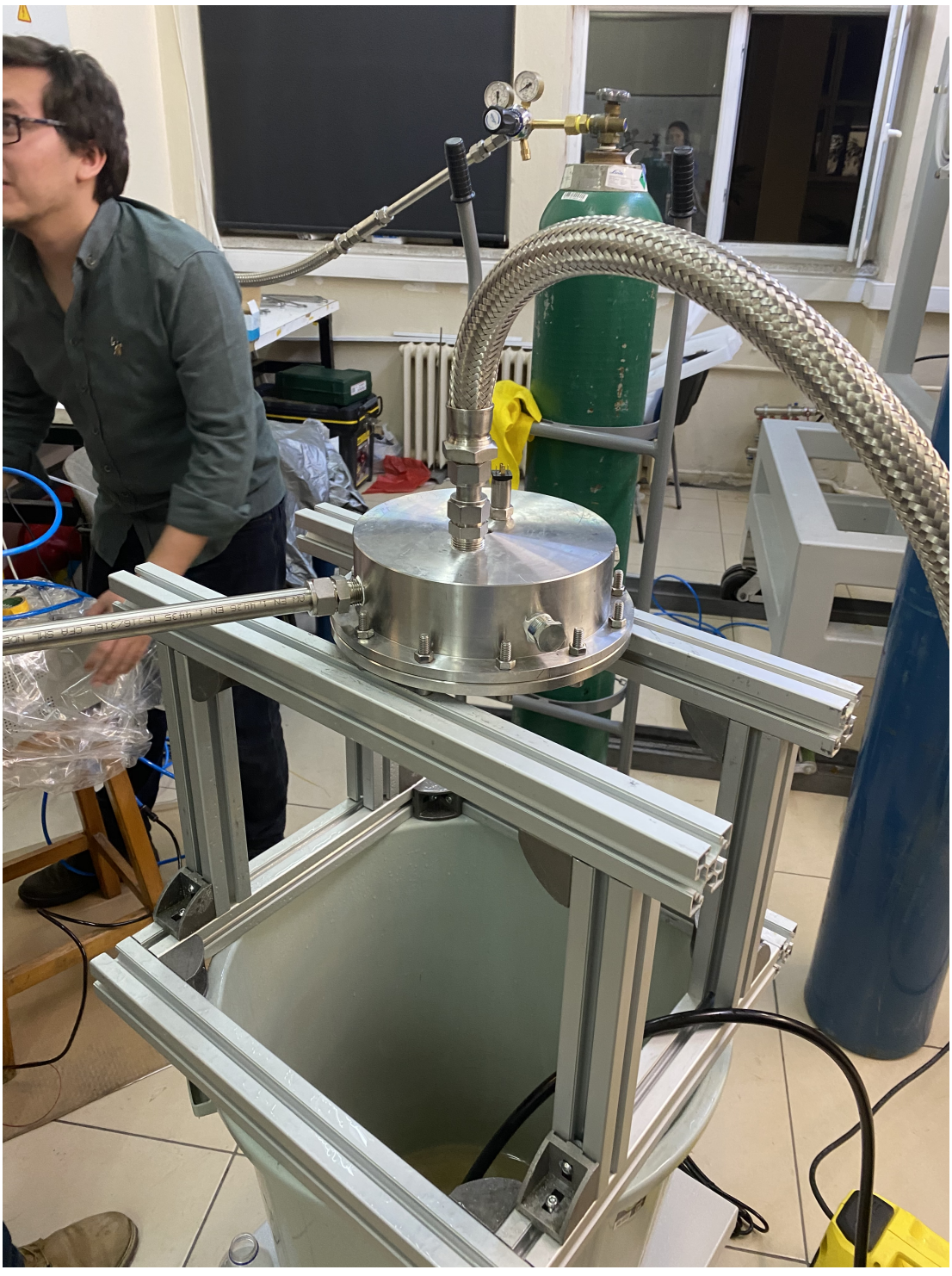

Figure 4.1. Water test setup.

During a water test, the pressure drop across the injector and the mass flow rate are measured and recorded. Using Equation 3.14, the discharge coefficient is calculated. In Figure 4.2, triplet impingement of water during the water tests can be seen.

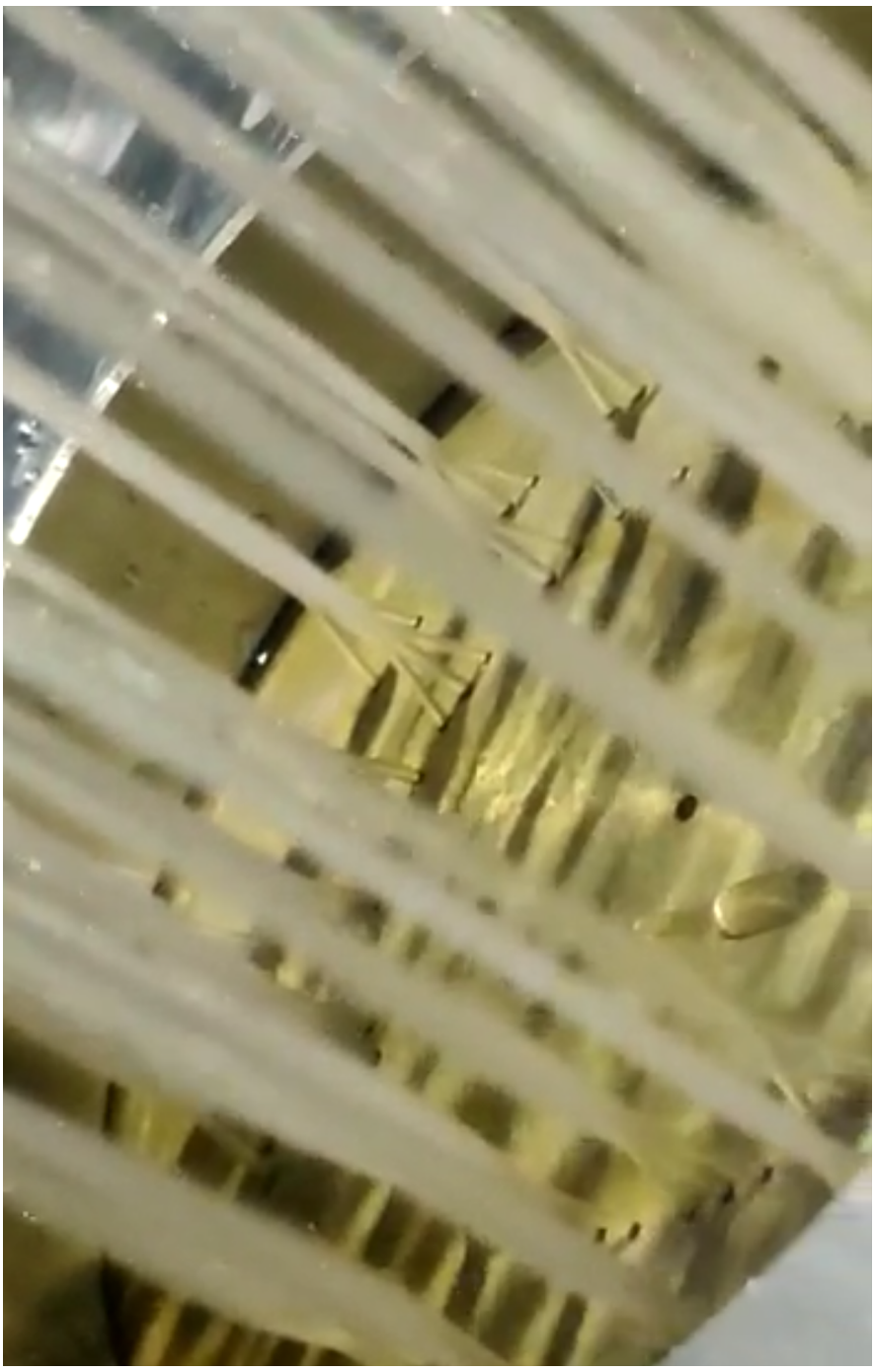

Figure 4.2. Triplet impingement of water at low pressure drop.

4.0.1. First Injector Water Tests

First injector water test results for the oxidizer flow are presented in Table 4.1.

Table 4.1. First injector water test results for the oxidizer orifices.

Pressure drop, $\mathbf{\Delta P}$	$5.3bar$
Mass flow rate, $\mathbf{\dot{m}_o}$	$3.2kg/s$
Discharge coefficient, $\mathbf{C_d}$	0.69

The calculated C_d in Table 4.1 is the average discharge coefficient for the oxidizer orifices. C_d is a dimensionless property for characterizing the flow and pressure loss behavior of passages. C_d of real injectors are less than 1 which is the ideal discharge condition. C_d is affected by the shape and manufacturing errors of the orifices. Empirical results for some geometries are presented in Figure 3.9. Even when using given geometries with calculated C_d values, an injector is tested to take the manufacturing errors into account and calculate the real C_d values. Once the C_d is calculated for the first injector oxidizer orifices, calculations for the actual scenario, in which LOX is the oxidizer, can be done using Equation 3.14. The results are presented in Table 4.2.

Table 4.2. First injector oxidizer flow with LOX.

Calculated discharge coefficient, $\mathbf{C_d}$	0.69
Required mass flow rate, $\mathbf{\dot{m}_o}$	$1.26kg/s$
Resulting pressure drop, $\mathbf{\Delta P}$	$0.7bar$

As it is seen in Table 4.2, the pressure drop across the injector for LOX is only $0.7bar$. For a chamber pressure of $30bar$, this only gives 2.3% stiffness ratio which is much lower than the criteria given in Section 3.3 and could cause buzz or chug instability [18]. First injector water test results for fuel flow are as given in Table 4.3.

Table 4.3. First injector water test results for fuel orifices.

Pressure drop, $\mathbf{\Delta P}$	$18.1 bar$
Mass flow rate, $\dot{\mathbf{m}}_\mathbf{f}$	$1.36 kg/s$
Discharge coefficient, $\mathbf{C_d}$	0.72

Once the C_d is calculated for the first injector fuel orifices, calculations for our fuel, ethanol - water mixture, can be done using Equation 3.14. The results are presented in Table 4.4.

Table 4.4. First injector fuel flow with ethanol - water mixture.

Calculated discharge coefficient, $\mathbf{C_d}$	0.72
Reuqired mass flow rate, $\dot{\mathbf{m}}_\mathbf{f}$	$1.01 kg/s$
Resulting pressure drop, $\mathbf{\Delta P}$	$11.9 bar$

The pressure drop in the oxidizer side of the injector is insufficient for a stable combustion. As previously expressed in Section 3.3, another injector with smaller oxidizer flow area is designed.

The pressure drop across the injector for fuel flow results in high pressure in the fuel dome As previously expressed in Section 3.3, another injector with larger fuel flow area is designed to lower the pressure drop.

4.0.2. Second Injector Water Tests

With a %60 reduction in total oxidizer injection area and a %50 increase in total fuel injection area, a new injector is designed and manufactured. With this new injector design, only the number and diameter of the injection holes are changed. Hole angles are kept the same as the prior design. For this reason, the new design is done with the assumption of the discharge coefficients remaining the same for both the oxidizer and

the fuel orifices. In Tables 4.5 and 4.6, the expectations for the pressure drops across this injector are given.

Table 4.5. Changes and expectations for the new injector oxidizer side.

Total oxidizer injection area, $\mathbf{A_o}$	1→0.40
Discharge coefficient, $\mathbf{C_d}$	Remains same, 0.69
Pressure drop, $\mathbf{\Delta P}$	$0.7bar \rightarrow 4.6bar$

Table 4.6. Changes and expectations for the new injector fuel side.

Total fuel injection area, $\mathbf{A_f}$	1→1.50
Discharge coefficient, $\mathbf{C_d}$	Remains same, 0.72
Pressure drop, $\mathbf{\Delta P}$	$11.9bar \rightarrow 5.3bar$

Upon testing this new injector water, it was seen that the oxidizer C_d has remained the same, 0.69. However, the C_d on the fuel side is calculated as 0.52 for this new injector. This means, to get a $1.01kg/s$ mass flow rate of %75 ethanol - %25 water mixture with this injector, the pressure drop needs to be $9.9bar$ instead of $5.3bar$. We believe this difference is caused by a manufacturing error that we cannot identify.

4.1. Cold Flow Tests

Many water tests are conducted to find the C_d values for both the oxidizer and the fuel side of the injector. After these tests are completed, several cold flow tests are done with the injector. Cold flow tests are only conducted for the second design of the injector since the first design did not give acceptable results with the water tests and therefore retired from the project.

In the cold flow tests, the overall feed system and the cryogenic valves are tested with liquid nitrogen and water. For the cold flow tests, the injector is mounted on the thrust stand where the load cell would be mounted in the full test assembly. The

injector is assembled with the thrust plate and the thrust plate is mounted to the thrust stand from its central hole with a threaded rod and several nuts. The feed system is set up as it would be in the full test assembly.

Figure 4.3 shows a photo of the cold flow test setup. Cold flow tests are carried out in a parking lot in our campus whereas the hot flow and hot fire tests are conducted in a test side outside the campus. A photo of one of the cold flow tests of the injector with liquid nitrogen as oxidizer and water as fuel can be seen in Figure 4.4.

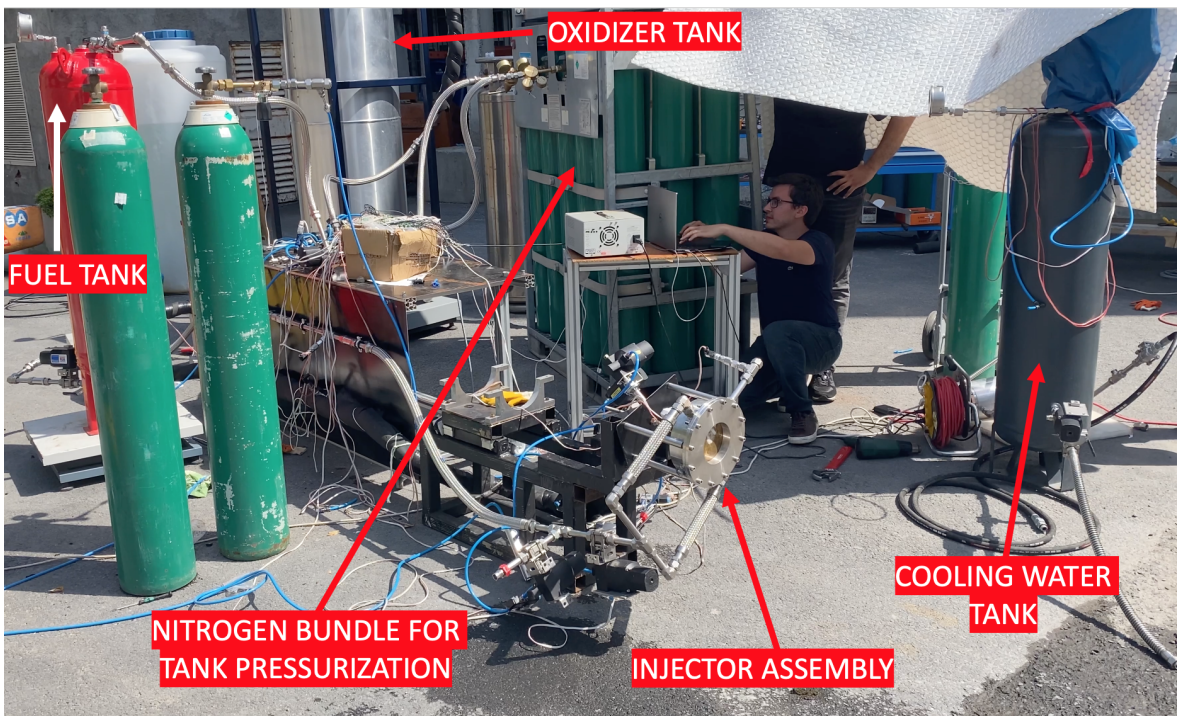

Figure 4.3. Cold flow test setup.

Prior to the test beginning, liquid nitrogen alone is fed into the oxidizer line to cool the line. Both of the propellant tanks are pressurized to $80bar$ in the cold flow tests. The pressure against time graphs for one of the tests are presented in Figures 4.5 and 4.6.

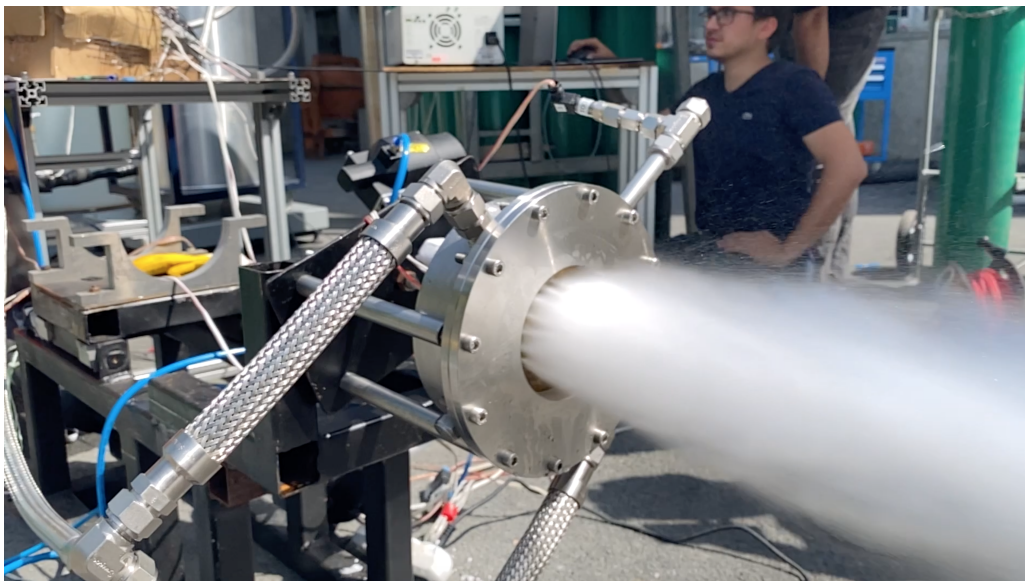

Figure 4.4. Cold flow test of the injector.

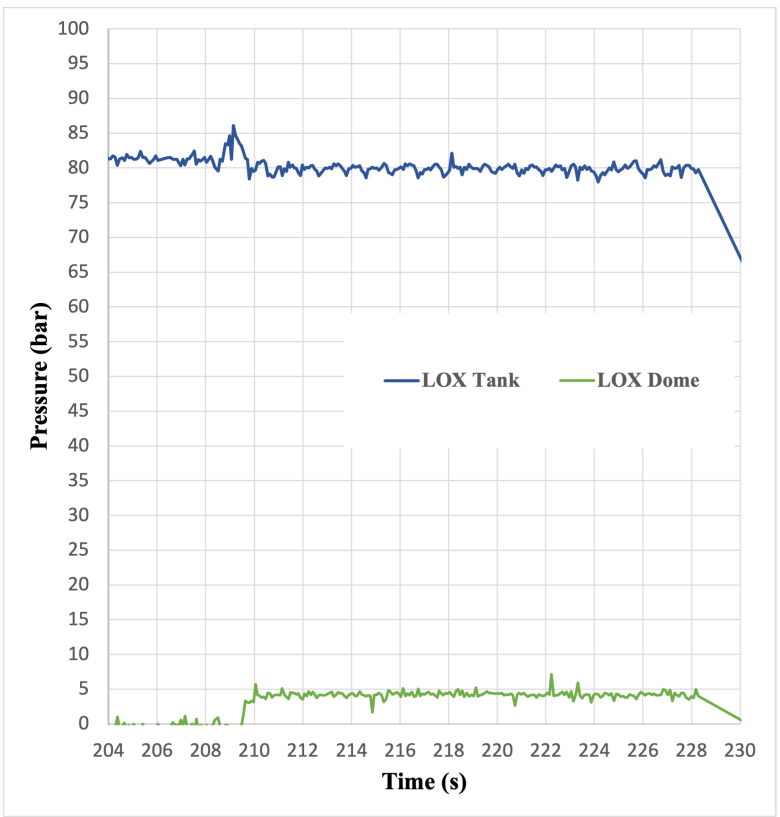

Figure 4.5. Pressure in the cold flow test with liquid nitrogen as the oxidizer.

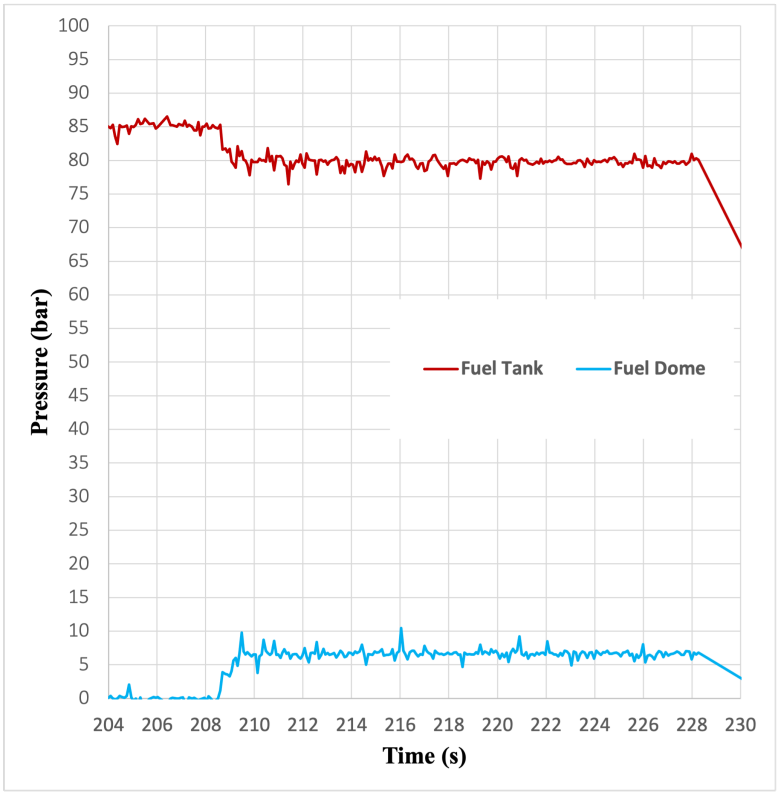

Figure 4.6. Pressure in the cold flow test with water as the fuel.

From Figure 4.5, a 4.5bar pressure drop across the oxidizer orifices is measured. Oxidizer tank pressure oscillates between 77 - 80bar in this test. From Figure 4.6, a 7bar pressure drop across the fuel orifices is observed. Fuel tank pressure in this test varies between 76bar and 80bar. In Figures 4.7 and 4.8, the mass of the tanks against time graphs are presented.

The cold flow test gives 1.06kg/s mass flow rate for liquid nitrogen and 0.88kg/s mass flow rate for water. Making the appropriate calculations, this results in a 1.26kg/s mass flow rate for liquid oxygen which is the designed mass flow rate. 0.88kg/s water mass flow rate gives 0.80kg/s mass flow rate for ethanol - water mixture. This is 21% less than the designed mass flow rate. This would give an OF ratio of 1.58 for the real propellants which is 26% higher than the designed value.

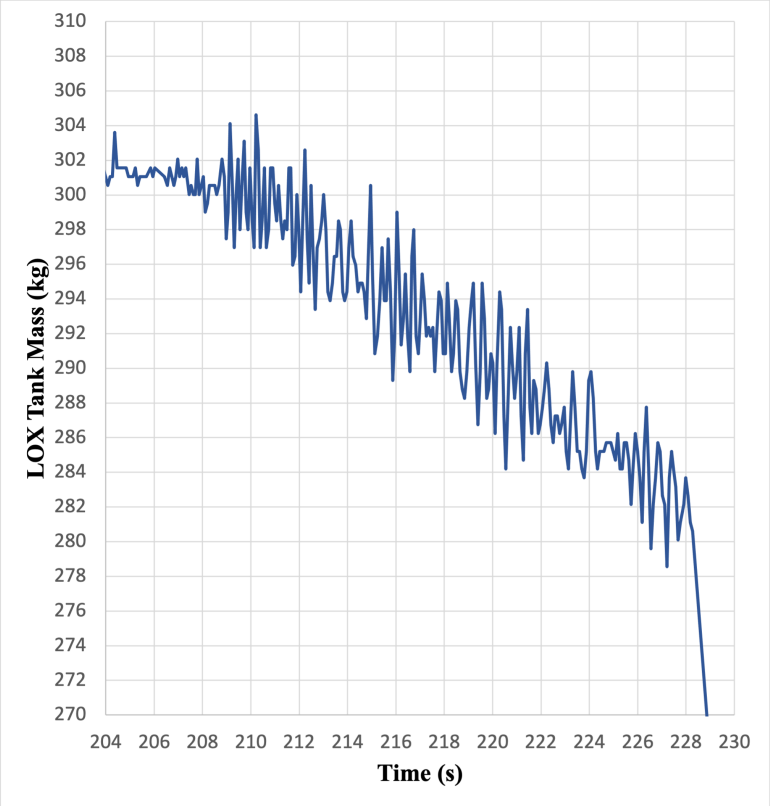

Figure 4.7. Mass of the oxidizer tank in cold flow test with liquid nitrogen.

The C_d calculations for the oxidizer side holds true after the cold flow test. The C_d calculations for the fuel is 0.49 here, which was obtained in some of the water tests. The previously given 0.52 value is the average of multiple tests. The results here are accepted to be consistent with the water tests.

There are two aspects to be considered for the insufficient mass flow rate of the fuel: injector manufacturing defects and cavitating venturi manufacturing defects. The cavitating venturi is designed for supplying $1.01 kg/s$ mass flow rate for ethanol - water mixture. Regardless of the downstream behaviour, this mass flow rate should be supplied by the cavitating venturi. This suggests a manufacturing defect in the fuel cavitating venturi. Otherwise it would have supplied the calculated mass flow rate as in the case of oxidizer venturi. If the fuel cavitating venturi worked as it was designed, we would have seen a much higher pressure drop across the injector for supplying the rated mass flow rate.

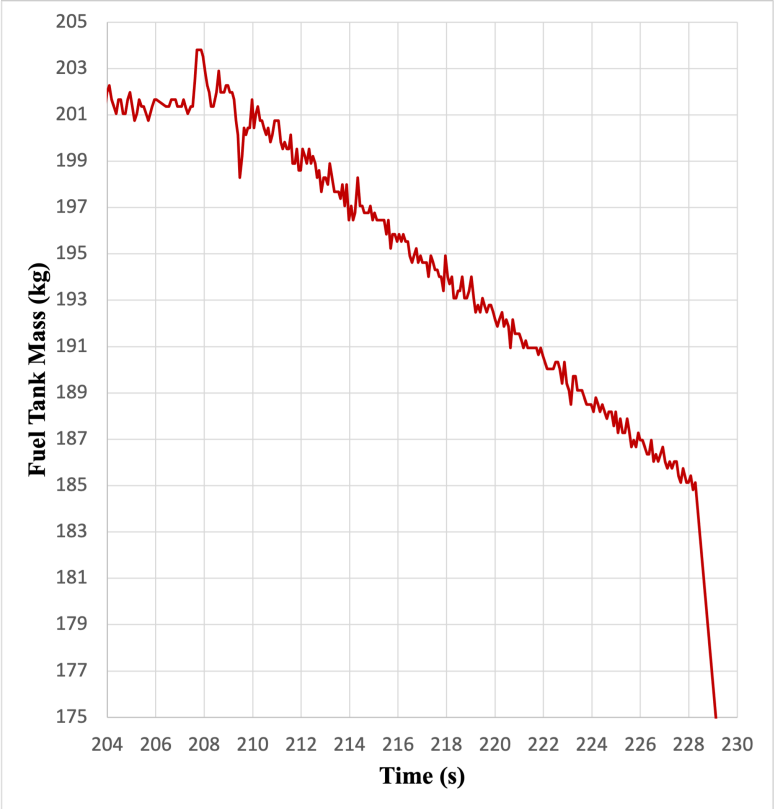

Figure 4.8. Mass of the fuel tank in cold flow test with water.

4.2. Open Hot Flow Tests

The first open hot flow test is conducted with gaseous oxygen and ethanol - water mixture. In this test, both tanks are pressurized to $10bar$. This test was devoted to testing the igniter. Therefore, no significant pressure or mass flow rate measurements were done in this test. Similar to the cold flow tests, injector is mounted on the thrust stand in the open hot flow tests. The igniter is placed in front of the injector. The igniter is elevated to the injector center's level with the pneumatic piston manually by opening and closing a switch connected to the solenoid valve. Lowering the igniter to take it out of the open fire is also done manually in these tests. Igniter movement is later automated within the LabVIEW software for the full hot fire test. Test setup can be seen in Figure 4.9. The second open hot flow test is done with gaseous oxygen and ethanol - water mixture with both tanks at $30bar$ pressure.



Figure 4.9. Open hot flow test setup.

The final open hot flow test is conducted with LOX and ethanol - water mixture. In this test, both tanks are pressurized to $80bar$. Pressure and tank mass measurements for the oxidizer side during this test are presented in Figures 4.10 and 4.11.

Figure 4.10 shows a 25 bar dome pressure for the oxidizer side. This suggests that liquid oxygen evaporates in the dome. The mass against time graph for the oxidizer tank is given in Figure 4.11. The mass flow rate of liquid oxygen for this test is calculated as $0.88kg/s$. This is inconsistent with cold flow tests. Looking at Figure 4.10, it is seen that the oxidizer tank pressure gradually decreases from $80bar$ to $73bar$. This is one of the reasons for the reduced mass flow rate here. This issue rises from insufficient supply pressure to the bang - bang controller. We later resolved this issue by increasing the supply pressure from the nitrogen bundle. However, the main issue with the reduced mass flow rate seems to be caused by icing and therefore flow area narrowing in the venturi.

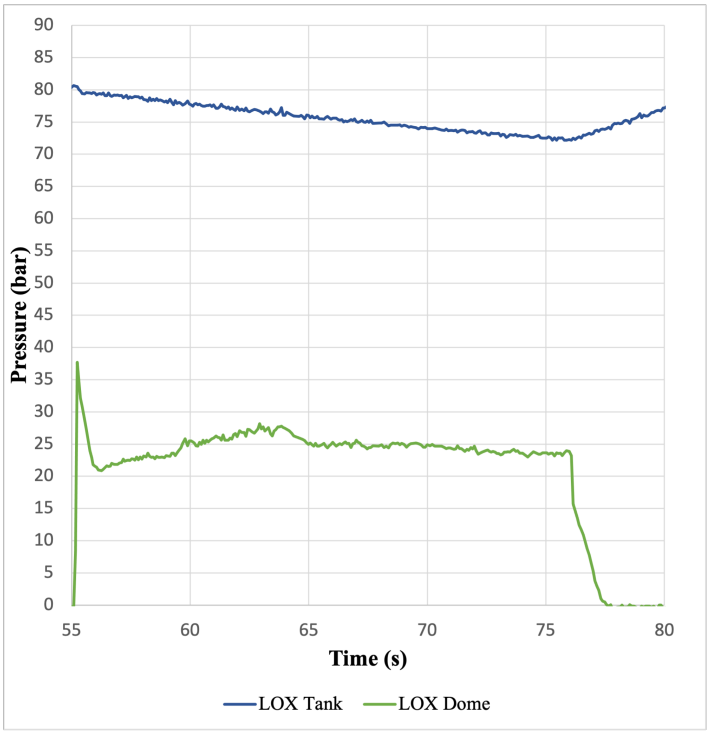

Figure 4.10. Pressure measurements in open hot flow test for LOX.

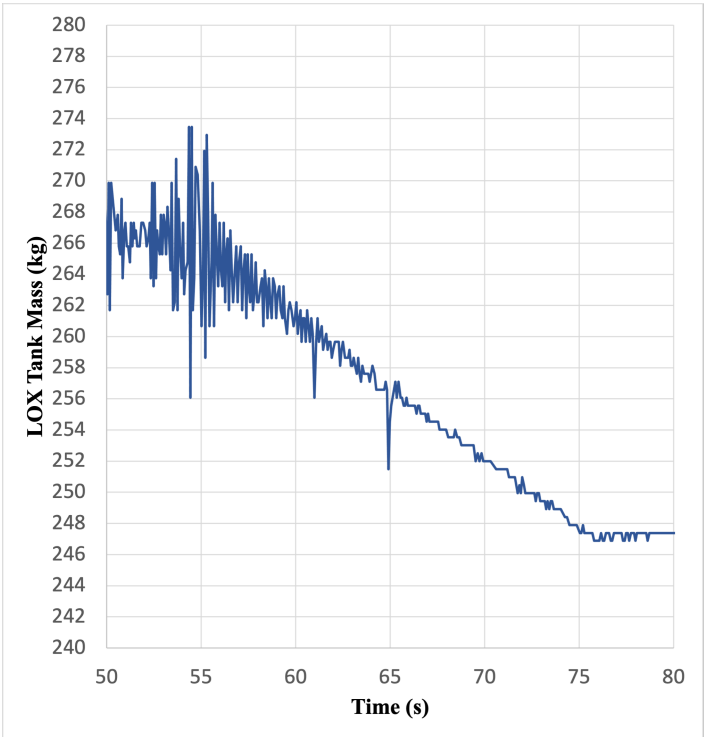

Figure 4.11. Mass of the oxidizer tank - car in open hot flow test at 80 bar.

Pressure and tank mass measurements for the fuel side are presented in Figures 4.12 and 4.13. Figure 4.12 shows a 7.5 bar dome pressure for the fuel side. This is as expected.

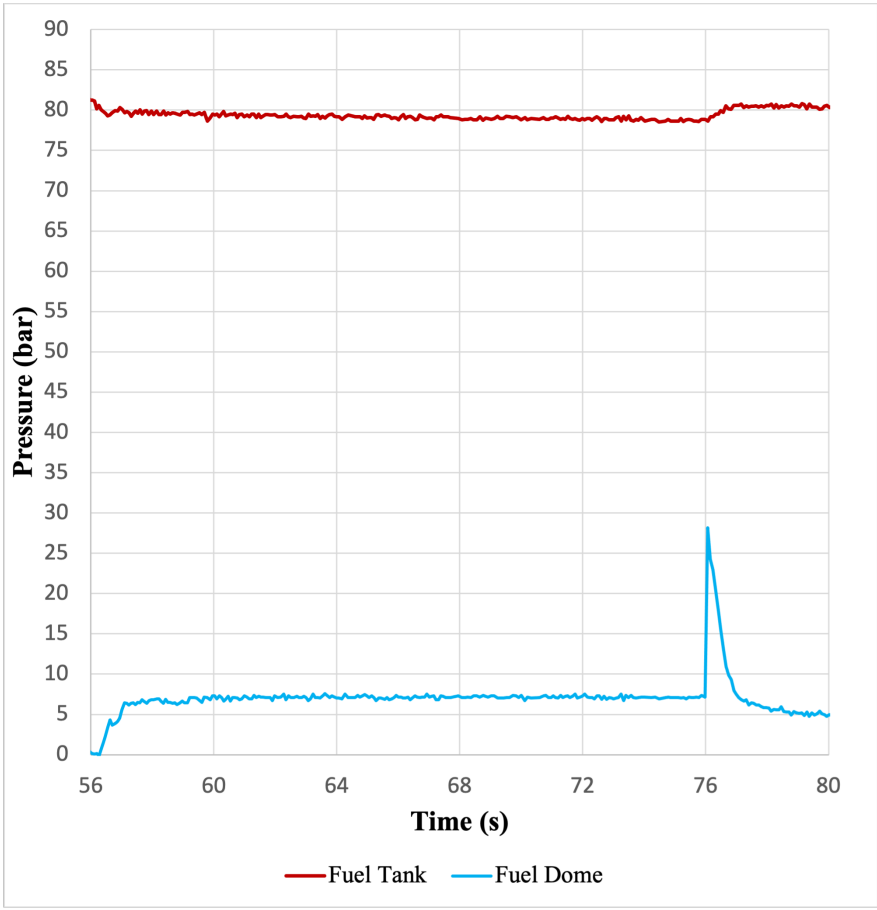

Figure 4.12. Pressure measurements in open hot flow test for fuel.

The mass flow rate of fuel is calculated as $0.84kg/s$ from Figure 4.13. With this pressure drop and mass flow rate of ethanol - water mixture, the C_d for the fuel side is calculated as 0.50 which is once again consistent with the water tests.

The measured mass flow rate for the oxidizer side is $0.88kg/s$ which is 30% less than the designed value, $1.26kg/s$. For the fuel side, the mass flow rate is measured as $0.84kg/s$ and this is 17% less than the designed value, $1.01kg/s$. This gives an OF ratio of 1.05 which is 16% less than the designed 1.25 OF ratio.

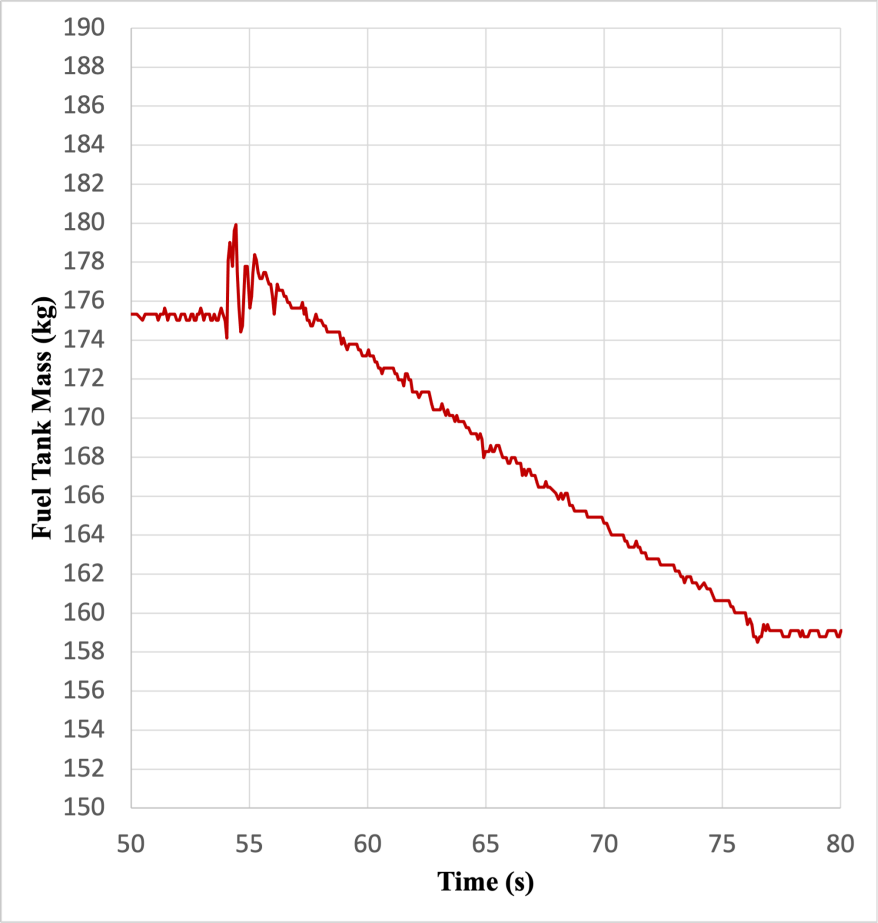

Figure 4.13. Mass of the fuel tank in open hot flow test at 80 bar.

A photo of this test with liquid oxygen as oxidizer and ethanol - water mixture as fuel at 80 bar tank pressure can be seen in Figure 4.14.



Figure 4.14. Injector open hot flow test with liquid oxygen and ethanol - water mixture.

5. HOT FIRE TEST

BUSTLab Liquid Rocket Engine is hot fire tested in September 2021. The first design was for a $50bar$ chamber pressure, $10kN$ target thrust, $294s$ of Isp, gaseous oxygen as oxidizer and kerosene as fuel configuration. This configuration results in $2.39kg/s$ mass flow rate for the oxidizer and $1.06kg/s$ mass flow rate for the fuel, giving a total mass flow rate of $3.45kg/s$. Due to the reasons explained in the previously, the hot fire test is carried out with ethanol - water mixture as fuel, liquid oxygen as oxidizer. The targeted mass flow rate is $1.26kg/s$ for the liquid oxygen and $1.01kg/s$ for the ethanol - water mixture, giving $2.27kg/s$ total mass flow rate. At $30bar$ chamber pressure, $5.65kN$ thrust is targeted with $254s$ of Isp. Assembly of the BUSTLab Liquid Rocket Engine mounted on the thrust stand can be seen in Figure 5.1.

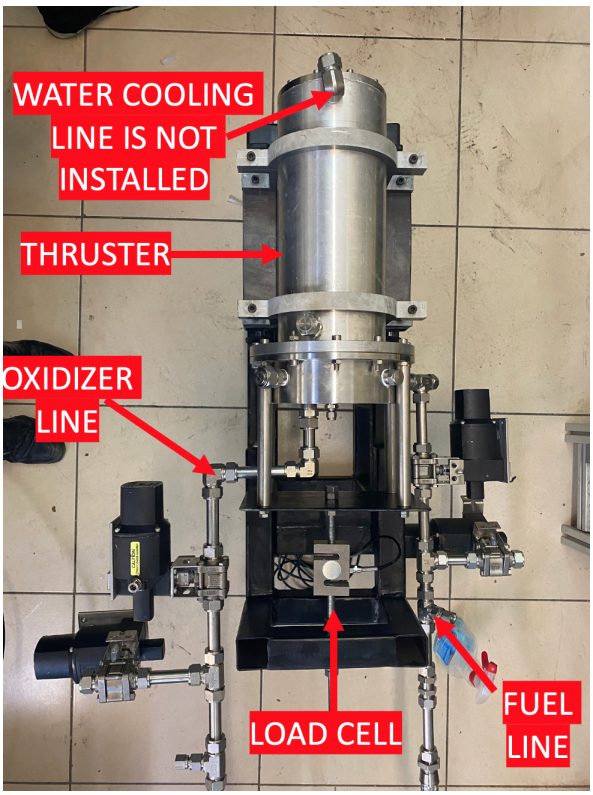

Figure 5.1. BUSTLab Liquid Rocket Engine hot fire thruster assembly on the thrust stand.

Hot fire test setup at the test site can be seen in Figure 5.2.

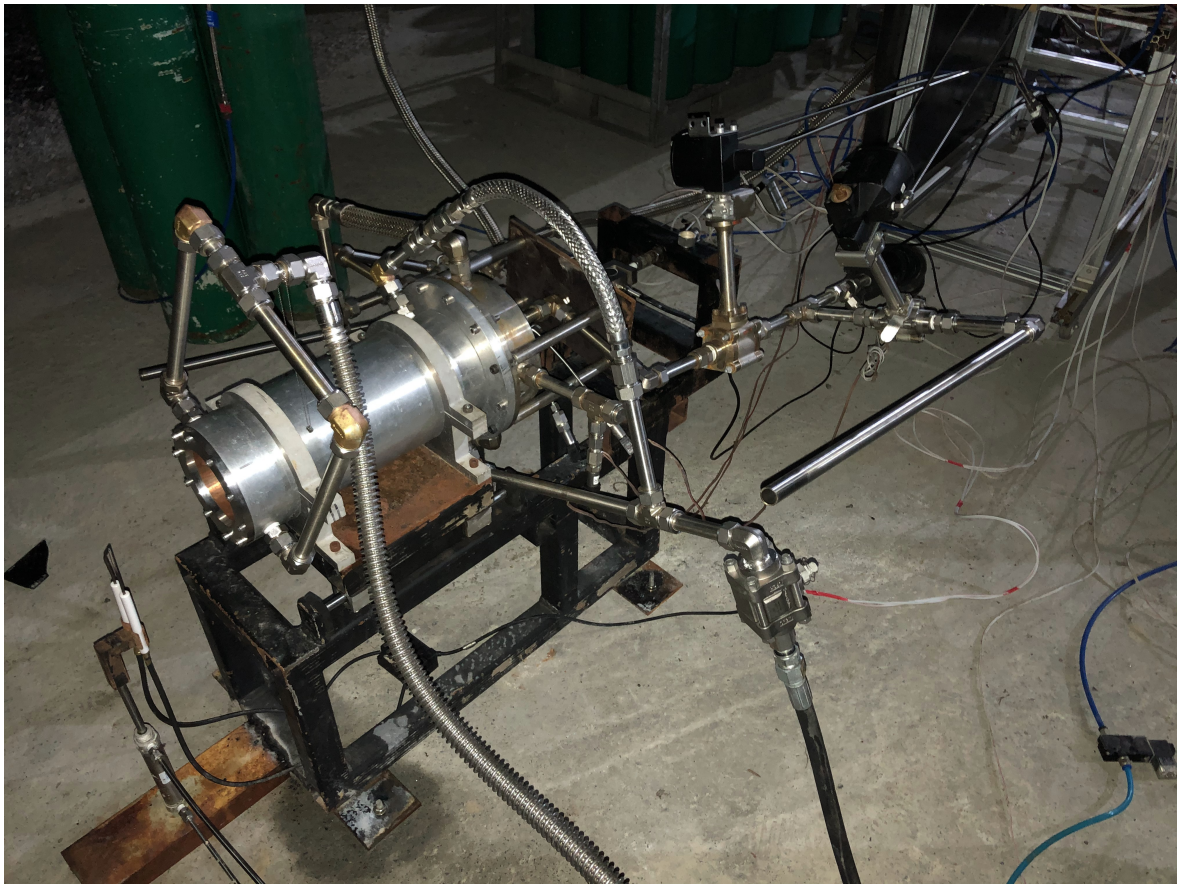

Figure 5.2. BUSTLab Liquid Rocket Engine hot fire test setup.

The essential elements of this setup can be listed as follows:

- Thruster
- Thrust stand
- Igniter
- Feed line installation desk and feed line elements
- Oxidizer tank
- Fuel tank
- 2 × scale for measuring tank masses
- Cooling water tank

- 1 × nitrogen bottle for pneumatic actuators
- 1 × nitrogen bottle for water tank pressurization
- 1 × nitrogen bundle (15 bottles) for oxidizer tank presssurization
- 1 × nitrogen bundle (15 bottles) for fuel tank presssurization
- 2 × NI USB6008 - 1 x NI USB6009
- 1 × Power source for control board
- 1 × laptop computer

The thrust stand is fixed to the concrete floor with 4 steel dowels. The dowels press and fix the the thrust stand through 4 metal plates welded to the thrust stand. For the hot fire test, the igniter is welded to the thrust stand. The igniter's pneumatic piston is screwed to a thick steel U - bar. This U - bar is welded to the thrust stand to align and fix its position.

Similar to the open hot flow tests, the oxidizer line is cooled with liquid nitrogen prior to the test. The oxidizer tank itself is also cooled with liquid nitrogen first. An outlet just before the oxidizer dome is employed for cooling the line. Once nitrogen starts exiting this outlet in liquid form, the line is accepted to have cooled. After the line is cooled and liquid nitrogen in the tank is fully drained, liquid oxygen is loaded to the oxidizer tank. Liquid oxygen is transferred from an industrial dewar at $8bar$ pressure. The loading is done with a braided transfer hose at this pressure only. The oxidizer tank has an open outlet to the atmosphere during the loading for maintaining the pressure difference between the dewar and the tank. The fuel tank is simply loaded by pouring the fuel through a funnel.

All of the valves in the test setup are in normally - closed condition. The only exception to this is for the emergency depressurization outlets located on the desk where the tank pressurization lines are mounted.

The oxidizer tank pressure against time graph during the hot fire test is shown in Figure 5.3. This figure shows an oxidizer dome pressure level around $65bar$. This

suggests that the oxidizer is not in liquid phase in the dome. We do not now if it is a liquid - gaseous mixture or completely in the gaseous phase in the dome. Since the mass flow rate of the oxidizer line is passively controlled by the cavitating venturi, the mass flow rate is not affected by this phase change. The cavitating venturi sets the mass flow rate from the upstream tank pressure. In order to pass this set mass flow rate, the injector responds to this phase change with the increased dome pressure; therefore, the increased pressure drop.

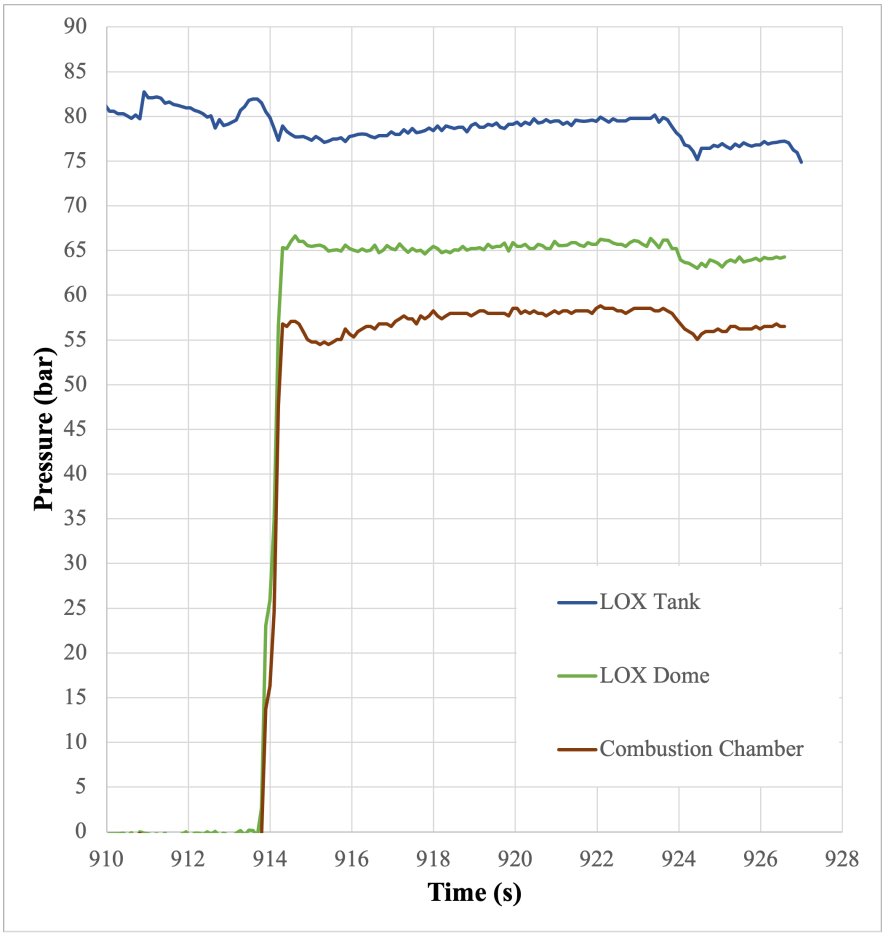

Figure 5.3. Pressure measurements on oxidizer side during hot fire test.

The oxidizer tank - car mass against time graph during the hot fire test is presented in Figure 5.4. This figure shows a linear trend in the change of tank mass, i.e., mass flow rate of the oxidizer. The mass flow rate is calculated by drawing a trend line

on the graphs. Mass flow rate calculations are done by calculating the slope of this line. For the hot fire test, the oxidizer mass flow rate is calculated as $0.83 kg/s$.

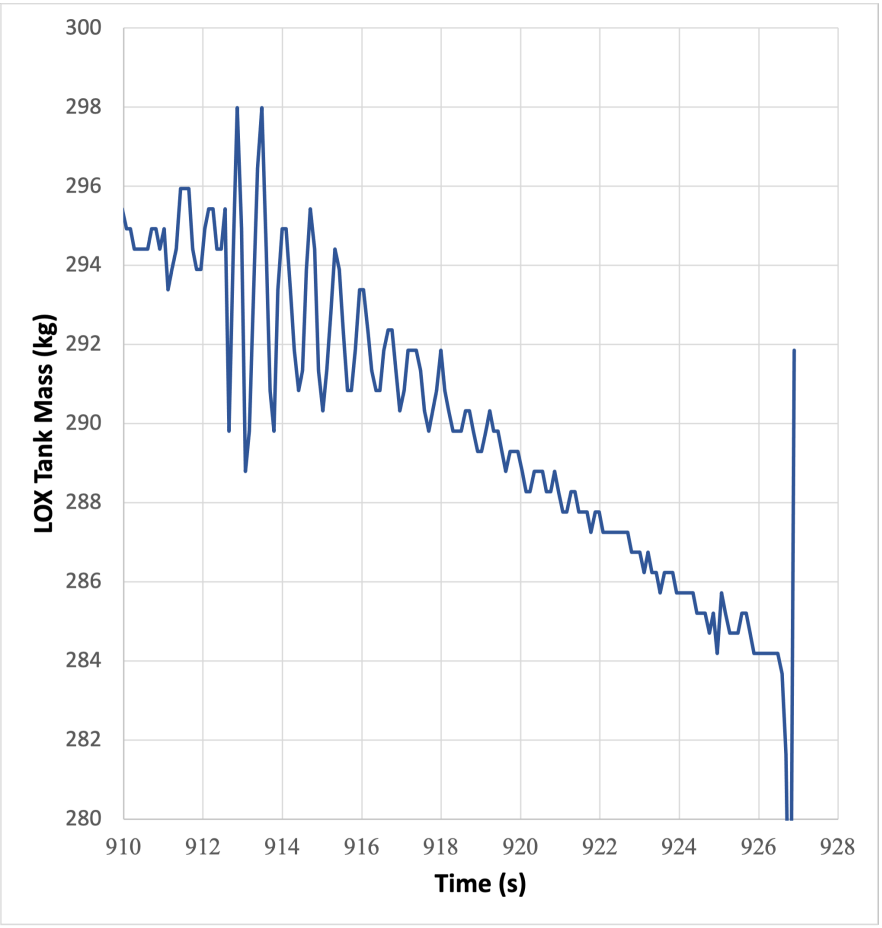

Figure 5.4. Oxidizer tank mass during hot fire test.

Looking at Figure 5.5, it is seen that fuel dome pressure rises up to $44 bar$ during the test. Like the oxidizer, we believe the fuel evaporates in the dome. Since the mass flow rates of the propellants are calculated, we conclude that neither of the propellants are in the liquid phase. With the calculated mass flow rates, the chamber pressure can be estimated. Looking at the dome pressures and calculating the pressure drops tells us the mass flow rate of the propellants would be much higher than the measured values if they were liquids.

Figure 5.5 shows that combustion chamber pressure is measured higher than the fuel dome pressure, around $57bar$. This suggests that the combustion chamber pressure measurement is incorrect because it cannot be higher than the fuel dome pressure.

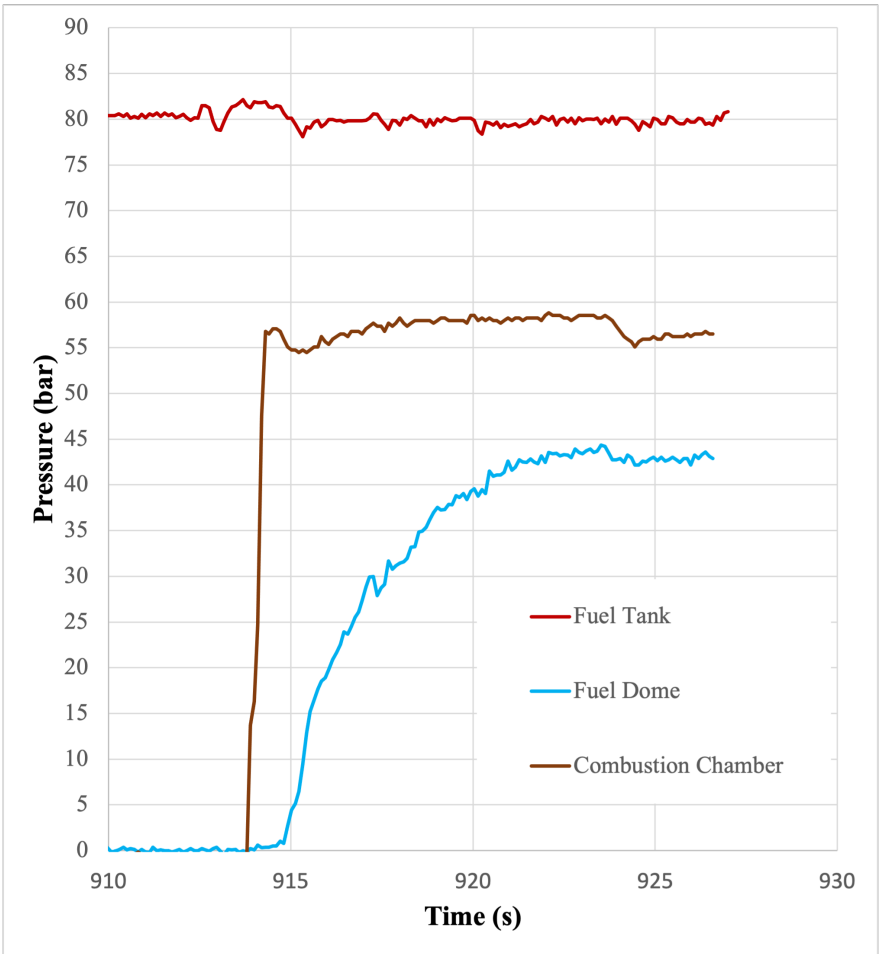

Figure 5.5. Pressure measurements on fuel side during hot fire test.

Looking at Figure 5.3, it is seen that combustion chamber pressure measurement trend is similar to that of the oxidizer dome. This suggests that the sealing of the combustion chamber pressure sensor from the oxidizer dome has failed. This might be caused by the failure of the o - ring used for this sealing. As a result of this sealing failure, the oxidizer dome pressure with a $7bar$ pressure drop is measured by this sensor. This also hints that some unknown amount of oxidizer is fed into the combustion chamber through the hole drilled on the injector face center for chamber pressure measurement.

The fuel tank mass against time graph during the hot fire test is presented in Figure 5.6. For the hot fire test, the fuel mass flow rate is calculated as $0.89kg/s$.

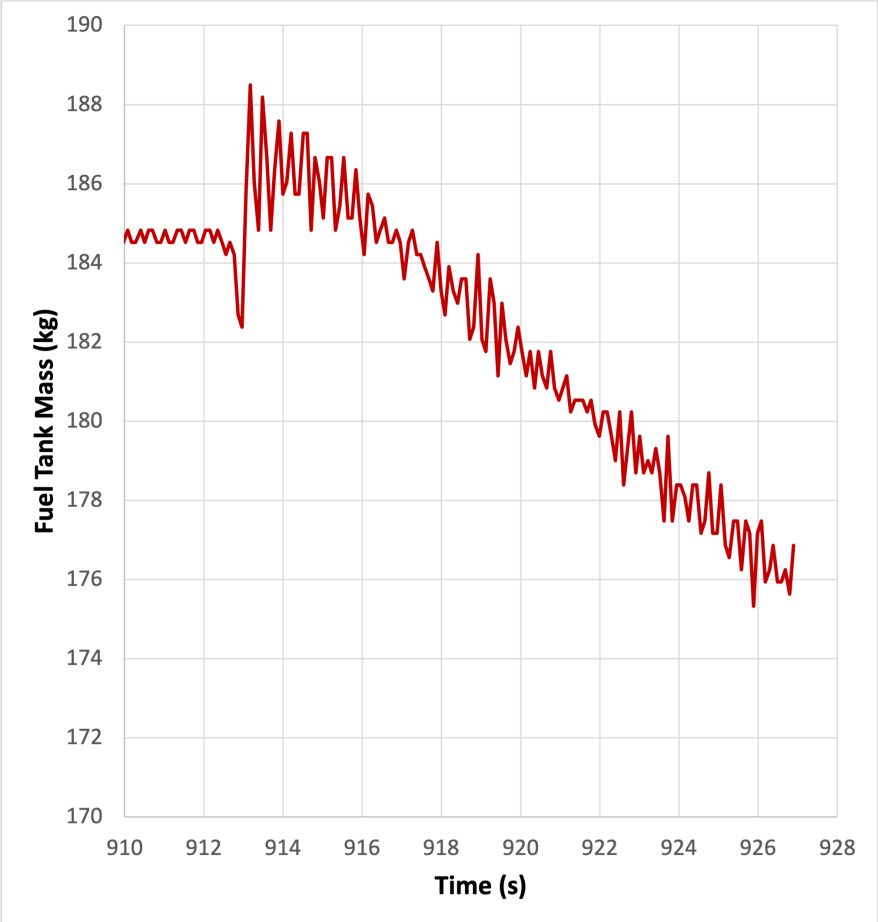

Figure 5.6. Fuel tank mass during hot fire test.

Figure 5.4 shows a $0.83kg/s$ mass flow rate for the LOX and Figure 5.6 show $0.89kg/s$ mass flow rate for the fuel. This gives a total mass flow rate of $1.72kg/s$ which is 24% lower than the designed $2.27kg/s$ and an OF ratio of 0.93 which is %26 lower than the designed 1.25 OF ratio.

The BUSTLab Liquid Rocket Engine Hot Fire Test begins at $t = 913s$. The test is originally planned to last for 20 seconds. However, 12 seconds from the beginning, at $t = 925s$, the hot fire test has ended with an explosion in the engine. The test was cut short with this explosion. With the safety precautions taken before the test, the

damage is limited to the test setup only. After the investigation, it is guessed that the explosion occured in the dome of the engine. With the data we have of this test, we cannot exactly determine the cause of the explosion. However, we are guessing that the explosion may have been caused by a sealing failure in the dome. With the huge temperature gradient across the dome and the combustion chamber, the injector might have bent resulting in sealing failure.

During the hot fire test, the thrust measurements could not be taken due to the load cell failure. With the measured mass flow rates and therefore OF ratio, we used NASA's CEA software and MATLAB to calculate the produced thrust. Propellants, OF ratio and chamber pressure are used as inputs to find γ, $\mathbb{M}$, T_c and P_e. These parameters are then used as inputs in our MATLAB code to calculate the thrust of the engine. The chamber pressure is iterated in CEA software until the measured $1.72 kg/s$ is obtained from the MATLAB code. The iteration ended at $21.2 bar$ chamber pressure. This gives a thrust around $3.62 kN$ with $215 s$ Isp. This theoretical calculation suggests a 35.9% drop in the designed thrust and a 15.4% drop in the designed Isp. The overall design and test results are presented in Table 5.1. A photo from the hot firing of the engine can be seen in Figure 5.7.

Table 5.1. Design and test result comparison of the BUSTLab Liquid Rocket Engine.

	DESIGN	**HOT FIRE TEST**	**DIFFERENCE**
$\dot{\mathbf{m}}_{\mathbf{o}}$**(kg/s)**	1.26	0.83	-34.1%
$\dot{\mathbf{m}}_{\mathbf{f}}$**(kg/s)**	1.01	0.89	-11.9%
$\dot{\mathbf{m}}_{\mathbf{total}}$**(kg/s)**	2.27	1.72	-24.2%
OF Ratio	1.25	0.93	-25.6%
Thrust(kN)	5.65	3.62	-35.9%
Isp(s)	254	215	-15.4%



Figure 5.7. BUSTLab Liquid Rocket Engine hot firing.

6. CONCLUSION

In this study, a bipropellant rocket engine is developed with a focus on the injector. The design, manufacturing and testing of the injector and the engine are carried out as part of this development. The initial design is done for a $10kN$ thrust, $50bar$ chamber pressure, $294s$ Isp engine with kerosene fuel and gaseous oxygen oxidizer. The total mass flow rate for this design was $3.45kg/s$ with 2.25 OF ratio. The manufacturing of the thrust chamber is done according to this design. However, after the difficulties in kerosene accessibility and gaseous oxygen upstream pressure requirements are seen, the fuel is changed to the mixture of 75% ethanol and 25% water, and the oxidizer is changed to liquid oxygen with an OF ratio of 1.25. LOX is not chosen as the oxidizer initially because we did not want to work with the cryogenic fluids as they significantly increase the difficulties in the feed system design and operation, and we had not prior experience with them. After these changes, our design has become a $5.65kN$ thrust, $30bar$ chamber pressure, $2.27kg/s$ total mass flow rate and $254s$ Isp engine.

BUSTLab Liquid Rocket Engine has a triplet impinging injector. This injector type is chosen for this study because it has simpler manifolding compared to other types. Another reason is impinging injector manufacturing process requires no welding and it can be carried out with computerized machining methods only. Two different versions are designed and manufactured for the injector.

The first injector is manufactured for $RP-1$ and GOX propellants. This injector is water tested many times. In these tests, it is seen that the total oxidizer flow area is too large for LOX, giving inadequate pressure drop, $0.7bar$, for a stable combustion. For the fuel side, it is seen that the total flow area is too small which requires high pressure drop, $11.9bar$, across the injector. This results in higher pressures than needed in the fuel dome. In order to solve these issues, a second injector is designed. This design reduces the oxidizer flow area to 40% and increases the fuel flow area to 150%

of the first design. The C_d values for the first injector are calculated as 0.69 for the oxidizer orifices and 0.72 for the fuel orifices. The second version of the injector is designed with the assumption that the C_d values will stay the same or close to the first design test results.

Unlike the first injector, the second design has simple distribution of the triplet elements across the injector face. This is done to alleviate the manufacturing difficulty and cut the manufacturing costs to reasonable levels. On paper, this design increases the oxidizer pressure drop to $4.6bar$ and reduces the fuel pressure drop to $5.3bar$. These calculations are done for the same discharge coefficient values with the prior injector design. Nevertheless, the water tests showed that this design has 0.52 discharge coefficient for the fuel side, whereas the oxidizer side remained the same. We believe the huge difference in the fuel side discharge coefficient is caused by a manufacturing error that we have not been able identify. This injector is used in the cold flow, open hot flow and hot fire tests.

Cold flow tests are carried out with liquid nitrogen and water. 1.06kg/s mass flow rate for liquid nitrogen is obtained in these tests. Making the appropriate calculations, this give a liquid oxygen flow of $1.26kg/s$ which is the designed value. For the fuel side, 0.88kg/s mass flow rate is measured with water. This gives an ethanol - water mixture mass flow rate of $0.80kg/s$. The calculated fuel mass flow rate is 21% less than the design. The fuel cavitating venturi is designed to provide $1.01kg/s$ mass flow rate of ethanol - water mixture at $80bar$ tank pressure, at which the cold flow tests are conducted. We believe this difference is caused by a manufacturing error in the fuel cavitating venturi. Otherwise, the upstream mass flow rate is expected to be close to the designed value. If the cavitating venturi did work as expected, this would result in high pressure drop across the injector to compensate for the low C_d value and the resulting mass flow rate would still be $1.01kg/s$.

The third open hot flow test is conducted with both tanks filled with real propellants and pressurized to $80bar$. This test resulted in $0.88kg/s$ mass flow rate for the

oxidizer and $0.84kg/s$ for the fuel. The oxidizer side gave results as expected in the previous water and cold flow tests. In this test, the oxidizer tank pressure could not be kept at $80bar$. A linear decrease to $73bar$ resulted in lower upstream mass flow rate. However, we believe that the main issue with the lower oxidizer flow rate is caused by icing in the cavitating venturi resulting in the reduced flow area. The fuel side in this test gave lower mass flow rate measurements in agreement with the previous water and cold flow tests due to the manufacturing error in the cavitating venturi.

The hot fire test is originally planned for a 20 seconds of firing. During the test, $0.83kg/s$ oxidizer mass flow rate and $0.89kg/s$ of fuel mass flow rate are measured. Both the oxidizer and the fuel sides gave results consistent with open hot flow tests, suggesting once again an icing problem in the oxidizer venturi. In this test, no thrust measurements are performed due to a failure in the load cell. The combustion chamber pressure measurement is also inconclusive because of an o - ring failure. The pressure sensor assigned to measure the chamber pressure shows data close to that of the oxidizer dome suggesting a sealing failure between the oxidizer dome and the sensor. 12 seconds after the test beginning, the test was interrupted by an explosion in the engine. We believe this explosion is caused by a sealing failure in the dome between the oxidizer and fuel.

Since the thrust measurement with the load cell has failed in the hot fire test, an iterative method is used to calculate the produced thrust. With the measured OF ratio of 0.93 and known propellants, several CEA runs are done. By inputting the CEA outputs into the MATLAB code the mass flow rate is calculated. This way, the produced thrust is calculated to be around $3.62kN$ with $215s$ Isp. Table 5.1 shows the comparison of the designed engine and test results.

REFERENCES

1. Kitsikopoulos, H., "From Hero to Newcomen: The Critical Scientific and Technological Developments That Led to the Invention of the Steam Engine", *Proceedings of the American Philosophical Society*, Vol. 157, pp. 304–344, 2013.

2. Florenz, R. E., *The X3 100-kW Class Nested-Channel Hall Thruster: Motivation, Implementation, and Initial Performance.*, Ph.D. Thesis, The University of Michigan, 2014.

3. ""Best of the Best" Provides New Views, Commentary of Shuttle Launches", `https://youtu.be/vFwqZ4qAUkE?t=265`, accessed in March 2022.

4. Sutton, G. P. and O. Biblarz, *Rocket Propulsion Elements*, John Wiley & Sons, New York, NY, USA, 2016.

5. Surmacz, P. and G. Rarata, "Hybrid Rocket Propulsion Development and Application", *Progress in Astronautics*, Vol. 1, pp. 13–25, 2009.

6. Uramachi, H., D. Shiraiwa, T. Takai, N. Tanaka, T. Kaneko and K. Furukawa, "Green Propulsion Systems for Satellites—Development of Thrusters and Propulsion Systems Using Low-Toxicity Propellants", *Mitsubishi Heavy Industries Technical Review*, Vol. 56, No. 1, pp. 1–7, 2019.

7. Kokal, U., N. Turan, M. Celik and H. Kurt, "Design Improvements and Experimental Measurements of BURFIT-80 RF Ion Thruster", *53rd Joint Propulsion Conference*, p. 4891, Cleveland, OH, USA, 2017.

8. Turan, N., *Experimental Investigation of the Effects of Cathode Position on HK40 Hall Effect Thruster Performance and Cathode Coupling*, M.S. Thesis, Bogazici University, 2016.

9. Tummala, A. R. and A. Dutta, "An Overview of Cube-Satellite Propulsion Technologies and Trends", *Aerospace*, Vol. 4, No. 4, p. 58, 2017.

10. "A Close Up Look at the V2 Rocket Engine's Fuel Injector Inserts", `https://v2rockethistory.com/a-close-up-look-at-the-v2-rocket-engines-fuel-injector-inserts/`, accessed in April 2022.

11. Sutton, G. P., *History of Liquid Propellant Rocket Engines*, American Institute of Aeronautics and Astronautics, Reston, VA, USA, 2005.

12. Delpy, R. and J. Oswald, "PERSEUS Project 5kN LOX/Ethanol Rocket Engine Fire Tests", *7th European Conference for Aeronautics and Space Sciences (EUCASS)*, Milano, Italy, 2017.

13. Hansen, J. J., M. Hussein, S. Moehring, M. Stauffer, C. Acosta, J. Daly, N. Chennoju and P. Imper, "Student Design of a Bipropellant Liquid Rocket Engine and Associated Infrastructure", *AIAA Propulsion and Energy Forum*, p. 3918, 2020.

14. Trillo, J. E., *Design of a 500 lbf Liquid Oxygen and Liquid Methane Rocket Engine for Suborbital Flight*, M.S. Thesis, University of Texas El Paso, 2016.

15. Yang, L.-J. and Q.-F. Fu, "Theoretical Investigation on the Dynamics of a Gas-Liquid Coaxial Swirl Injector", *Journal of Propulsion and Power*, Vol. 27, No. 1, pp. 144–150, 2011.

16. "BPM-5 With Swirlers", `https://copenhagensuborbitals.com/bpm-5-with-swirlers`, accessed in February 2022.

17. "The Swirlers Have Landed", `https://copenhagensuborbitals.com/the-swirlers-have-landed/`, accessed in February 2022.

18. Dressler, G., "Summary of Deep Throttling Rocket Engines With Emphasis on Apollo LMDE", *42nd Joint Propulsion Conference*, Sacramento,CA,USA, 2006.

19. Nilsen, C., S. Meyer and S. Meriam, "Purdue Liquid Oxygen-Liquid Methane Sounding Rocket", *AIAA Scitech 2019 Forum*, San Diego, CA, USA, 2019.

20. Dressler, G. and J. Bauer, "TRW Pintle Engine Heritage and Performance Characteristics", *36th Joint Propulsion Conference*, Las Vegas, NV, USA, 2000.

21. Nardi, R., V. Perez and A. Pimenta, "Experiments With Pintle Injector Design and Development", *51st Joint Propulsion Conference*, Orlando, FL, USA, 2015.

22. Farr, R. and T. Sanders, "RS-88 Pad Abort Demonstrator Thrust Chamber Assembly Testing at NASA Marshall Space Flight Center, November-December 2003", *41st Joint Propulsion Conference*, p. 4422, Tucson, AZ, USA, 2005.

23. Nardi, R., S. Neto, A. Pimenta and V. Perez, "Dimensioning a Simplex Swirl Injector", *50th Joint Propulsion Conference*, p. 3602, Cleveland, OH, USA, 2014.

24. Rezende, R. N., *Liquid Rocket Engine: Thrust Chamber Parametric Modeling*, SAE International, Kansas City, MO, USA, 2018.

25. Anderson, W. E., M. Long, S. Heister and V. Yang, "Liquid Bipropellant Injectors", *Liquid Rocket Thrust Chambers, Progress in Astronautics and Aeronautics*, Vol. 42, pp. 141–165, 2004.

26. Kramer, S. B., N. Putnam and A. Chwick, "The Rocket: an Old Idea, an Old Challenge", *Astronautics*, Vol. 4, p. 15, 1959.

27. Schmucker, R., *Flow Processes In Overexpanded Chemical Rocket Nozzles. Part 1: Flow Separation*, NASA, Pasadena, CA, USA, 1984.

28. Cowles, F. B. and C. R. Foster, *Experimental Study Of Gas-Flow Separation In Overexpanded Exhaust Nozzles For Rocket Motors*, NASA, Pasadena, CA, USA, 1949.

29. Summerfield, M., C. R. Foster and W. C. Swan, "Flow Separation in Overexpanded Supersonic Exhaust Nozzles", *Journal of Jet Propulsion*, Vol. 24, No. 5, pp. 319–321, 1954.

30. Frey, M. and G. Hagemann, "Status of Flow Separation Prediction in Rocket Nozzles", *34th Joint Propulsion Conference*, p. 3619, Cleveland, OH, USA, 1998.

31. Rachov, P. P., H. Tacca and D. Lentini, "Electric Feed Systems for Liquid Propellant Rockets", *Journal of Propulsion and Power*, Vol. 29, No. 5, pp. 1171–1180, 2013.

32. Spiller, D., A. Stabile and D. Lentini, "Design and Testing of a Demonstrator Electric—Pump Feed System for Liquid Propellant Rocket Engines", *Aerotecnica Missili & Spazio*, Vol. 92, No. 3, pp. 123–130, 2013.

33. Beck, P. and J. Tulp, "Rocket lab: Liberating the Small Satellite Market", *31st Small Satellite Conference*, Logan, UT, USA, 2017.

34. Darley, M. and P. Beck, "Return to Sender: Lessons Learned From Rocket Lab's First Recovery Mission", *36th Small Satellite Conference*, Logan, UT, USA, 2022.

35. McRight, P., C. Popp, C. Pierce, A. Turpin, W. Urbanchock and M. Wilson, "Confidence Testing of Shell-405 and S-405 Catalysts in a Monopropellant Hydrazine Thruster", *41st Joint Propulsion Conference*, p. 3952, Tucson, AZ, USA, 2005.

36. Evans, D. and T. Price, *The Status Of Monopropellant Hydrazine Technology*, NASA, Pasadena, CA, USA, 1968.

37. Malm, J., "Inclusion of Substances of Very High Concern in the Candidate List", `https://echa.europa.eu/documents/10162/c5b972a9-f57f-4fd5-8177-04b4e46c5e93`, accessed in April 2022.

38. Nosseir, A. E., A. Cervone and A. Pasini, "Review of State of the Art Green

Monopropellants: For Propulsion Systems Analysts and Designers", *Aerospace*, Vol. 8, No. 1, p. 20, 2021.

39. Mayer, A. and W. Wieling, "Green Propulsion Research at TNO the Netherlands", *Transactions On Aerospace Research*, Vol. 253, No. 4, pp. 1–24, 2018.

40. Baek, S., W. Jung, H. Kang and S. Kwon, "Development of High-Performance Green-Monopropellant Thruster With Hydrogen Peroxide and Ethanol", *Journal of Propulsion and Power*, Vol. 34, No. 5, pp. 1256–1261, 2018.

41. Gill, G. and W. Nurick, "Liquid Rocket Engine Injectors", *NASA Special Publication (SP)*, NASA Technical Reports, 1976.

42. "Coaxial Swirl Injector", `https://copenhagensuborbitals.com/tag/coaxial-swirl-injector/`, accessed in February 2022.

43. Zong, N. and V. Yang, "Cryogenic Fluid Dynamics of Pressure Swirl Injectors at Supercritical Conditions", *Physics of Fluids*, Vol. 20, No. 5, pp. 74–88, 2008.

44. Hulka, J. and J. Schneider, "Single Element Injector Cold Flow Testing for STME Swirl Coaxial Injector Element Design", *29th Joint Propulsion Conference*, Monterey, CA, USA, 1993.

45. Hiraiwa, T., T. Saito, T. Tomita, N. Azuma, K. Okita, K. Obase and T. Kaneko, "Research Works of Ethanol Propulsion System for the Future Rocket-Plane Experimental Vehicle", *47th Joint Propulsion Conference*, p. 6114, Atlanta, GA, USA, 2011.

46. Youngblood, S. H., *Design and Testing of a Liquid Nitrous Oxide and Ethanol Fueled Rocket Engine*, M.S. Thesis, New Mexico Institute of Mining and Technology, Socorro, NM, USA, 2015.

47. Casiano, M. J., J. R. Hulka and V. Yang, "Liquid Propellant Rocket Engine Throt-

tling: a Comprehensive Review", *Journal of Propulsion and Power*, Vol. 26, No. 5, pp. 897–923, 2010.

48. Bazarov, V., V. Yang and P. Puri, "Design and dynamics of jet and swirl injectors", *Liquid Rocket Thrust Chambers: Aspects of Modeling, Analysis, and Design*, Vol. 200, pp. 19–103, 2004.

49. Lacava, P. T., D. Bastos-Netto and A. P. Pimenta, "Design Procedure and Experimental Evaluation of Pressure-Swirl atomizers", *24th International Congress of the Aeronautical Sciences*, Yokohama, JAPAN, 2004.

50. Escher, D. W., *Design and Preliminary Hot Fire and Cold Flow Testing of Pintle Injectors*, Ph.D. Thesis, Pennsylvania State University, 1996.

51. Austin, B. L., S. Heister and W. Anderson, "Characterization of Pintle Engine Performance for Nontoxic Hypergolic Bipropellants", *Journal of Propulsion and Power*, Vol. 21, No. 4, pp. 627–635, 2005.

52. Phillip, J., S. Youngblood, M. Grubelich, W. V. Saul and M. J. Hargather, "Development and Testing of a Nitrous-Oxide/Ethanol Bipropellant Rocket Engine", *52nd Joint Propulsion Conference*, pp. 50–92, Salt Lake City, UT, USA, 2016.

53. Lopez, I., *Design of a 2000 lbf LOX/LCH4 Throttleable Rocket Engine for a Vertical Lander*, M.S. Thesis, The University of Texas at El Paso, El Paso, TX, USA, 2017.

54. Herrera, M., *Design and Testing of a 500 lbf Liquid Oxygen/Liquid Methane Engine*, M.S. Thesis, The University of Texas at El Paso, El Paso, TX, USA, 2019.

APPENDIX A: NOZZLE THEORY

The heart of a rocket engine is the thrust chamber where chemical reactions take place. These chemical reactions create a high temperature - high enthalpy environment in the chamber. Thermodynamic relations are used to calculate the design parameters and performance of a rocket. The following assumptions are used for ideal rocket nozzle calculations:

(i) Combustion products are homogeneous.
(ii) Working fluid is in gaseous phase. Liquid or solid phases of matter have negligible mass
(iii) Combustion products obey ideal gas law.
(iv) The flow is adiabatic (no heat transfer to the thrust chamber walls).
(v) Friction and boundary layer effects are neglected.
(vi) There are no shock waves or discontinuities in the nozzle.
(vii) The propellant flow is steady and constant.
(viii) The expansion is uniform and steady.
(ix) Transient effects (start and shut off) are negligible.
(x) Combustion products are exhausted axially.
(xi) Any axial cross - section of the chamber has uniform velocity, pressure, temperature and density.
(xii) Frozen flow conditions apply (gas composition is fixed).
(xiii) Stored propellants are at room temperature and cryogenics are at their boiling temperatures.

With these assumptions, a quasi one - dimensional theory can be developed. With the equations derived, engine design parameters and performance parameters can be calculated. Real rockets have 1 - 6% performances below the calculations made with these assumptions [4]. The small error in calculations with ideal rocket assumptions are explained by [4]:

(i) Perfect injection and mixing in ideal rocket assumption can be approached by a good injector.

(ii) All of the combustion products are at elevated temperatures well above their saturation conditions and they behave close to ideal.

(iii) Wall frictions are generally small in real nozzles.

(iv) Heat transfer to the walls is generally 1% - 2% percent of the total energy of the flow.

(v) Variation in propellant feed rate and chamber pressure is less than 5% of the rated working condition.

(vi) A well designed supersonic nozzle has no normal shocks or discontinuities present and the energy conversion from thermal to kinetic is smooth.

Using the assumptions above, thermodynamic relations are used to derive the rocket equations. The stagnation enthalpy, as given in A.1, is constant throughout the process:

$$h_0 = h + \frac{V^2}{2}. \tag{A.1}$$

For an isentropic flow, the change in enthalpy or temperature between any two sections changes the kinetic energy in the other way. An increase in the enthalpy results in a decrease in the kinetic energy and a decrease in the enthalpy results in an increase in the kinetic energy:

$$h_0 = h_a + \frac{V_a^2}{2} = h_b + \frac{V_b^2}{2}. \tag{A.2}$$

Reorganizing Equation A.2:

$$h_a - h_b = \frac{V_b^2 - V_a^2}{2} = c_p(T_a - T_b). \tag{A.3}$$

Mass flow rate at any section from continuity equation is shown in Equation A.4:

$$\dot{m}_a = \dot{m}_b \equiv \dot{m} = AV\rho = \frac{AV}{v}. \tag{A.4}$$

In this equation ρ is the density and v is the specific volume.

Ideal gas law is written as in Equation A.5:

$$p_x v_x = RT_x = \frac{R_{univ}}{\mathbb{M}} T_x. \tag{A.5}$$

R_{univ} is the universal gas constant and $\mathbb{M}$ is the molecular mass or molecular weight of the combustion products.

c_p (specific heat at constant pressure) and c_v(specific heat at constant volume) relations for ideal gases are:

$$\gamma = \frac{c_p}{c_v} \ (specific\ heat\ ratio) \tag{A.6}$$

$$c_p - c_v = R \tag{A.7}$$

$$c_v = \frac{R}{\gamma - 1} \tag{A.8}$$

$$c_p = \frac{\gamma R}{\gamma - 1}. \tag{A.9}$$

The specific entropy relations for two different sections of the flow are as given in Equations A.10 and A.11:

$$s(T_b, v_b) - s(T_a, v_a) = c_v \ln \frac{T_b}{T_a} + Rln\frac{v_b}{v_a} \tag{A.10}$$

$$s(T_b, p_b) - s(T_a, p_a) = c_p \ln \frac{T_b}{T_a} - Rln\frac{p_b}{p_a}. \tag{A.11}$$

For an isentropic flow of an ideal gas, specific entropy is constant. Equations A.10 and A.11 reduce to:

$$0 = c_v ln\frac{T_b}{T_a} + R \ln \frac{v_b}{v_a} \tag{A.12}$$

$$0 = c_p ln \frac{T_b}{T_a} - R \ln \frac{p_b}{p_a}. \quad \text{(A.13)}$$

Introducing the ideal gas relations in Equations A.8 and A.9 into Equations A.12 and A.13:

$$0 = \frac{R}{\gamma - 1} \ln \frac{T_b}{T_a} + R \ln \frac{v_b}{v_a} \quad \text{(A.14)}$$

$$0 = \frac{\gamma R}{\gamma - 1} \ln \frac{T_b}{T_a} - R \ln \frac{p_b}{p_a}. \quad \text{(A.15)}$$

Reorganizing Equations A.14 and A.15:

$$\frac{1}{\gamma - 1} \ln \frac{T_b}{T_a} = \ln \frac{v_a}{v_b} \quad \text{(A.16)}$$

$$\frac{\gamma}{\gamma - 1} \ln \frac{T_b}{T_a} = \ln \frac{p_b}{p_a}. \quad \text{(A.17)}$$

Solving Equations A.16 and A.17:

$$\frac{T_b}{T_a} = \left(\frac{v_a}{v_b} \right)^{\gamma - 1} \quad (constant\ s,\ constant\ \gamma) \quad \text{(A.18)}$$

$$\frac{T_b}{T_a} = \left(\frac{p_b}{p_a} \right)^{(\gamma - 1)/\gamma} \quad (constant\ s,\ constant\ \gamma). \quad \text{(A.19)}$$

Finally, Equations A.18 and A.19 are combined and reorganized into Equation A.20:

$$\frac{T_a}{T_b} = \left(\frac{p_a}{p_b} \right)^{(\gamma - 1)/\gamma} = \left(\frac{v_b}{v_a} \right)^{\gamma - 1}. \quad \text{(A.20)}$$

The relations in Equation A.20 hold for any point in an isentropic flow.

The stagnation or total values of pressure and temperature refer to the condition at which the flow is stopped, flow velocity goes to zero, isentropically. Dividing

Equation A.1 with c_p, we can find the stagnation temperature for the flow:

$$T_0 = T + \frac{V^2}{2c_p}. \tag{A.21}$$

With the assumption of adiabatic flow established earlier, we can say that the stagnation temperature remains unchanged throughout the flow process.

The stagnation pressure relation and the local pressure relation is derived as follows: Equation A.20 is solved for p_a/p_b and Equation A.21 is substituted for the T_0 in this equation. Since the velocity is small in the combustion chamber, the combustion pressure can be taken as equal to the stagnation pressure:

$$\frac{p_a}{p_b} = \left(\frac{T_a}{T_b}\right)^{\gamma/(\gamma-1)} = \left(\frac{v_b}{v_a}\right)^{\gamma} \tag{A.22}$$

$$\frac{p_0}{p} = \left(\frac{T_0}{T}\right)^{\gamma/(\gamma-1)} = \left(\frac{v}{v_0}\right)^{\gamma} \tag{A.23}$$

$$\frac{p_0}{p} = \left(1 + \frac{V^2}{2c_pT}\right)^{\gamma/(\gamma-1)} = \left(\frac{v}{v_0}\right)^{\gamma}. \tag{A.24}$$

Independent of pressure, the local speed of sound is defined as:

$$c = \sqrt{\gamma RT}. \tag{A.25}$$

The Mach number is the ratio of the flow speed to the local speed of sound. The Mach number is a dimensionless flow parameter. A Mach number $M < 1$ means the flow is at subsonic speeds and a Mach number $M > 1$ means the flow is at supersonic speeds. Sonic conditions correspond to a Mach number $M = 1$. At the throat, all supersonic rocket nozzles must have sonic conditions. It is calculated as:

$$M = \frac{V}{c} = \frac{V}{\sqrt{\gamma RT}}. \tag{A.26}$$

Using Equations A.3, A.9 and A.25, the relationship of T_0 to M is derived as:

$$\frac{1}{2}\frac{(\overbrace{V_0^2}^{\Rightarrow 0} - V^2)}{c^2} = \frac{c_p(T - T_0)}{c^2} \tag{A.27}$$

$$\frac{1}{2}\frac{-V^2}{c^2} = -\frac{1}{2}M^2 = \frac{c_p(T - T_0)}{\gamma RT} \tag{A.28}$$

$$-\frac{1}{2}M^2 = \frac{c_p}{\gamma R}\left(1 - \frac{T_0}{T}\right) \tag{A.29}$$

$$-\frac{1}{2}M^2 = \frac{\gamma R}{(\gamma - 1)\gamma R}\left(1 - \frac{T_0}{T}\right) \tag{A.30}$$

$$-\frac{1}{2}(\gamma - 1)M^2 = 1 - \frac{T_0}{T} \tag{A.31}$$

$$\frac{T_0}{T} = 1 + \frac{1}{2}(\gamma - 1)M^2 \tag{A.32}$$

$$T_0 = T\left[1 + \frac{1}{2}(\gamma - 1)M^2\right]. \tag{A.33}$$

Solving Equation A.33 for M:

$$M = \sqrt{\frac{2}{\gamma - 1}\left(\frac{T_0}{T} - 1\right)}. \tag{A.34}$$

With the established adiabatic and isentropic flow assumptions and using Equations A.20 and A.32, stagnation pressure and Mach number relation is derived:

$$\left(\frac{p_0}{p}\right)^{(\gamma-1)/\gamma} = 1 + \frac{1}{2}(\gamma - 1)M^2 \tag{A.35}$$

$$p_0 = p\left[1 + \frac{1}{2}(\gamma - 1)M^2\right]^{\gamma/(\gamma-1)}. \tag{A.36}$$

Rewriting Equation A.4:

$$v = \frac{AV}{\dot{m}}. \tag{A.37}$$

Rewriting Equation A.20:

$$\frac{p_a}{p_b} = \left(\frac{v_b}{v_a}\right)^{\gamma}. \tag{A.38}$$

Using Equations A.33, A.36, A.37 and A.38:

$$p_0 = p_a \left[1 + \frac{1}{2}(\gamma - 1)M_a^2\right]^{\gamma/(\gamma-1)} \tag{A.39}$$

$$p_0 = p_b \left[1 + \frac{1}{2}(\gamma - 1)M_b^2\right]^{\gamma/(\gamma-1)} \tag{A.40}$$

$$\frac{p_a}{p_b} = \left[\frac{1 + \frac{1}{2}(\gamma - 1)M_b^2}{1 + \frac{1}{2}(\gamma - 1)M_a^2}\right]^{\gamma/(\gamma-1)} \tag{A.41}$$

$$\left(\frac{v_b}{v_a}\right)^{\gamma} = \left[\frac{1 + \frac{1}{2}(\gamma - 1)M_b^2}{1 + \frac{1}{2}(\gamma - 1)M_a^2}\right]^{\gamma/(\gamma-1)} \tag{A.42}$$

$$\left(\frac{A_b V_b}{A_a V_a}\right)^{\gamma} = \left[\frac{1 + \frac{1}{2}(\gamma - 1)M_b^2}{1 + \frac{1}{2}(\gamma - 1)M_a^2}\right]^{\gamma/(\gamma-1)} \tag{A.43}$$

$$\frac{A_b V_b}{A_a V_a} = \left[\frac{1 + \frac{1}{2}(\gamma - 1)M_b^2}{1 + \frac{1}{2}(\gamma - 1)M_a^2}\right]^{1/(\gamma-1)} \tag{A.44}$$

$$\frac{A_b}{A_a} = \frac{V_a/c_a}{V_b/c_b}\frac{c_a}{c_b}\left[\frac{1 + \frac{1}{2}(\gamma - 1)M_b^2}{1 + \frac{1}{2}(\gamma - 1)M_a^2}\right]^{1/(\gamma-1)} \tag{A.45}$$

$$\frac{A_b}{A_a} = \frac{M_a}{M_b}\frac{\sqrt{\gamma R T_a}}{\sqrt{\gamma R T_b}}\left[\frac{1 + \frac{1}{2}(\gamma - 1)M_b^2}{1 + \frac{1}{2}(\gamma - 1)M_a^2}\right]^{1/(\gamma-1)} \tag{A.46}$$

$$\frac{A_b}{A_a} = \frac{M_a}{M_b}\sqrt{\frac{T_a}{T_b}}\left[\frac{1 + \frac{1}{2}(\gamma - 1)M_b^2}{1 + \frac{1}{2}(\gamma - 1)M_a^2}\right]^{1/(\gamma-1)} \tag{A.47}$$

$$\frac{A_b}{A_a} = \frac{M_a}{M_b}\sqrt{\frac{1 + \frac{1}{2}(\gamma - 1)M_b^2}{1 + \frac{1}{2}(\gamma - 1)M_a^2}}\left[\frac{1 + \frac{1}{2}(\gamma - 1)M_b^2}{1 + \frac{1}{2}(\gamma - 1)M_a^2}\right]^{1/(\gamma-1)} \tag{A.48}$$

$$\frac{A_b}{A_a} = \frac{M_a}{M_b}\left[\sqrt{\frac{1 + \frac{1}{2}(\gamma - 1)M_b^2}{1 + \frac{1}{2}(\gamma - 1)M_a^2}}\right]^{(\gamma+1)/(\gamma-1)} . \tag{A.49}$$

Equation A.49 gives the relations between the area ratios and Mach numbers for any points a and b in the nozzle. Figure A.1 presents a plot of area ratio (A/A_t), pressure ratio (p/p_0) and temperature ratio (T/T_0) along a converging - diverging nozzle as functions of Mach number (M) for $\gamma = 1.3$.

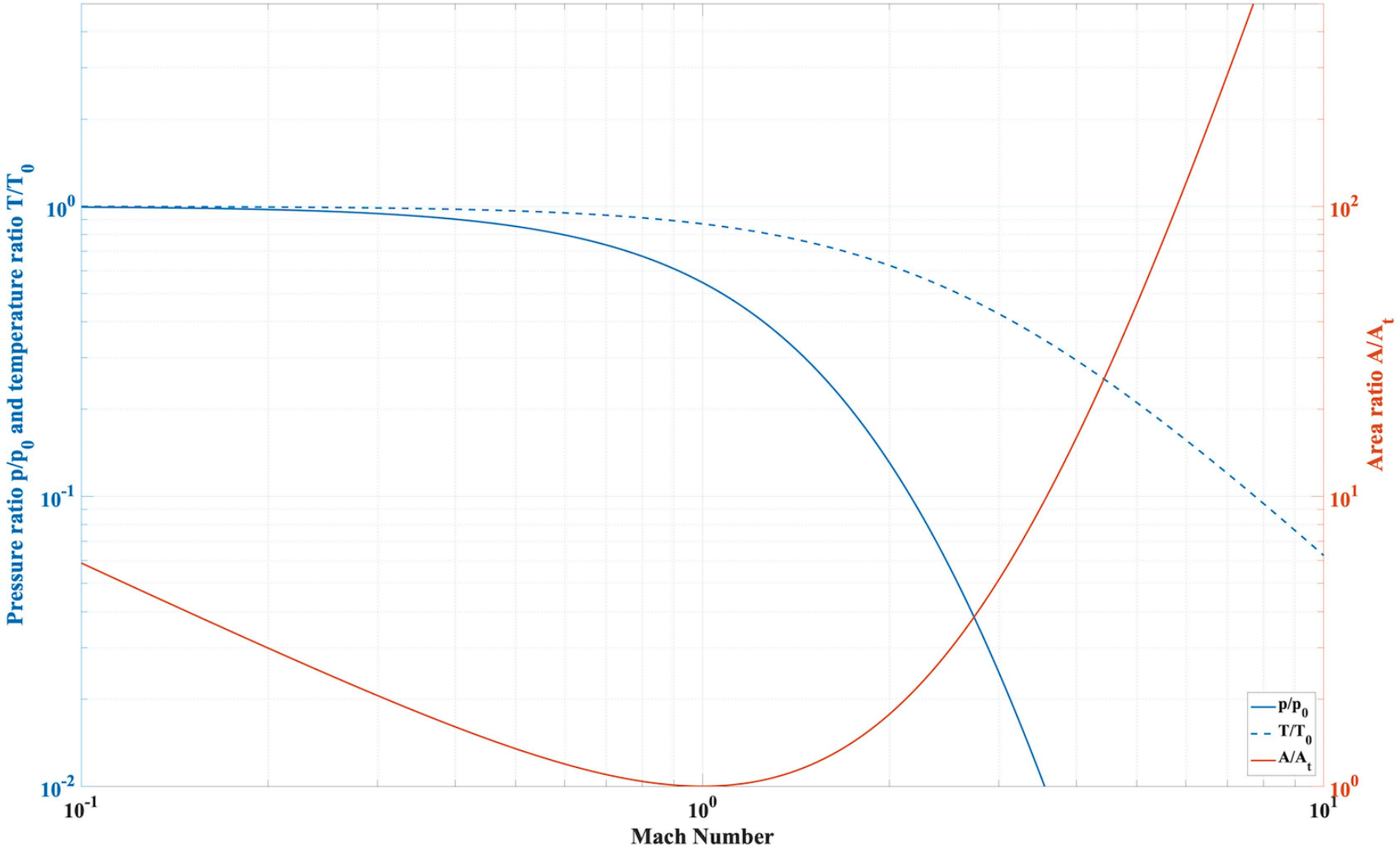

Figure A.1. Area ratio (A/A_t), pressure ratio (P/P_0) and temperature ratio (T/T_0) along a converging - diverging nozzle as functions of Mach number (M) for $\gamma = 1.3$.